

Micro and Nano-Tomography of Biological Tissues

Marco Stampanoni and Kevin Mader

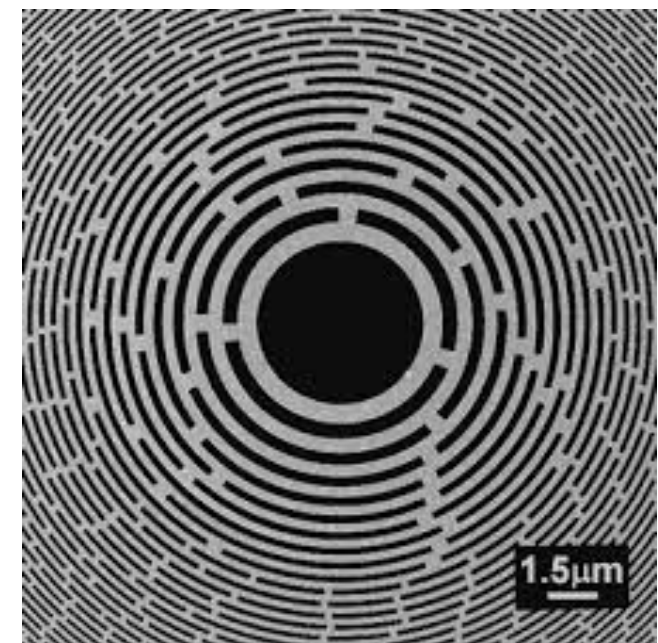
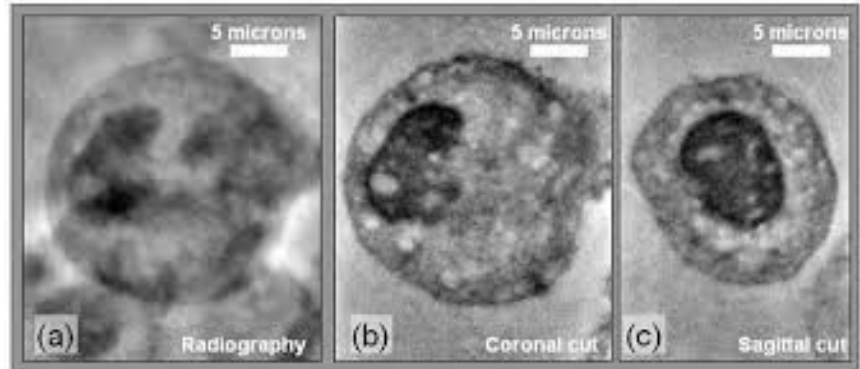
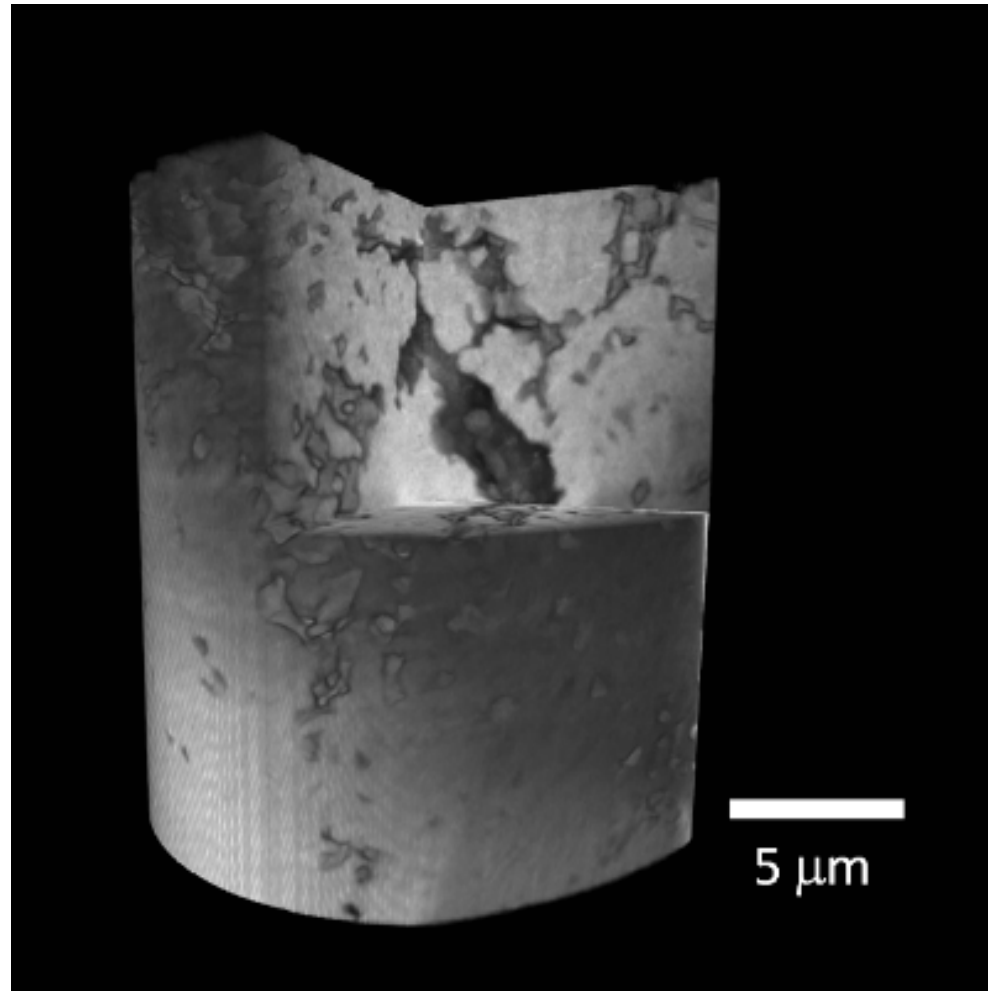
Swiss Light Source, Paul Scherrer Institut
Institute for Biomedical Engineering, University and ETH Zürich



ETH-227-0965-00 L



Nano-imaging



Moving to nanoimaging

- **Imaging geometries**

- **Focusing X-rays**

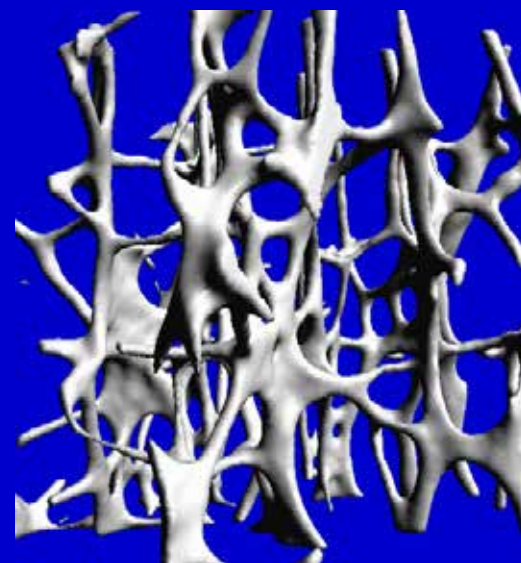
- Zone plates
- Compound Refractive Lenses
- Kirkpatrick-Baez systems

- **Phase contrast imaging in the nano scale**

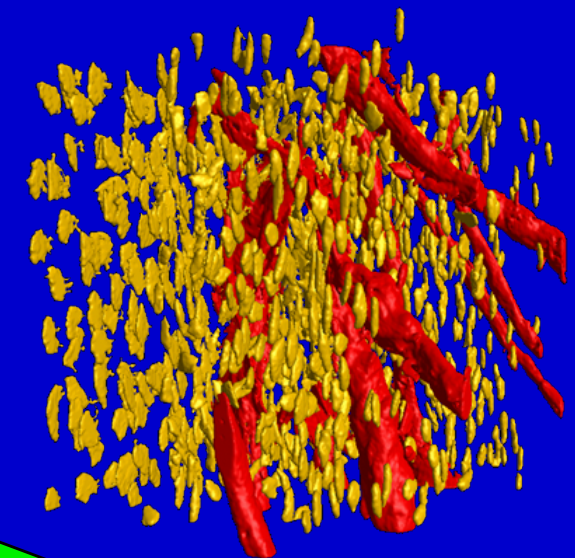
- PXM
- Zernike

- **Coherent Diffraction Imaging - Lensless imaging**

Towards nanotomography...



$$\Phi \propto \frac{SNR^2}{\Delta x^4 \cdot \Delta \mu^2}$$

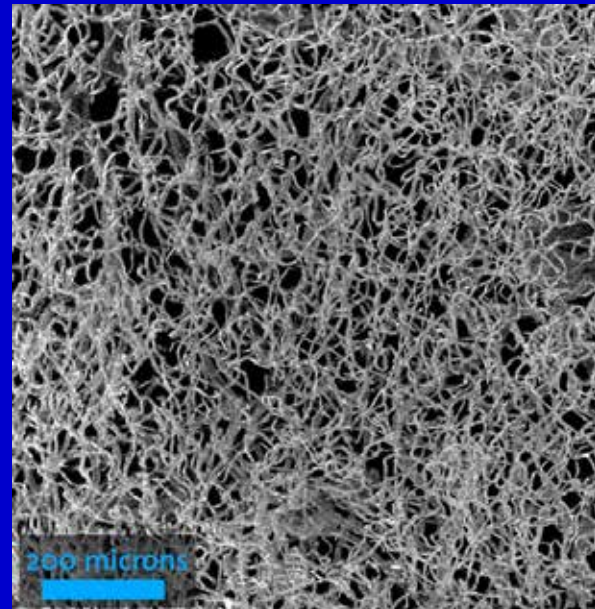


1000-500 µm
Hospital

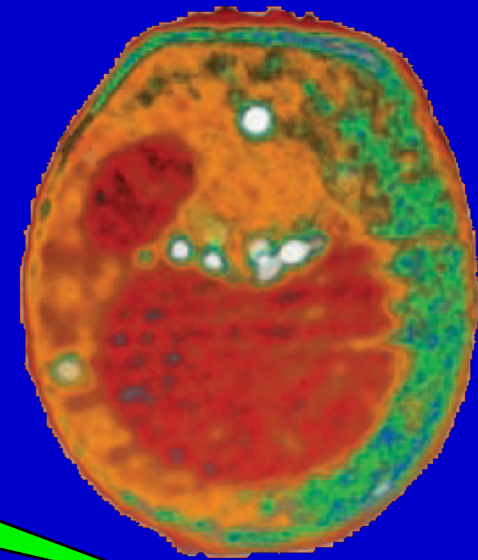
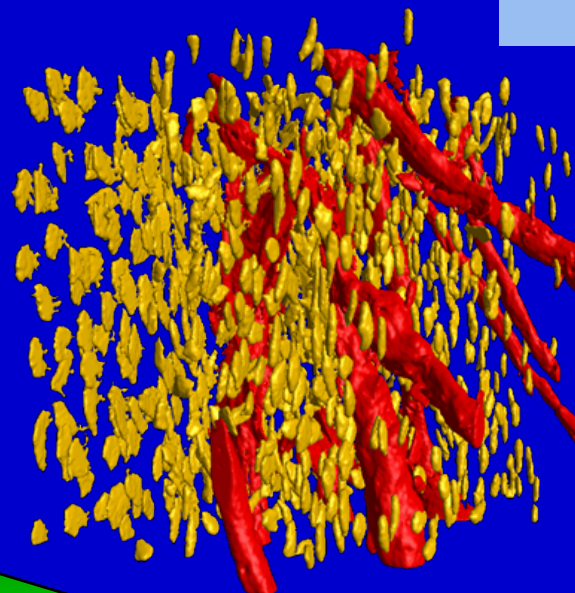
50-10 µm
Table Top micro CT

1-0.1 µm
SR - Tomographic Microscopy

Towards nanotomography...



$$\Phi \propto \frac{SNR^2}{\Delta x^4 \cdot \Delta \mu^2}$$



1-5 μm

SR - Tomographic Microscopy

0.5-1 μm

SR - Tomographic Microscopy

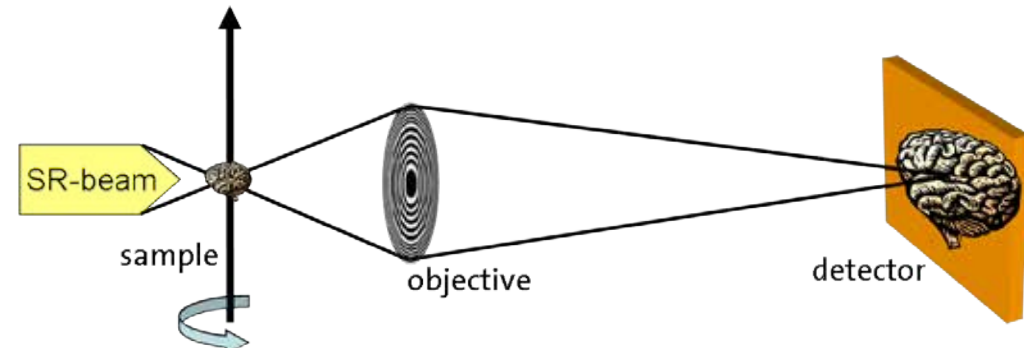
0.01-0.1 μm

SR-Nanoimaging

Classical geometries for nano-imaging

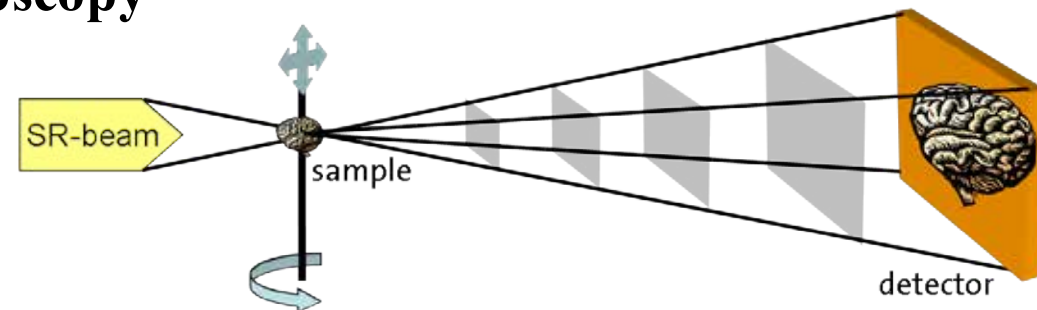
TXM: Transmission (full field) microscopy

- Absorption Radiography / Tomography
- Phase contrast Radiography / Tomography
- High resolution
- Dose “inefficient”



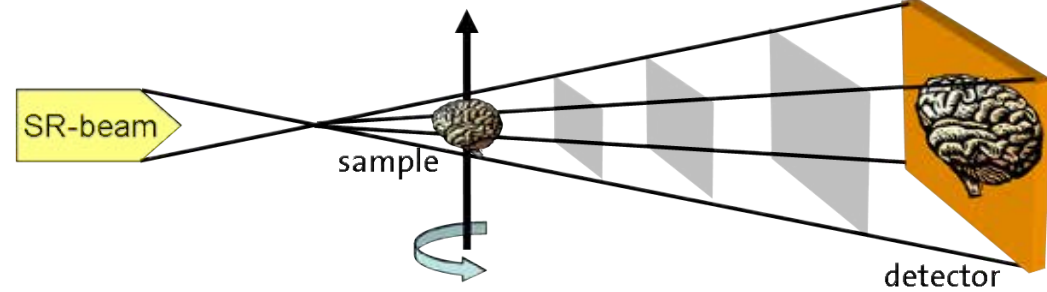
SXM: Scanning transmission microscopy

- Slow
- Dose “inefficient”
- Chemical sensitivity / Phase contrast

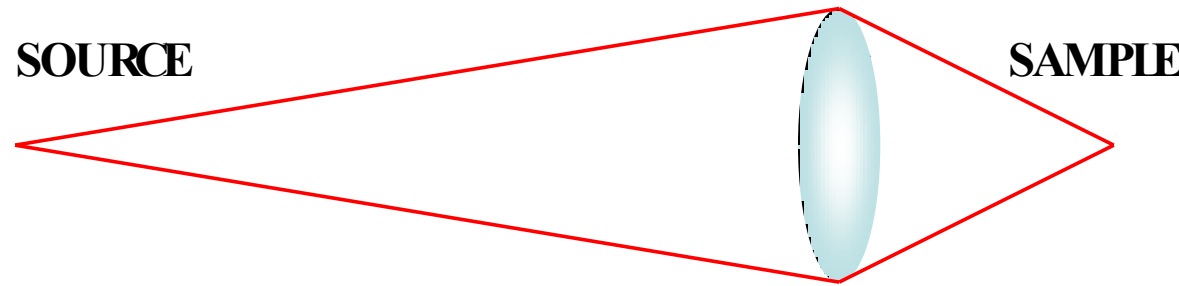


PXM: Projection microscopy

- Phase contrast Radiography / Tomography
- Fast
- High resolution
- Dose efficient



X-ray optics



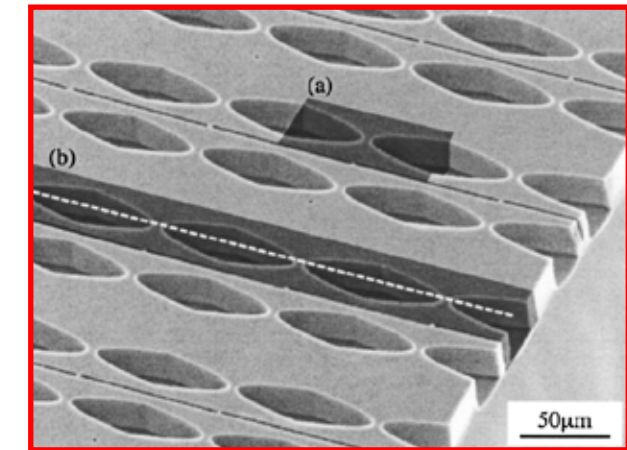
Diffractive lenses

Fresnel Zone plates
Crystals
Multilayers



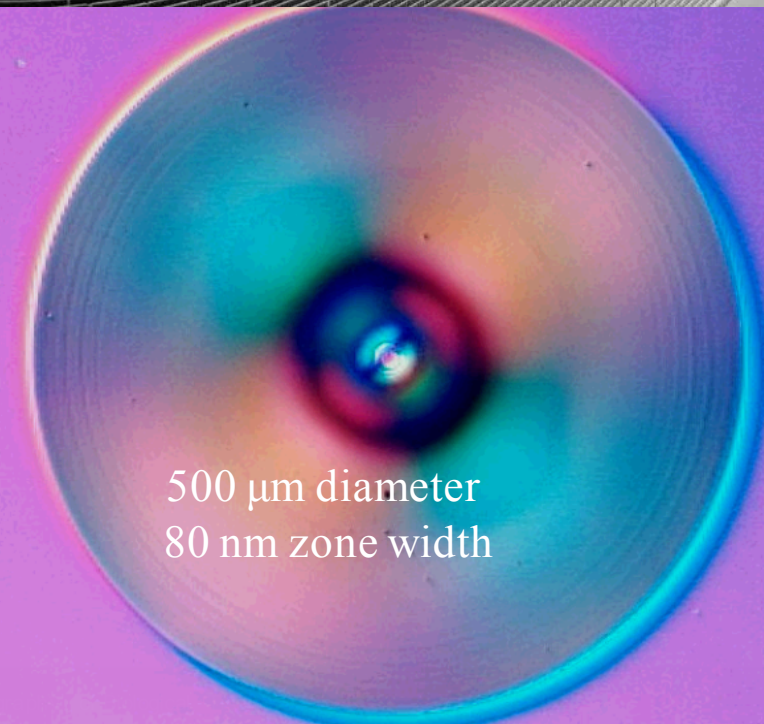
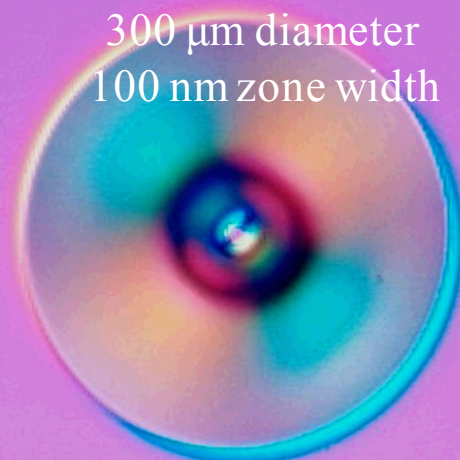
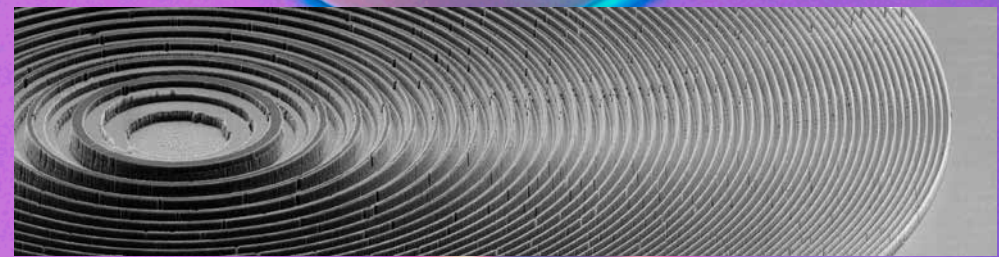
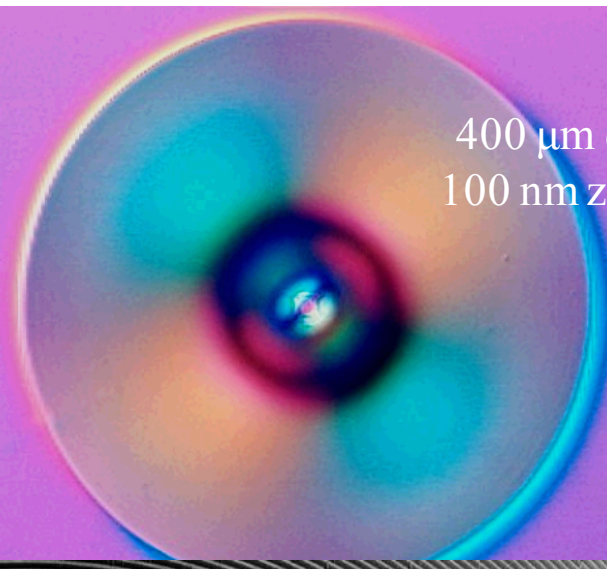
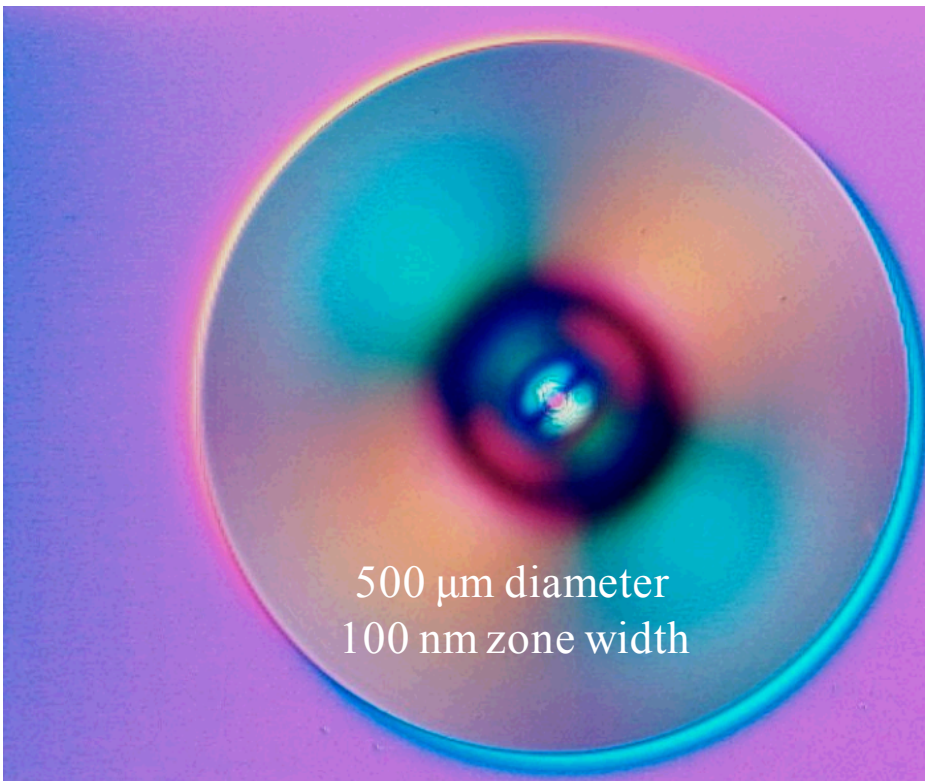
Mirrors

KB-systems
Wolter mirrors
Capillary optics
Microchannels



Refractive lenses

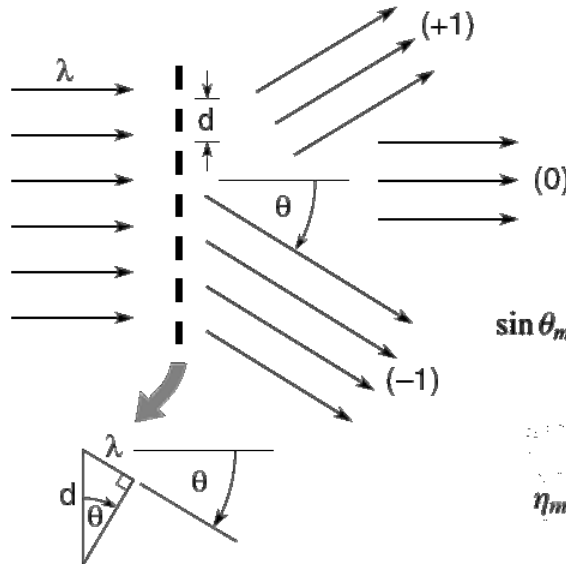
Compound refractive lenses



Fresnel zone plates

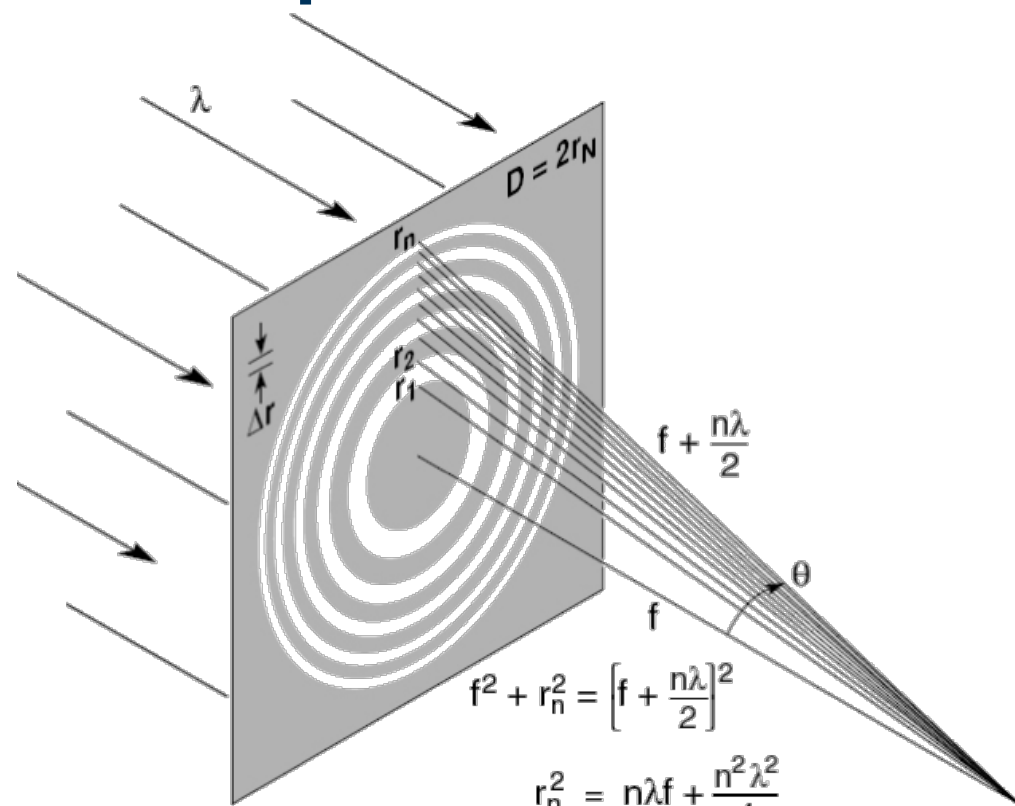


Diffraction from a transmission grating:



$$\sin \theta_m = \frac{m\lambda}{d}; \quad m = 0, \pm 1, \pm 2, \pm 3, \dots$$

$$\eta_m = \begin{cases} \frac{1}{4} & m = 0 \\ 1/m^2\pi^2 & m \text{ odd} \\ 0 & m \text{ even} \end{cases}$$

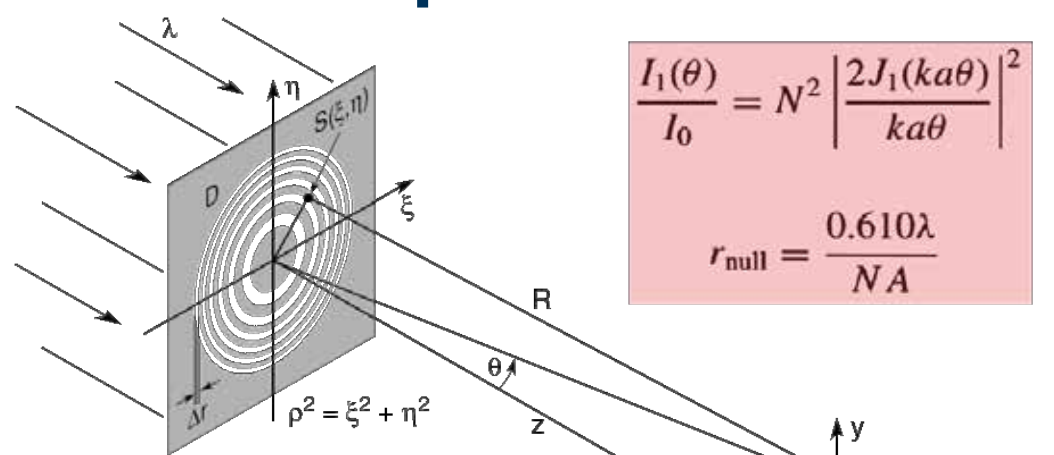


$$f^2 + r_n^2 = \left(f + \frac{n\lambda}{2} \right)^2$$

$$r_n^2 = n\lambda f + \frac{n^2\lambda^2}{4}$$

$$r_n \simeq \sqrt{n\lambda f}$$

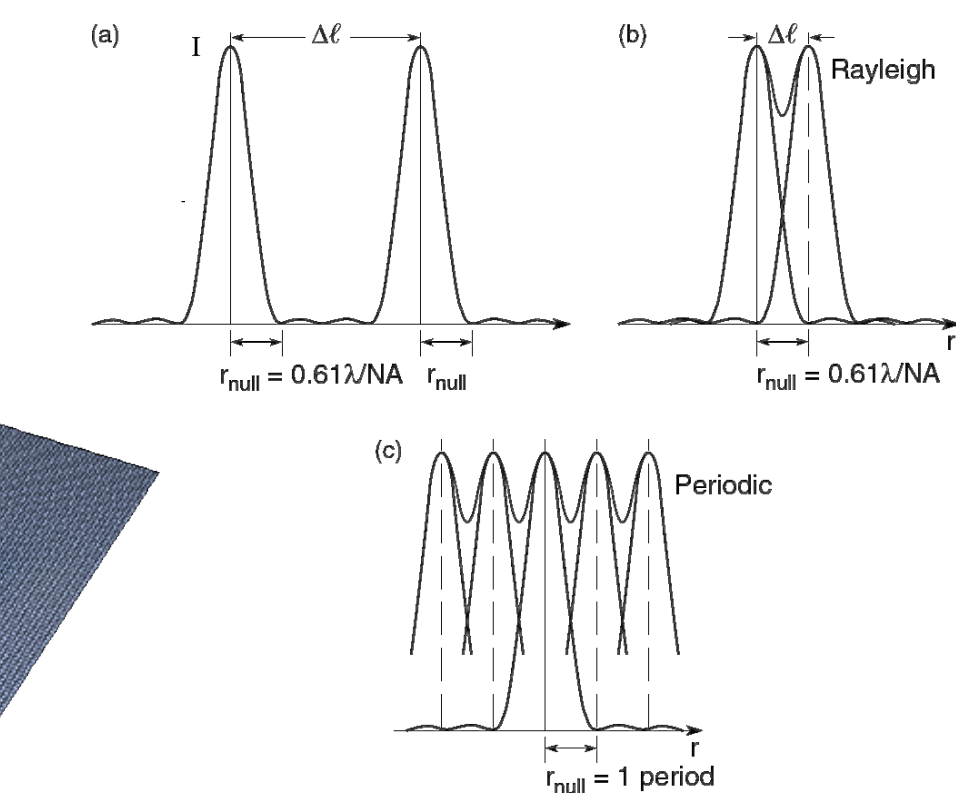
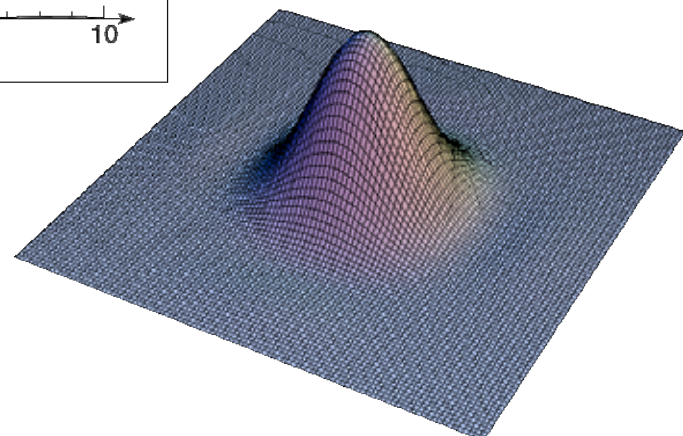
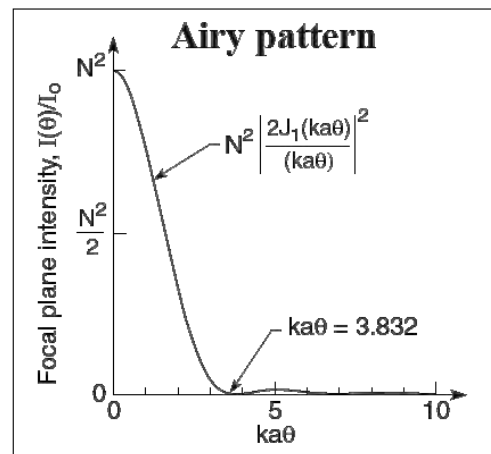
Spatial resolution of a zone plate



$$\frac{I_1(\theta)}{I_0} = N^2 \left| \frac{2J_1(ka\theta)}{ka\theta} \right|^2$$

$$r_{\text{null}} = \frac{0.610\lambda}{NA}$$

$$\Delta r_{Rayl.} = 1.22 \Delta r$$



Spatial resolution of a zone plate

nature

Vol 435 | 30 June 2005 | doi:10.1038/nature03719

LETTERS

Soft X-ray microscopy at a spatial resolution better than 15 nm

Weilun Chao^{1,2}, Bruce D. Harteneck¹, J. Alexander Liddle¹, Erik H. Anderson¹ & David T. Attwood^{1,2}

Analytical tools that have spatial resolution at the nanometre scale are indispensable for the life and physical sciences. It is desirable that these tools also permit elemental and chemical identification on a scale of 10 nm or less, with large penetration depths. A variety of techniques^{1–7} in X-ray imaging are currently being developed that may provide these combined capabilities. Here we report the achievement of sub-15-nm spatial resolution with a soft X-ray microscope—and a clear path to below 10 nm—using an overlay technique for zone plate fabrication. The microscope covers a spectral range from a photon energy of 250 eV (~3 nm wavelength) to 1.8 keV (~0.7 nm), so that primary K and L atomic resonances of elements such as C, N, O, Al, Ti, Fe, Co and Ni can be probed. This X-ray microscopy technique is therefore suitable for a wide range of studies: biological imaging in the water window^{8,9}; studies of wet environmental samples^{10,11}; studies of magnetic nanostructures with both elemental and spin-orbit sensitivity^{12–14}; studies that require viewing through thin windows, coatings or substrates (such as buried electronic devices in a silicon chip¹⁵); and three-dimensional imaging of cryogenically fixed biological cells¹⁶.

The microscope XM-1 at the Advanced Light Source (ALS) in Berkeley¹⁷ is schematically shown in Fig. 1. The microscope type is similar to that pioneered by the Göttingen/BESSY group (ref. 18, and references therein). A 'micro' zone plate (MZP) projects a full-field image to an X-ray-sensitive CCD (charge-coupled device), typically in one or a few seconds, often with several hundred images per day. The field of view is typically 10 µm, corresponding to a magnification of 2,500. The condenser zone plate (CZP), with a central stop, serves two purposes in that it provides partially coherent hollow-cone illumination¹, and, in combination with a pinhole, serves as the

monochromator. Monochromatic radiation of $\lambda/\Delta\lambda = 500$ is used. Both zone plates are fabricated in-house, using electron beam lithography¹⁸.

The spatial resolution of a zone plate based microscope is equal to $k_1 \lambda / N_{A_{MZP}}$, where λ is the wavelength, $N_{A_{MZP}}$ is the numerical aperture of the MZP, and k_1 is an illumination dependent constant, which ranges from 0.3 to 0.61. For a zone plate lens used at high magnification, $N_{A_{MZP}} = \lambda / 2\Delta r_{MZP}$, where Δr_{MZP} is the outermost (smallest) zone width of the MZP¹⁹. For the partially coherent illumination^{20–22} used here, $k_1 \approx 0.4$ and thus the theoretical resolution is $0.8\Delta r_{MZP}$, as calculated using the SPLAT computer program²³ (a two-dimensional scalar diffraction code, which evaluates partially coherent imaging). In previous results with a $\Delta r_{MZP} = 25$ nm zone plate, we reported² an unambiguous spatial resolution of 20 nm. Here we describe the use of an overlay nanofabrication technique that allows us to fabricate zone plates with finer outer zone widths, to $\Delta r_{MZP} = 15$ nm, and to achieve a spatial resolution of below 15 nm, with clear potential for further extension.

This technique overcomes nanofabrication limits due to electron beam broadening in high feature density patterning. Beam broadening results from electron scattering within the recording medium (resist), leading to a loss of image contrast and thus resolvability for dense features. This effect is reduced by writing only semi-isolated features. Here the dense zone plate pattern is subdivided into two less dense, complementary patterns, which are fabricated separately and then overlaid with high accuracy to yield the desired pattern. The overlay technique allows us to achieve pattern densities several times higher than would otherwise be possible. The required placement accuracy for zone plates is typically one-third the smallest feature size—thus about 5 nm for the optic reported here with a 15 nm outer zone width. As described below, the zone placement accuracy achieved here is better than 2 nm across the two-dimensional field, leaving significant room for further zone plate advances. Note that this high placement accuracy overlay technique permits the achievement of smaller zones without incurring the low diffraction

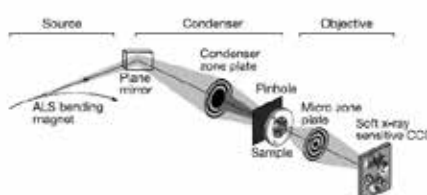


Figure 1 | A diagram of the soft X-ray microscope XM-1. The microscope uses a micro zone plate to project a full field image onto a CCD camera that is sensitive to soft X-rays. Partially coherent, hollow-cone illumination of the sample is provided by a condenser zone plate. A central stop and a pinhole provide monochromatization.



Figure 2 | An illustration of the overlay nanofabrication technique for micro zone plate fabrication. The zone plate is composed of even-numbered opaque zones (black and grey) and odd-numbered transparent zones (white). Set I (black), containing zones 2, 6, 10, ..., and its complement, set II (grey), are fabricated sequentially to form the desired overlaid micro zone plate.



Figure 3 | Scanning electron micrograph of a zone plate with 15 nm outermost zone. Shown in the inset is a more detailed view of the outermost zones. The zonal period, as indicated by the two black lines, is measured to be 30 nm. **The zone placement accuracy is measured to be 1.7 nm.**

W. Chao et al., Nature, Vol 435, June 2005

It worked only once...

Spatial resolution of a zone plate

PRL 99, 264801 (2007)

PHYSICAL REVIEW LETTERS

week ending
31 DECEMBER 2007

Zone-Doubling Technique to Produce Ultrahigh-Resolution X-Ray Optics

K. Jefimovs,^{1,2} J. Vila-Comamala,³ T. Pilvi,⁴ J. Raabe,¹ M. Ritala,⁴ and C. David¹¹*Paul Scherrer Institut, CH-5232 Villigen PSI, Switzerland*²*EMPA, CH-8600 Dübendorf, Switzerland*³*Laboratori de Llum Sincrotró, E-08193 Bellaterra, Spain*⁴*Laboratory of Inorganic Chemistry, University of Helsinki, FI-00014 Helsinki, Finland*
(Received 18 September 2007; published 28 December 2007)

A method for the fabrication of ultrahigh-resolution Fresnel zone plate lenses for x-ray microscopy is demonstrated. It is based on the deposition of a zone plate material (Ir) onto the sidewalls of a prepatterned template structure (Si) using an atomic layer deposition technique. This results in a doubling of the effective zone density, thus improving the achievable resolution of x-ray microscopes. Test structures with lines and spaces down to 15 nm were resolved in a scanning transmission x-ray microscope at 1 keV photon energy.

DOI: 10.1103/PhysRevLett.99.264801

PACS numbers: 41.50.+h, 07.85.Qe, 07.85.Tt

X-ray microscopy is an outstanding technique for the investigation of both inorganic and biological samples, as it possesses high spatial resolution, good penetration capability, combined with specific contrast mechanisms that can provide information on the elemental and even chemical composition of a specimen. Disciplines such as biology, materials science, chemistry, and environmental science are benefiting from the progress achieved in x-ray microscopes in recent years. The theoretically attainable resolution limit is much better than that of visible light microscopes, due to the 100–1000 times shorter wavelength. However, this limit has not been reached yet due to the limitations in the fabrication of the diffractive Fresnel zone plate (FZP) lenses used for imaging. In the hard x-ray regime sub-50 nm resolution has been reached [1,2]. In the soft x-ray regime, the daily working resolution is around 30 nm, while the smallest lines resolved are 15 nm wide [3].

There is an intimate relationship between the spatial resolution of a FZP-based microscope and the outermost zone width of the FZP, the two of them being essentially comparable. Electron-beam lithography tools, which are typically used to generate FZPs, are capable of writing with nanometer spot sizes and position accuracies. However, the obtainable structure sizes are determined by the range of secondary electrons created in the resist layer, which has a particularly detrimental consequence when writing dense patterns of lines such as gratings or FZPs. An approach has recently been reported which overcomes this nanofabrication limit by use of an overlay technique [3]. It is based on two separate exposure steps of complementary patterns to reduce the line density in each individual step. A FZP with 15 nm outermost zone width was demonstrated with this technique. Extremely small alignment tolerances of only a few nanometers are required between the two exposures, making the technique inherently complicated and resulting in a low fabrication yield.

Here we report on a powerful and, at the same time, much simpler nanofabrication method that overcomes the difficulty of high feature density patterning without any need for alignment. The method is very reproducible, as it only requires a single lithography step, and allows the fabrication of structures with extremely high aspect ratios, which increases the efficiency of ultrahigh-resolution optics. It is based on a deposition of a thin layer of a high refractive index material onto the sidewalls of a template structure made of a low-index material. This leads to a doubling of the effective line density of the deposited

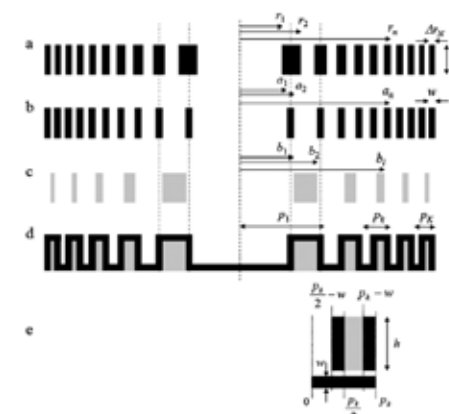


FIG. 1. (a) Schematic drawing of a Fresnel zone plate, (b) Fresnel zone plate with a constant width of the even zones equal to w , (c) low refractive index template structure, (d) low refractive index template structure coated by high refractive index zone plate material, and (e) fragment of the zone plate used for calculation of the local diffraction efficiency.

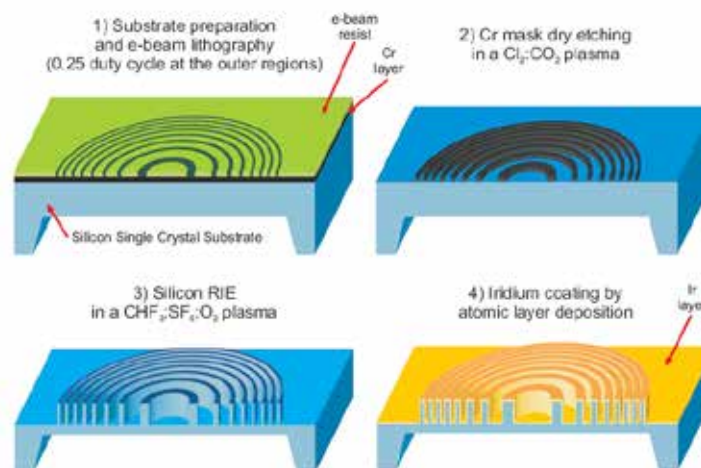


Figure 1. Zone-doubled FZP manufacturing steps: 1) electron-beam lithography, 2) pattern transfer to chromium layer by reactive ion etching, 3) pattern transfer to silicon by reactive ion etching and 4) iridium coating by atomic layer deposition.

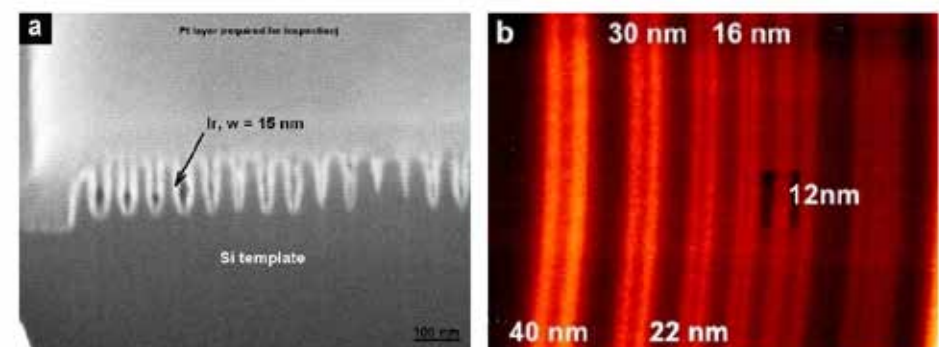
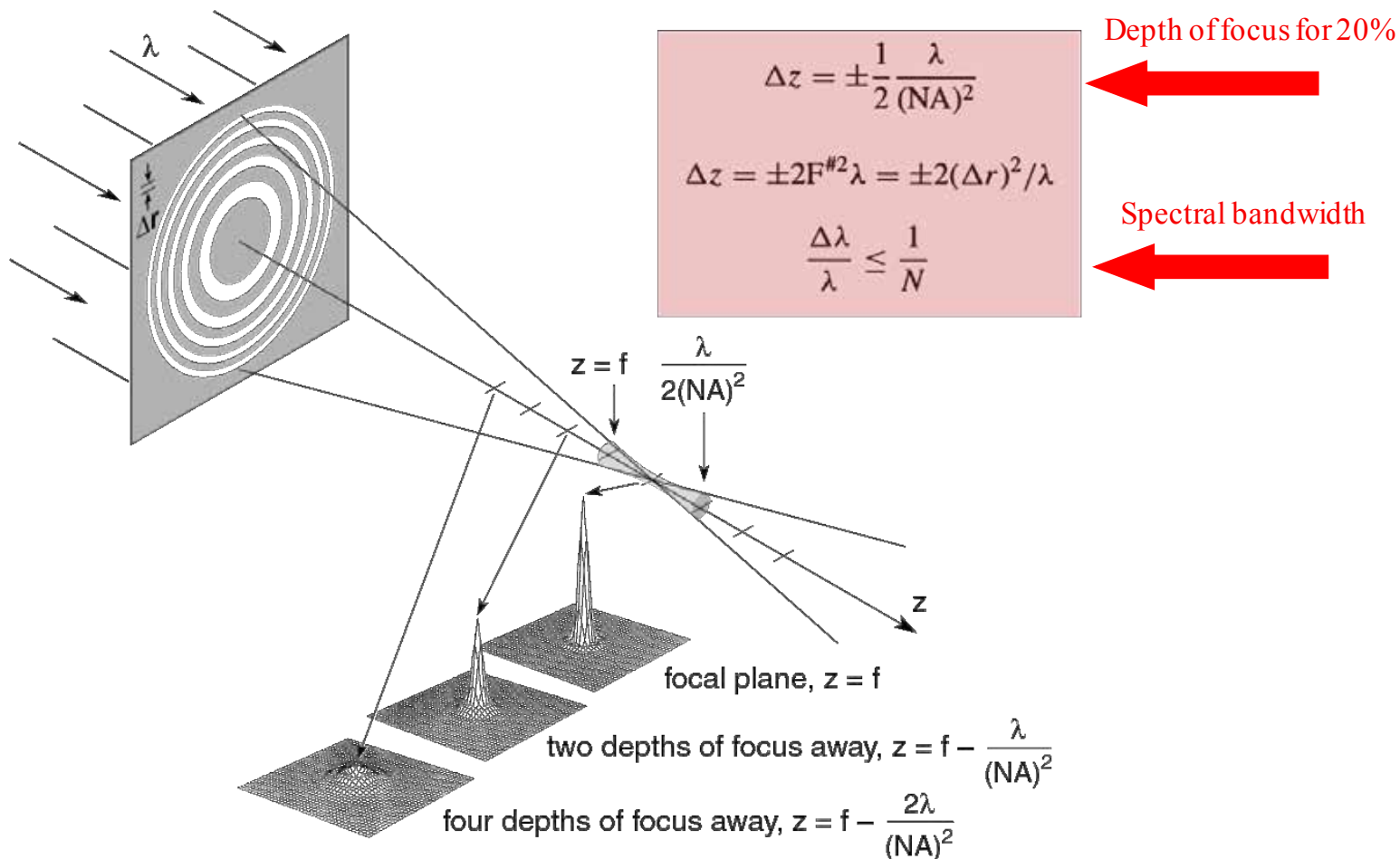


Figure 2. a) Cross section of zone-doubled FZP with an outermost zone width of 15 nm. b) STXM image of GaAs/AlGaAs heterostructure with several line widths. Smallest visible features consist of 3 lines of 12 nm width.

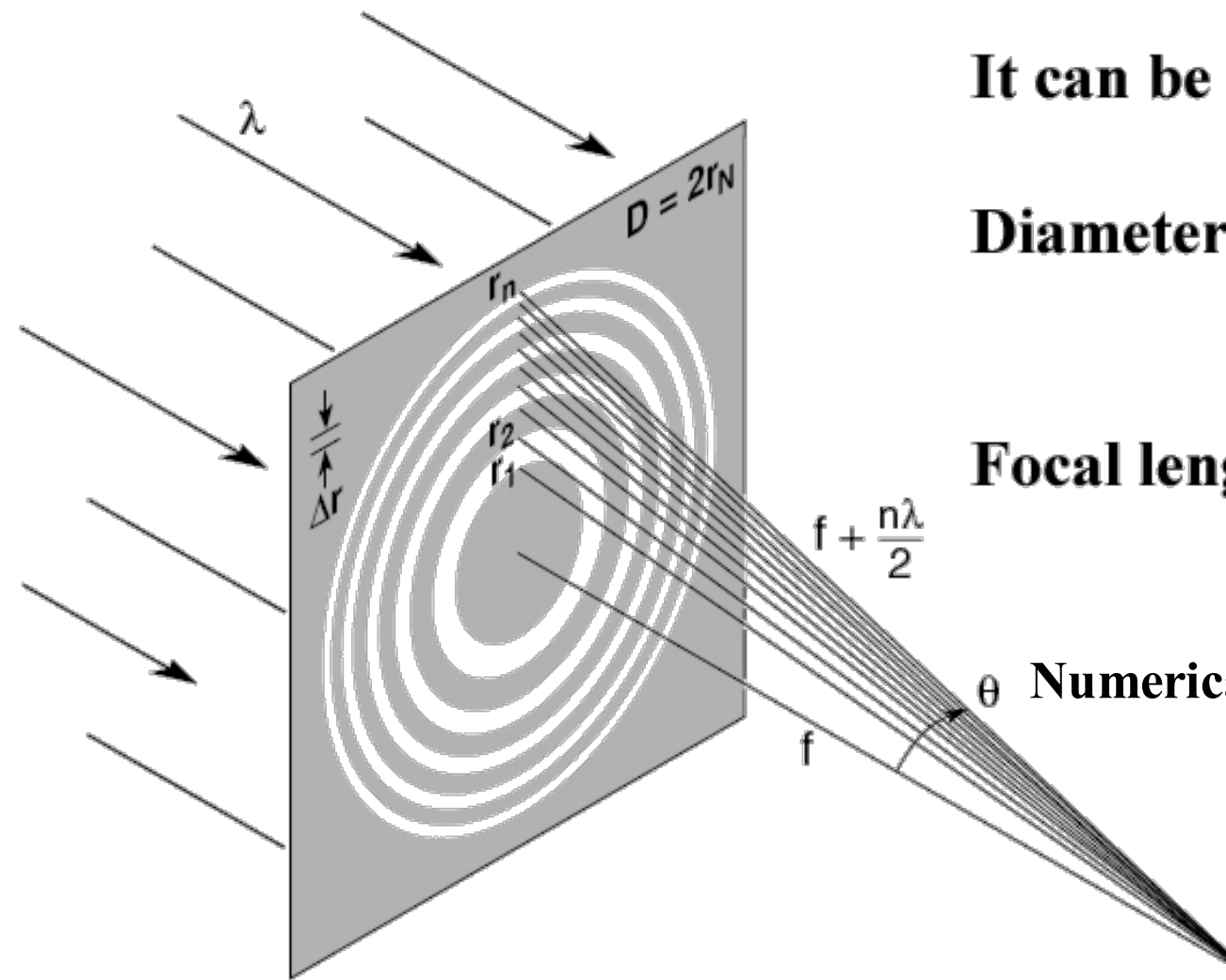
K. Jefimovs et al., PRL 99, 264801 (2007)

Depth of focus and spectral bandwidth

- The depth of focus of a lens or imaging system is the permitted displacement, away from the focal or image plane, for which the intensity on axis is diminished by some permissible small amount (20%) or image resolution is only slightly degraded.
- Focal plane intensity is also affected by the spectral bandwidth.



Fresnel zone plates: useful equations



It can be shown that:

Diameter :

$$D \simeq 4N \Delta r$$

Focal length:

$$f \simeq \frac{4N(\Delta r)^2}{\lambda}$$

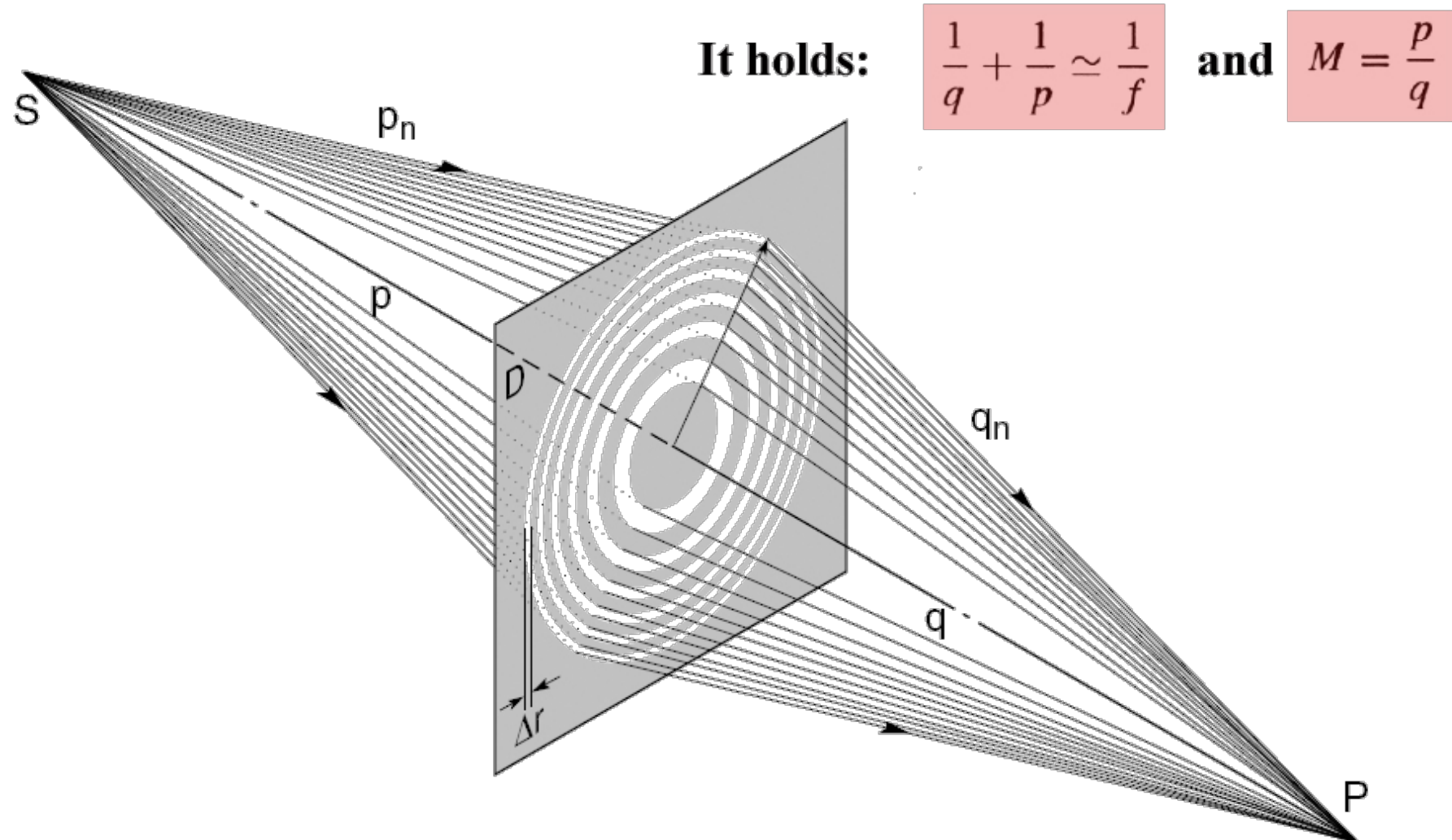
Numerical aperture:

$$NA \cong \frac{\lambda}{2\Delta r}$$

See also Exercise

Fresnel zone plates : point to point imaging

“Classical lens equation” is still valid!



See also Exercise

Summary zone plates

Resolution :

$$\delta_m = 1.22 \frac{\Delta r}{m}$$

Focal length :

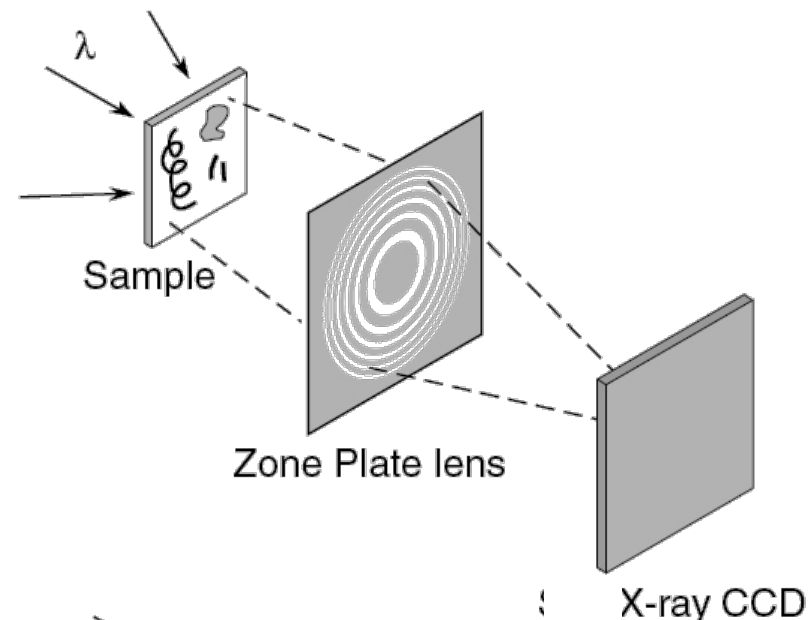
$$f_m = \frac{D\Delta r}{m\lambda}$$

Depth of focus :

$$DOF = \pm \frac{2\Delta r^2}{m\lambda}$$

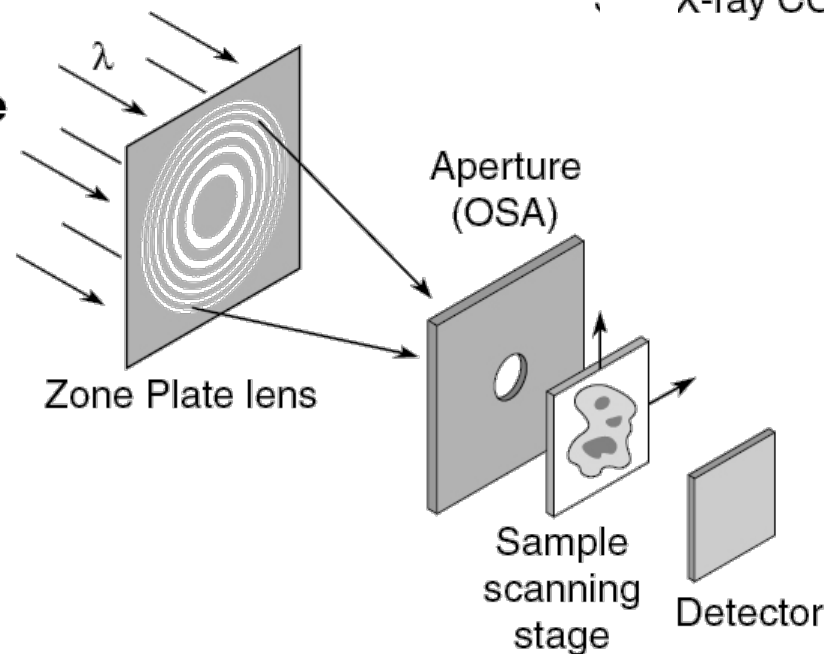
Zone plate X-ray microscopes

Full-Field Microscope



- Best spatial resolution
- Modest spectral resolution
- Shortest exposure time
- Bending magnet radiation
- Higher radiation dose
- Flexible sample environment (wet, cryo, labeled magnetic fields, electric fields, cement, ...)

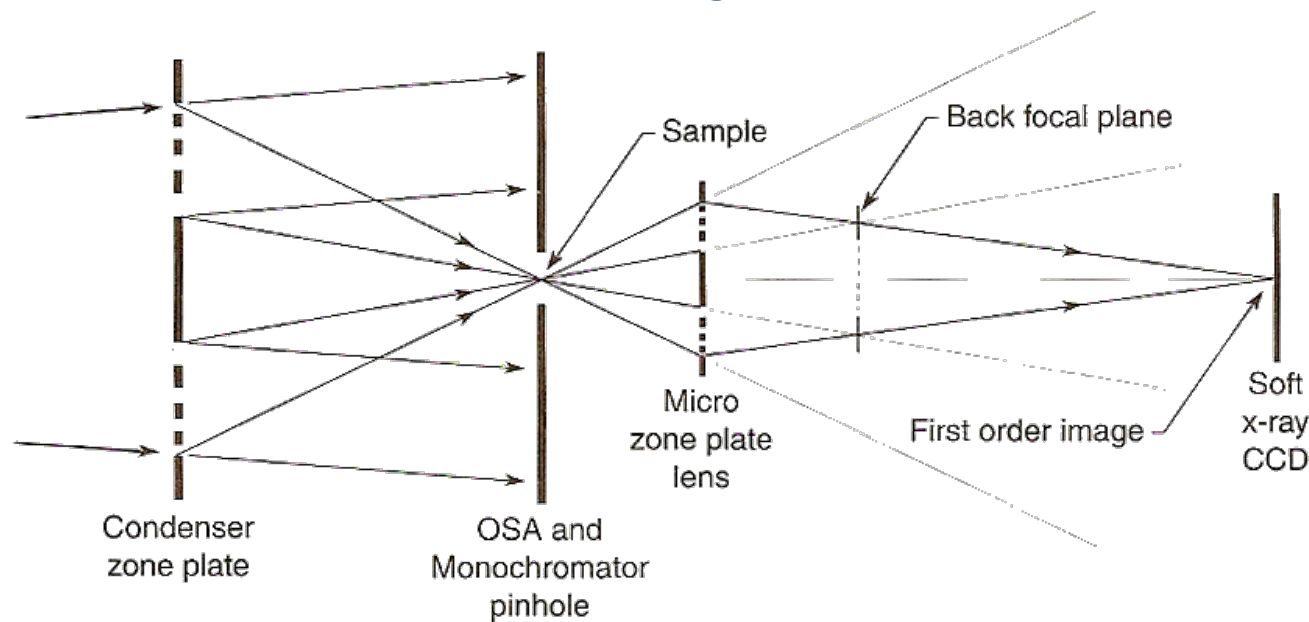
Scanning Microscope



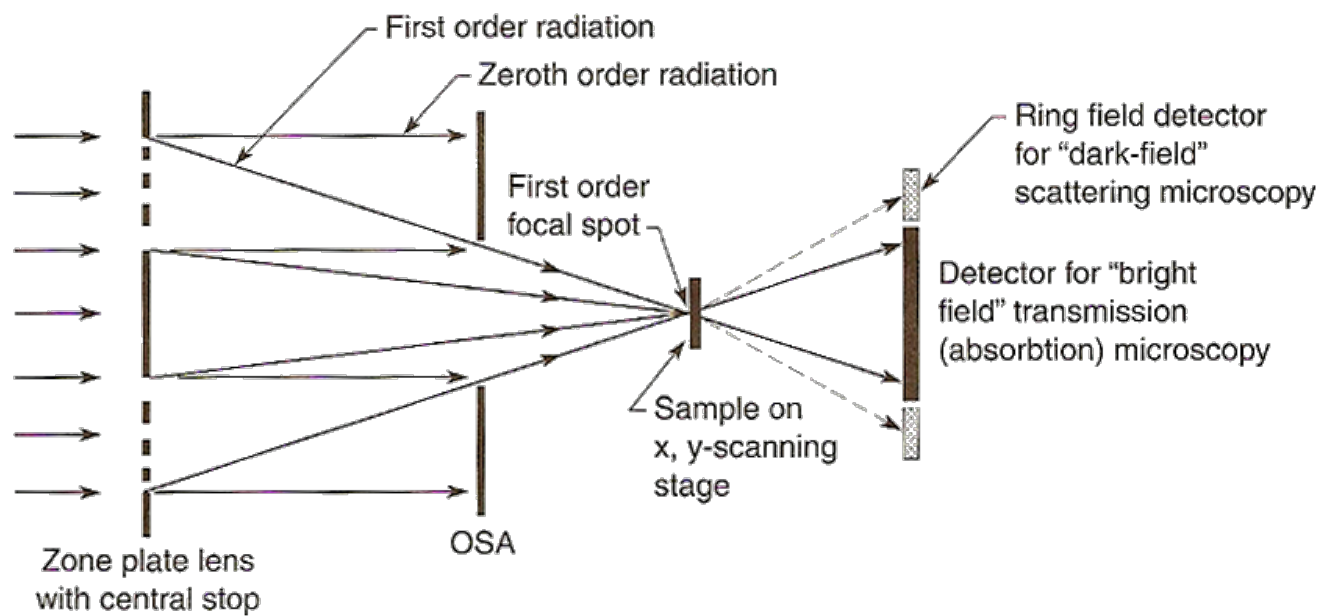
- Least radiation dose
- Next best spatial resolution
- Best spectral resolution
- Requires spatially coherent radiation
- Long exposure time
- Flexible sample environment
- Photoemission (restricted magnetic fields), fluorescence imaging

Zone-plate X-ray microscopes

TXM

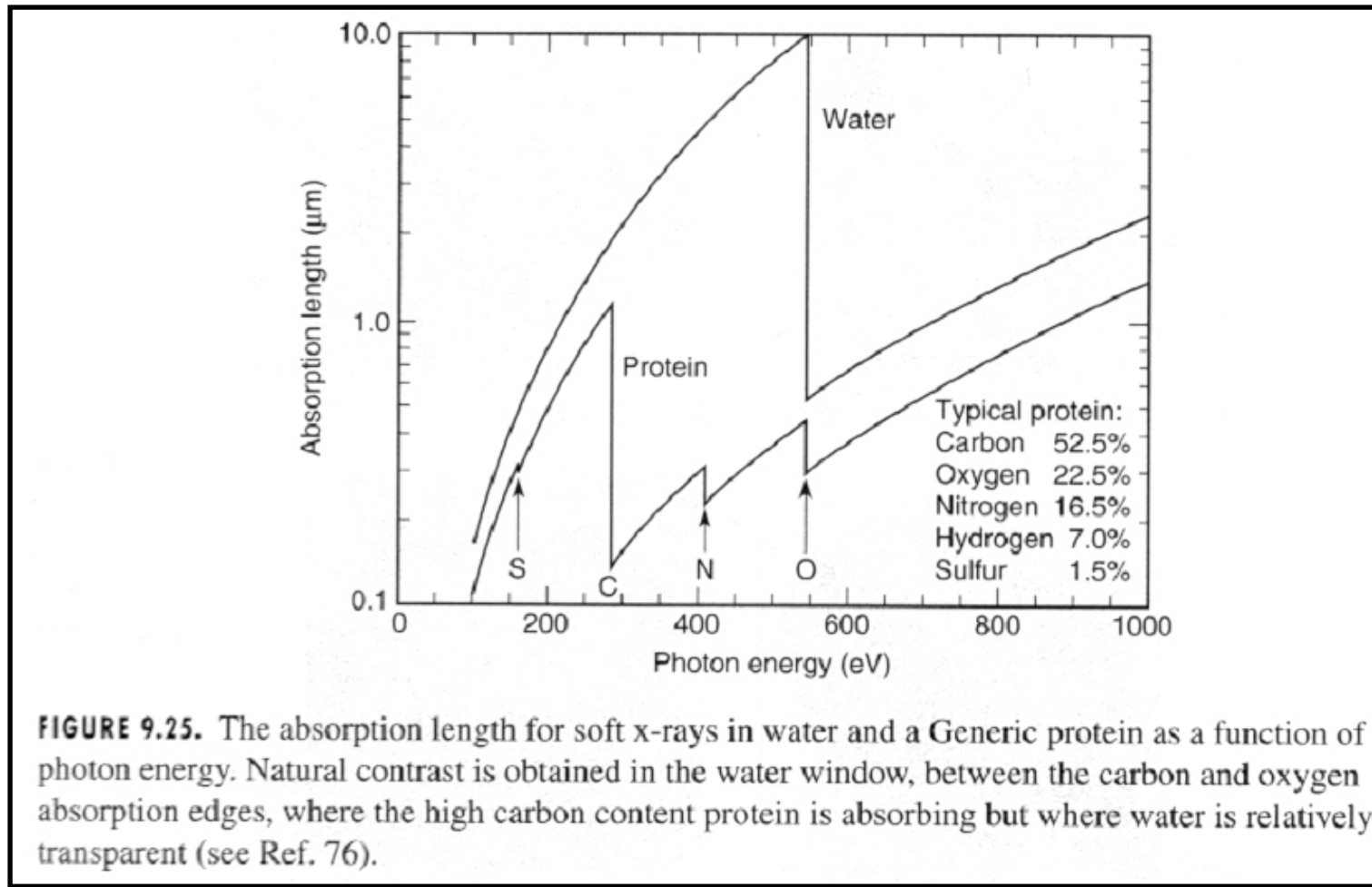


SXM



Full-field microscope in the water window

Between K shell absorption edges of oxygen (543 eV) and carbon (284 eV)



Ideal conditions for imaging proteins !

25 nm zone plate

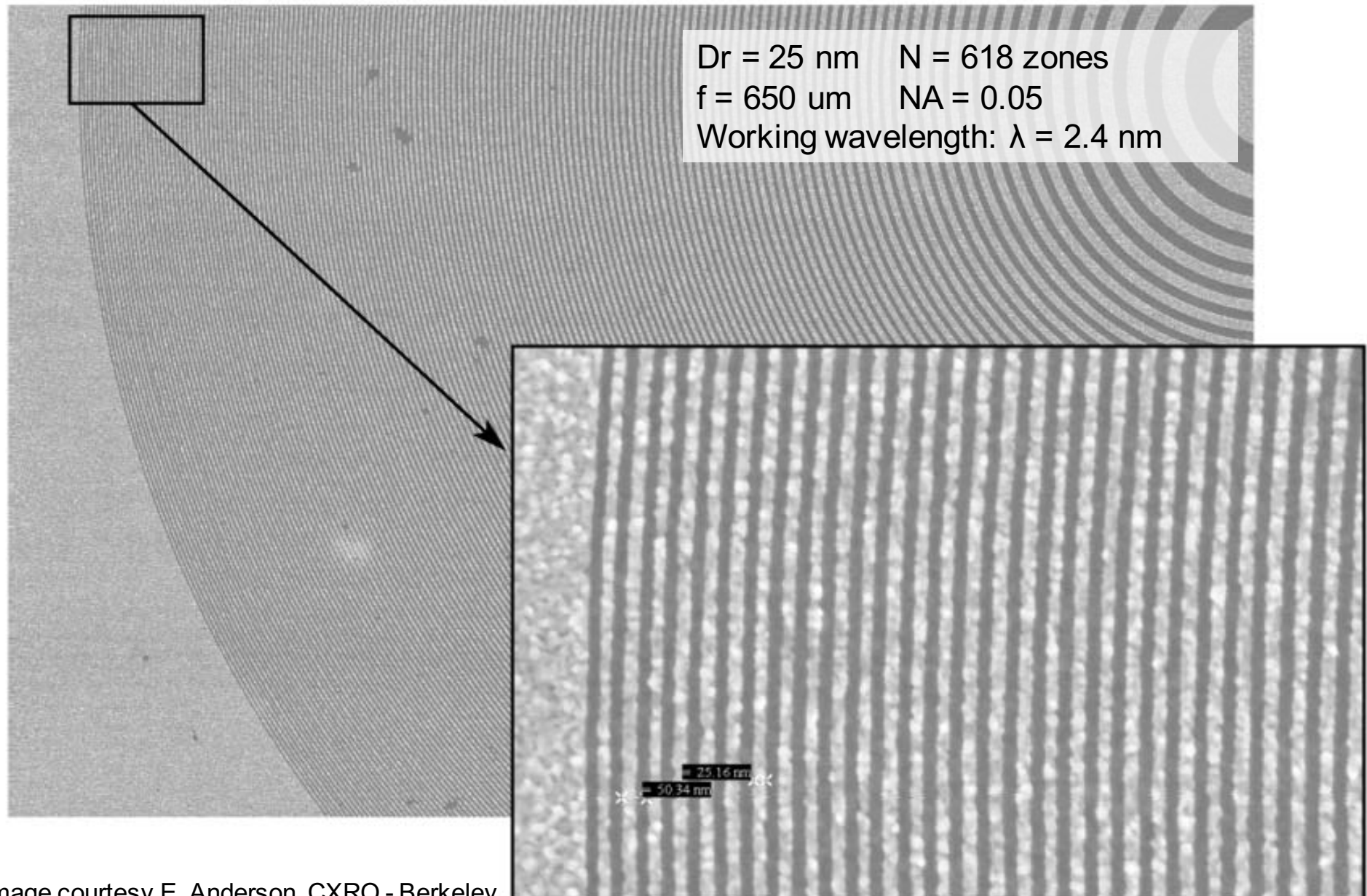
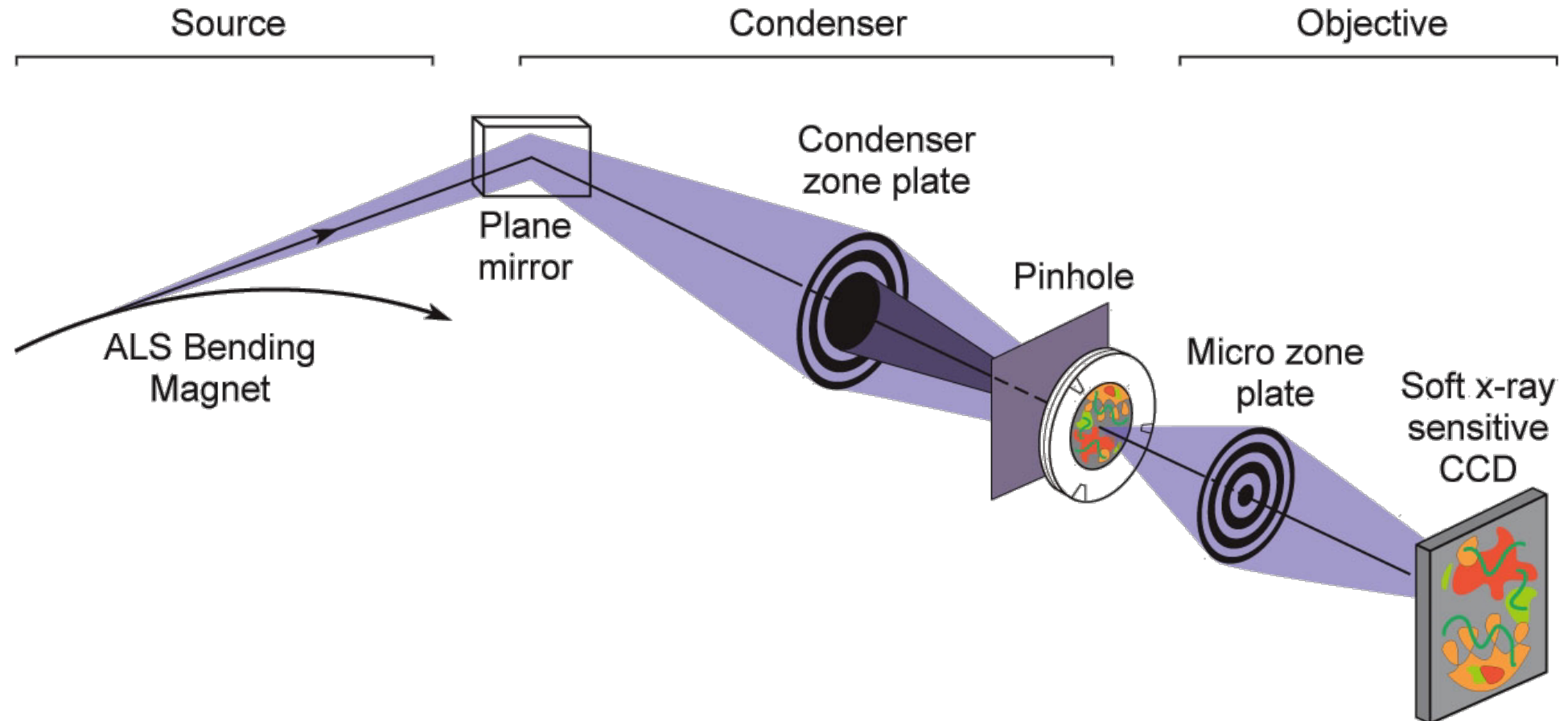
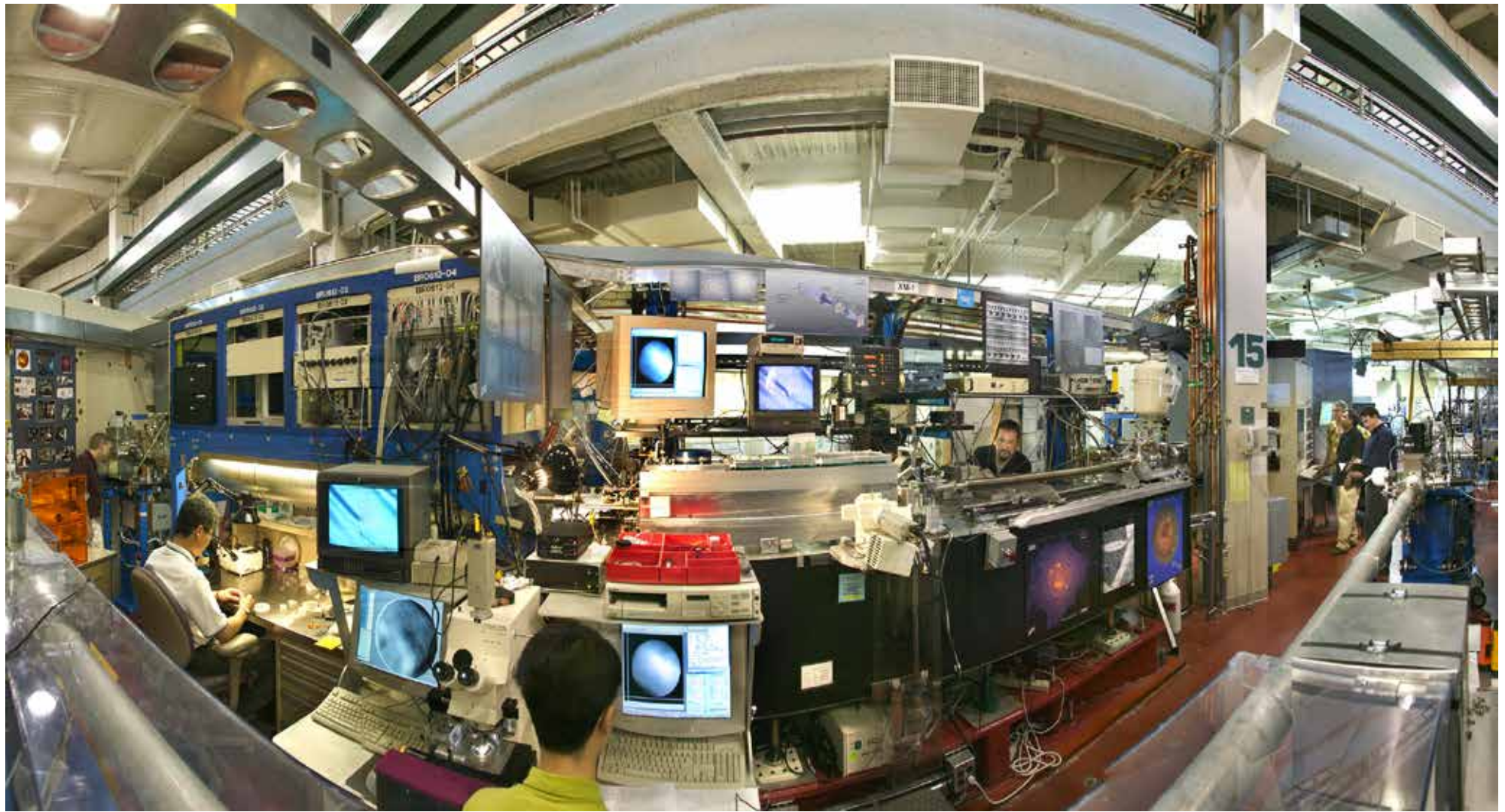


Image courtesy E. Anderson, CXRO - Berkeley

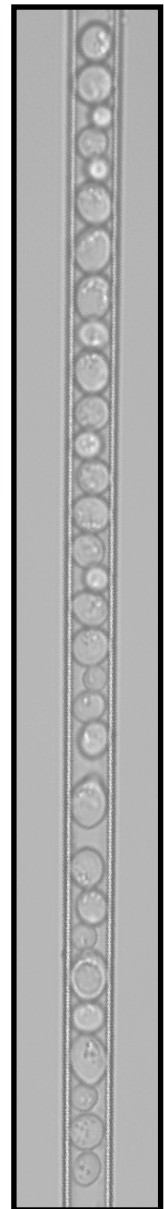
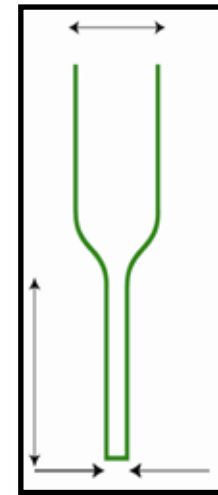
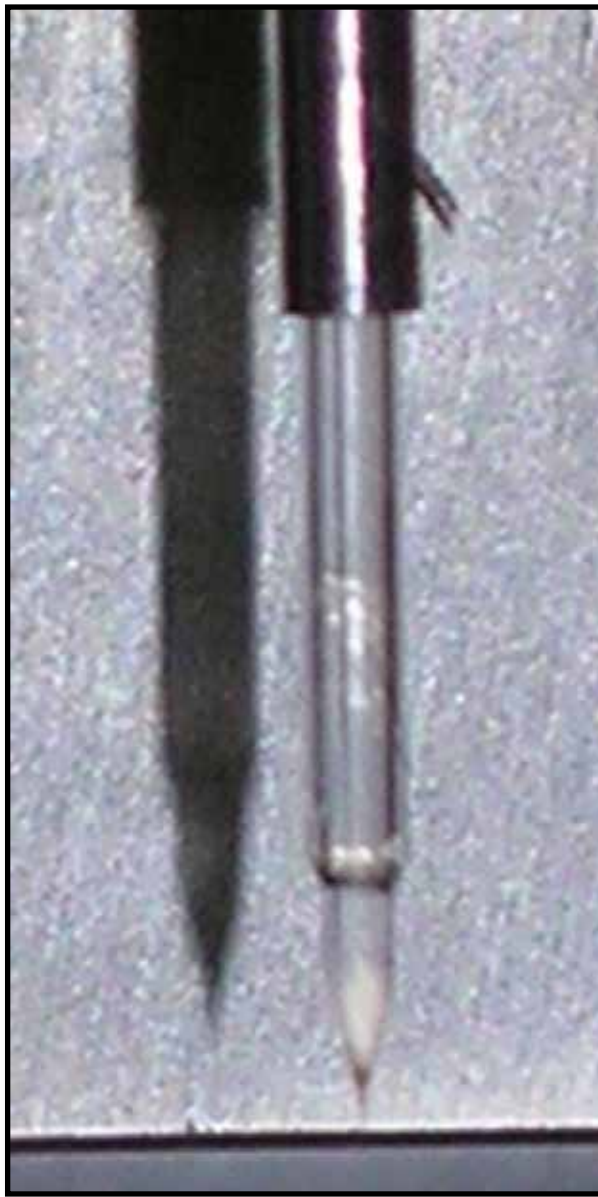
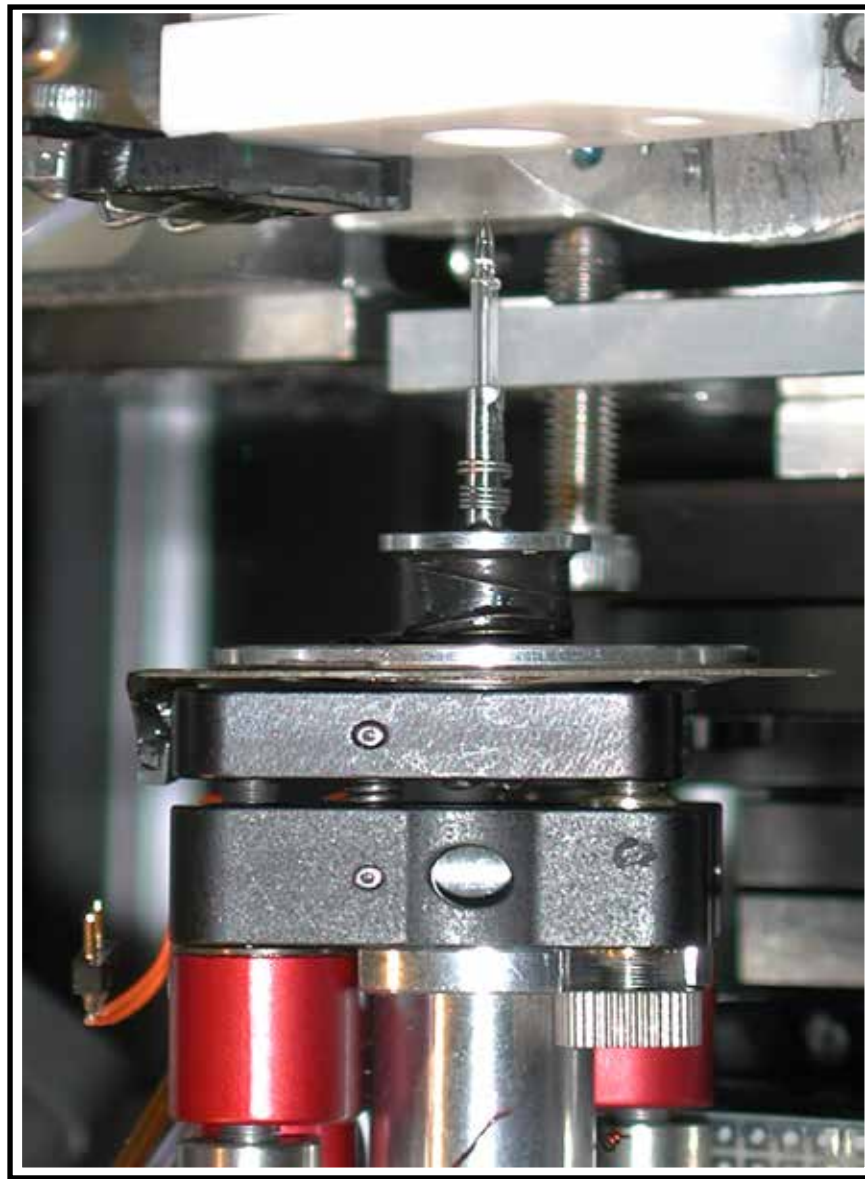
XM-1 microscope @ ALS



XM-1 microscope @ ALS

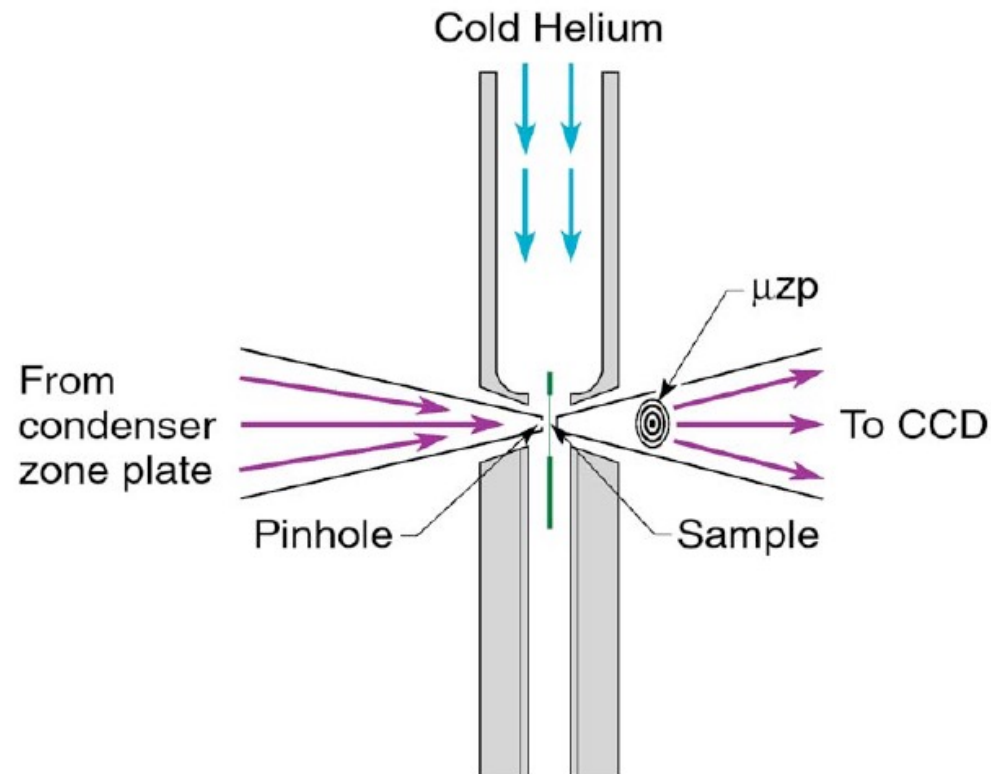


Cryo-cooled sample handler

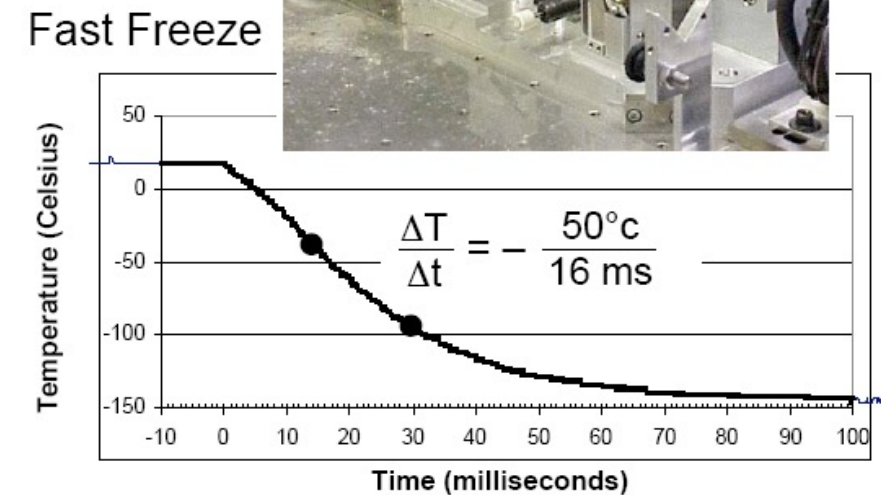
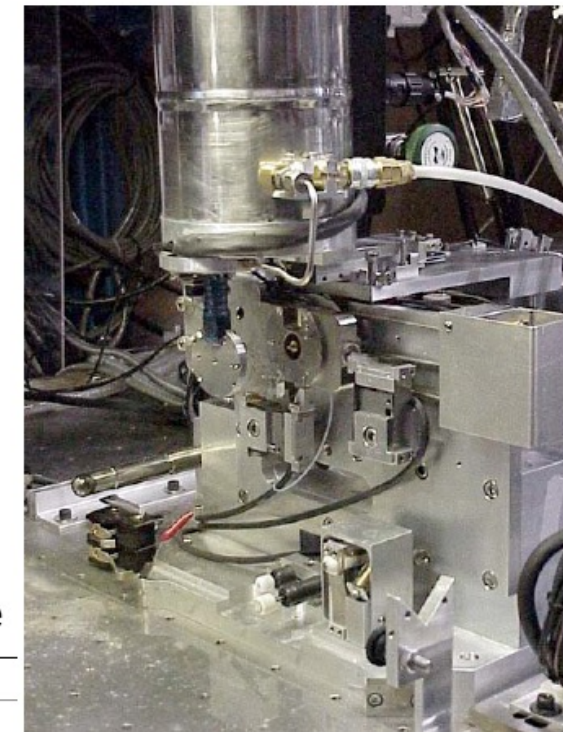


Images courtesy of C. Larabell, ALS/UCSF

Fast Freeze Cryo Fixation: Strong mitigation of radiation dose effects

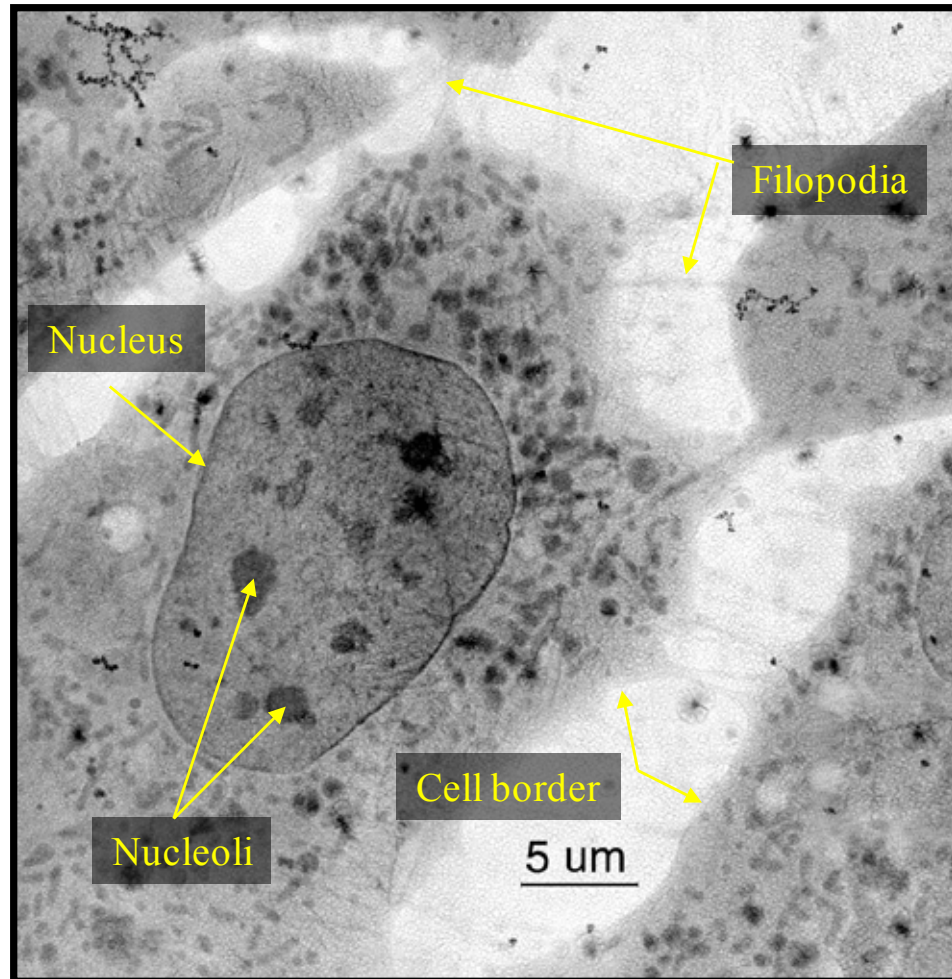


Helium passes through LN, is cooled,
and directed onto sample windows



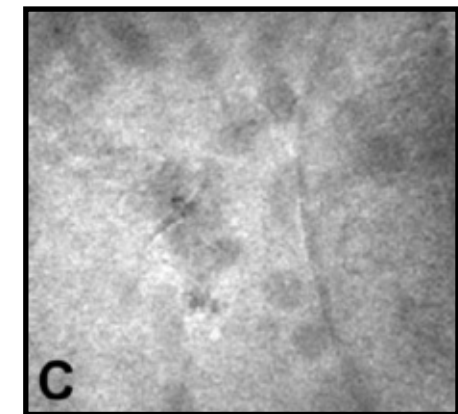
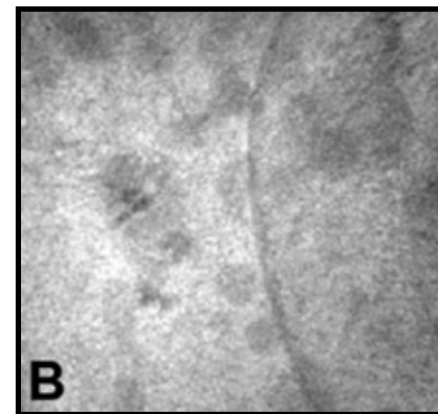
W. Meyer-Ilse, G. Denbeaux, L. Johnson, A. Pearson (CXRO-LBNL)

Cryo X-ray microscopy of 3T3 Fibroblasts



W. Meyer-Ilse et al., *Journal of Microscopy*, 2001, pp 395-403.

Whole cells - no fixatives, stains,
or contrast enhancement reagents



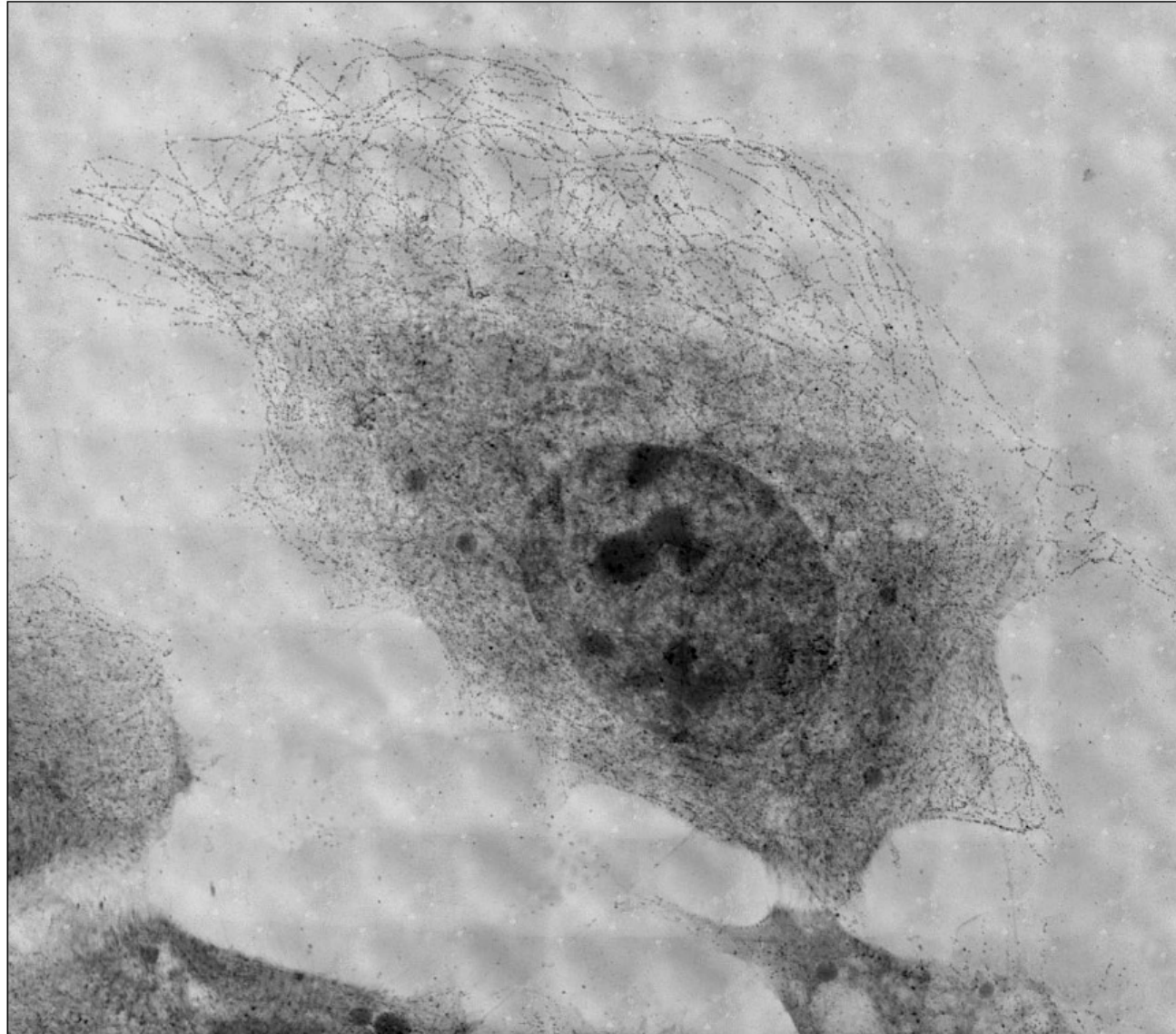
Cryo X-ray microscopy of whole, hydrated 3T3 cells.

Right: X-ray microscope image of a cell that was initially living, then rapidly frozen and examined under liquid nitrogen temperatures in the cryostage. No chemical fixatives or contrast enhancement agents were used. Images were obtained using a photon energy of 517 eV ($\lambda = 2.4$ nm), X-ray magnification of 2400, 0.034 NA, 20 nm pixel size; image size in pixels 2035 X2033.

Note that the image on the left is a composite of a series of 144 individual X-ray microscope images.

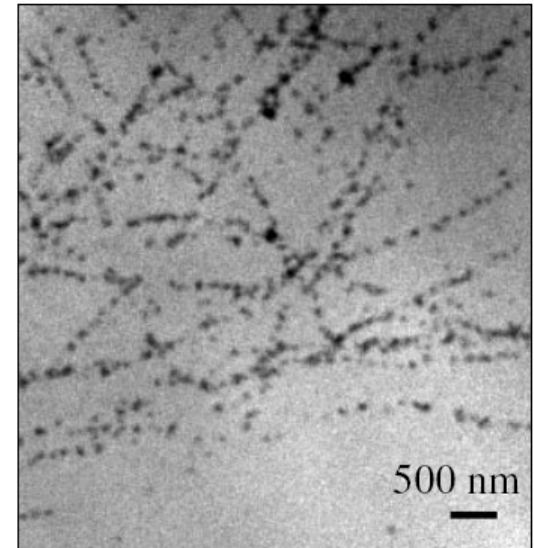
(B-C) One single image showing the first exposure of the edge of a cell nucleus (B) and the 40th exposure of that same region (C) demonstrating the stability of the cryofixed specimen.

Tubulin Network in Epithelial Cell



80113120-263

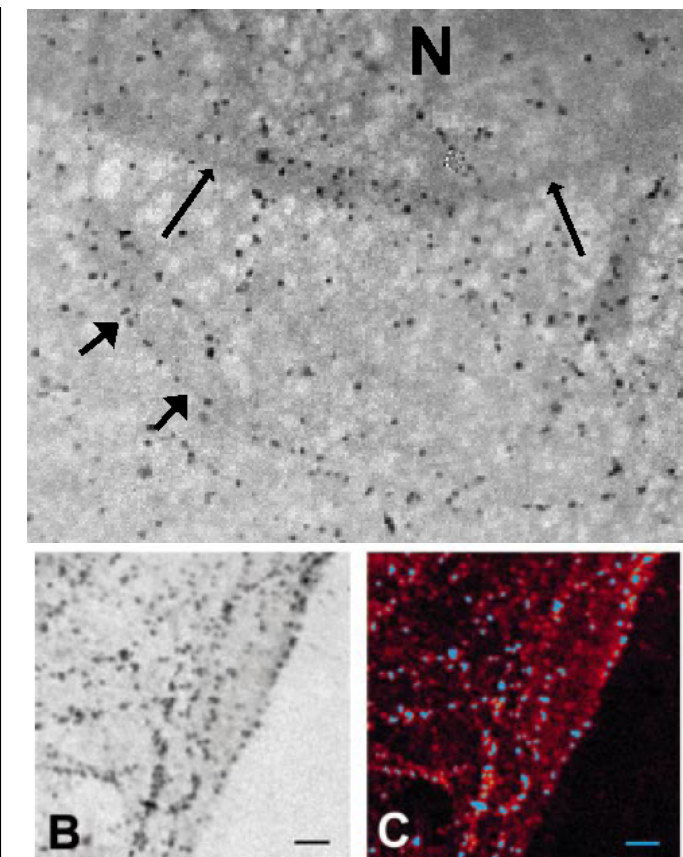
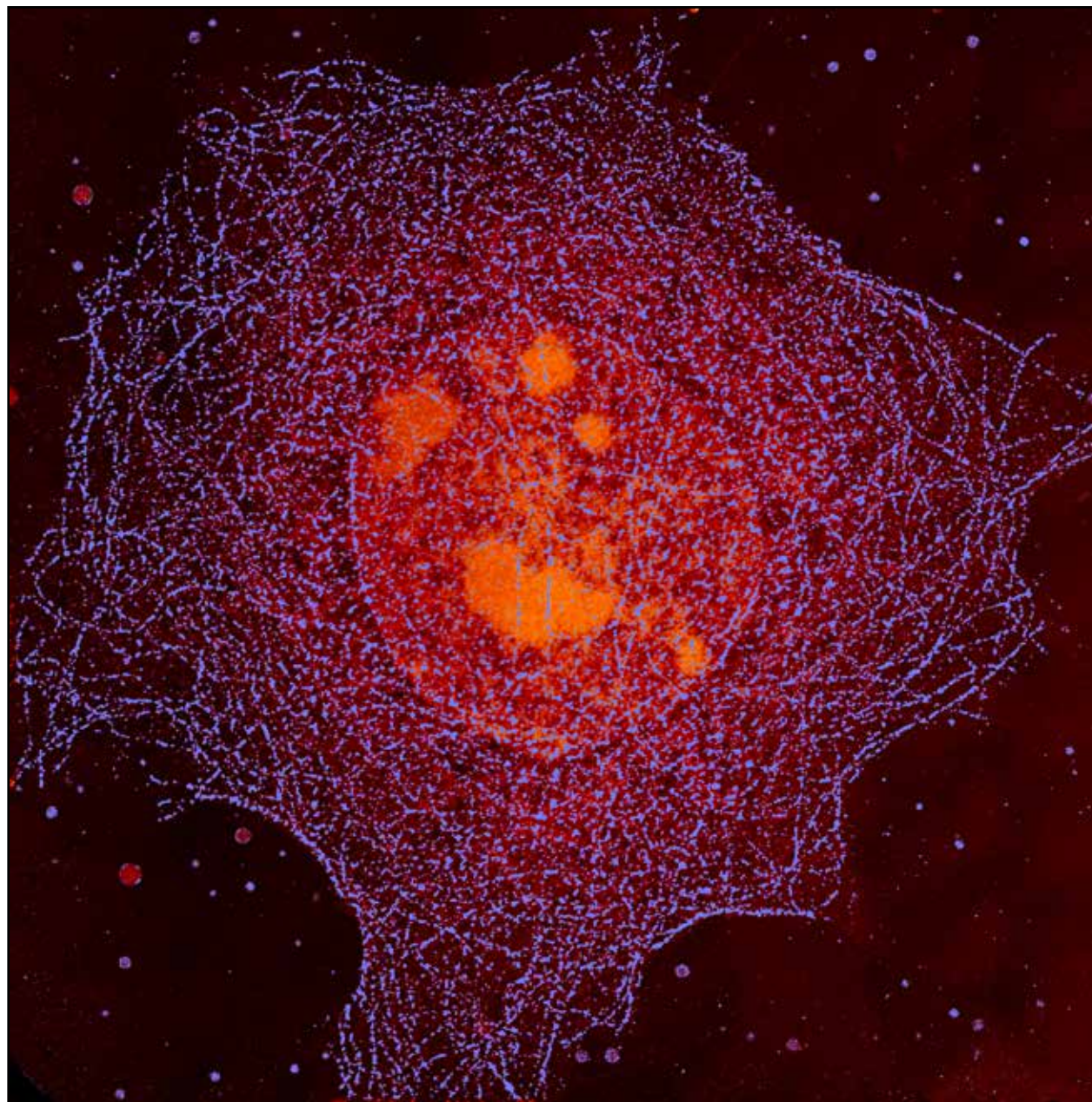
Immortalized mouse epithelial cells (EPH4), hydrated, labeled for tubulin with a FluronanoGold® antibody label, silver-enhanced.



80113182

Courtesy of A. Pearson/LBNL and C. Larabell/UCSF

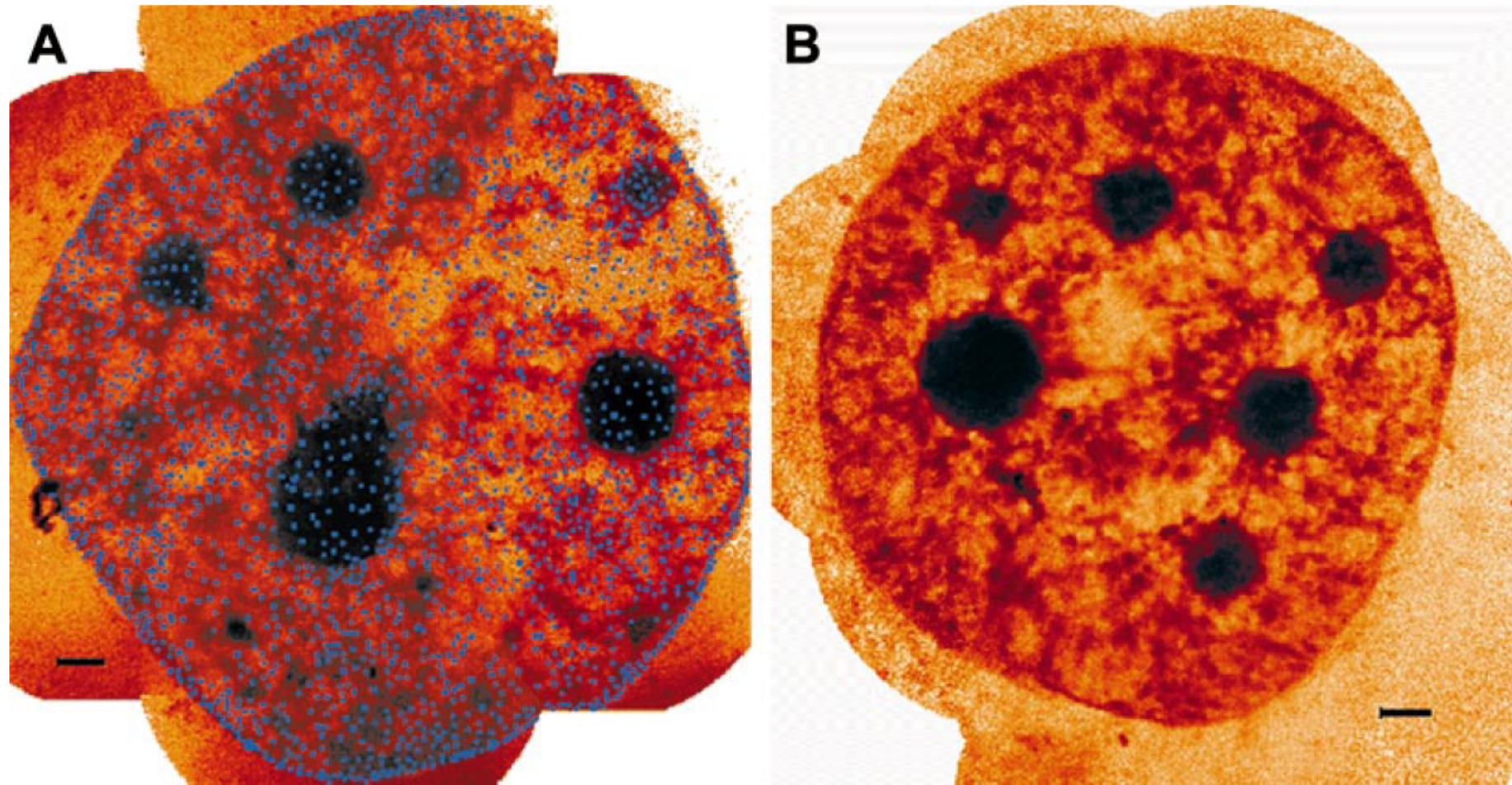
Immunolocalization of cytoplasmic proteins



X-ray microscope image of the labelled microtubule network (blue) in a whole, hydrated mouse mammary epithelial cell (EPH4). The cell nucleus containing several nucleoli (orange) is in the centre of the cell. (B) High magnification view of labelled microtubules before quantitative colour-coding. (C) Same field of view after colour coding of the microtubules.

W. Meyer-Lindenberg et al., *Journal of Microscopy*, 2001, pp 395-403.

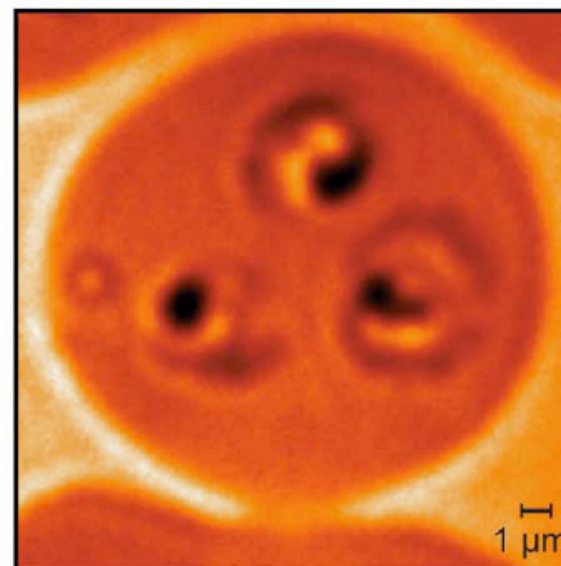
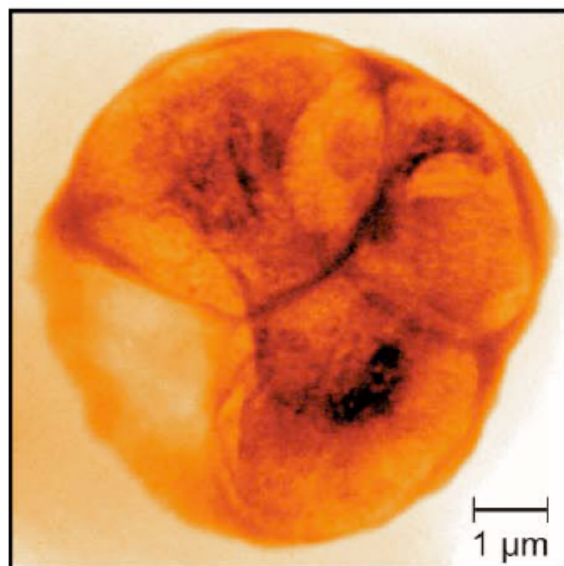
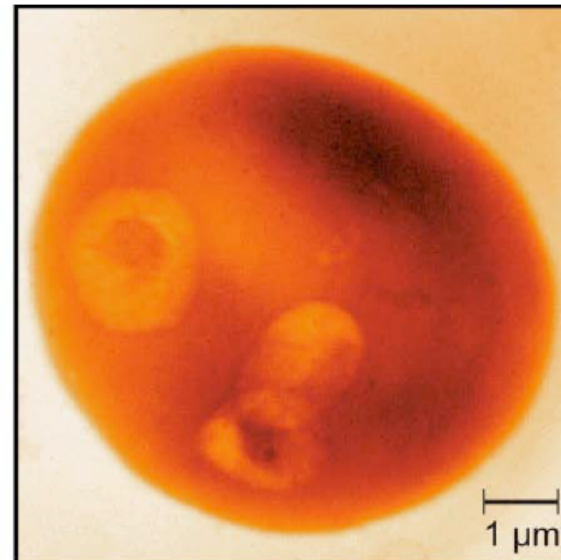
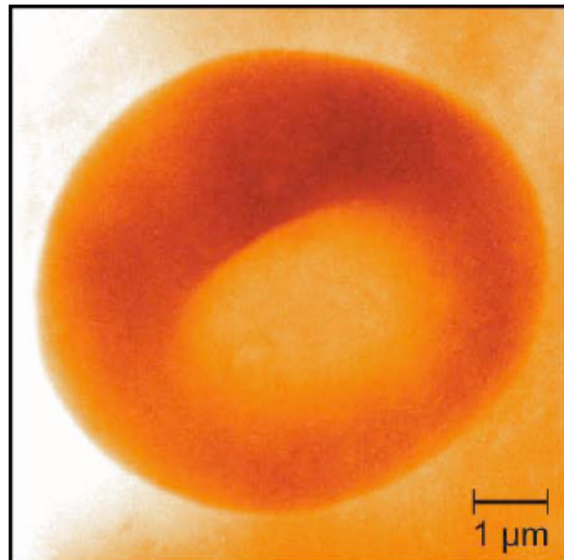
Nuclear pore complexes



Nuclei of human mammary epithelial tumour cells (T4) labelled for nuclear pore complex proteins. (A) Colorized X-ray micrograph of a single nucleus after silver enhancement. This image is a montage compiled from four individual X-ray microscope images. (B) Control: single nucleus that was exposed to secondary antibodies and silver enhancement (no primary antibodies). This image is a montage compiled from four individual X-ray microscope images. Magnification: 2400x, 0.034 NA with 20 nm pixel size at 517 eV ($\lambda = 2.4$ nm).

W. Meyer-Ilse et al., *Journal of Microscopy*, 2001, pp 395–403.

Malaria Infected Blood Cells

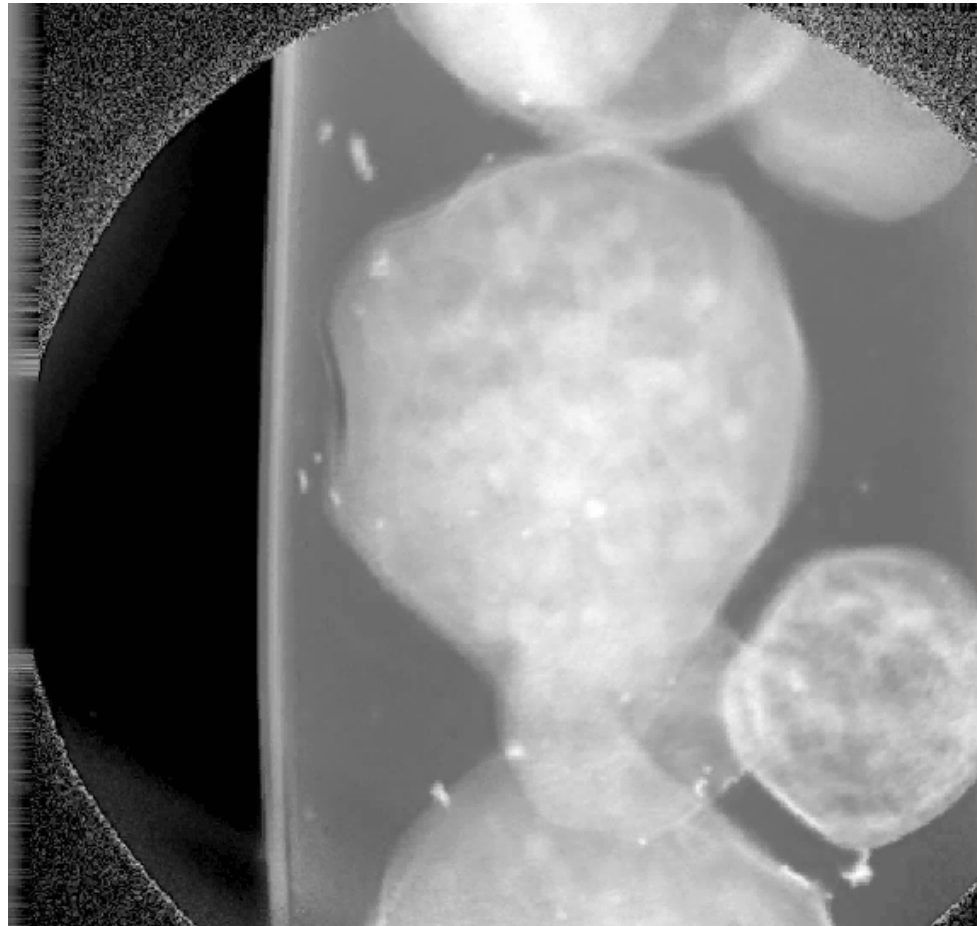


(Courtesy of C. Magowan and W. Meyer-Lindenberg, LBNL)

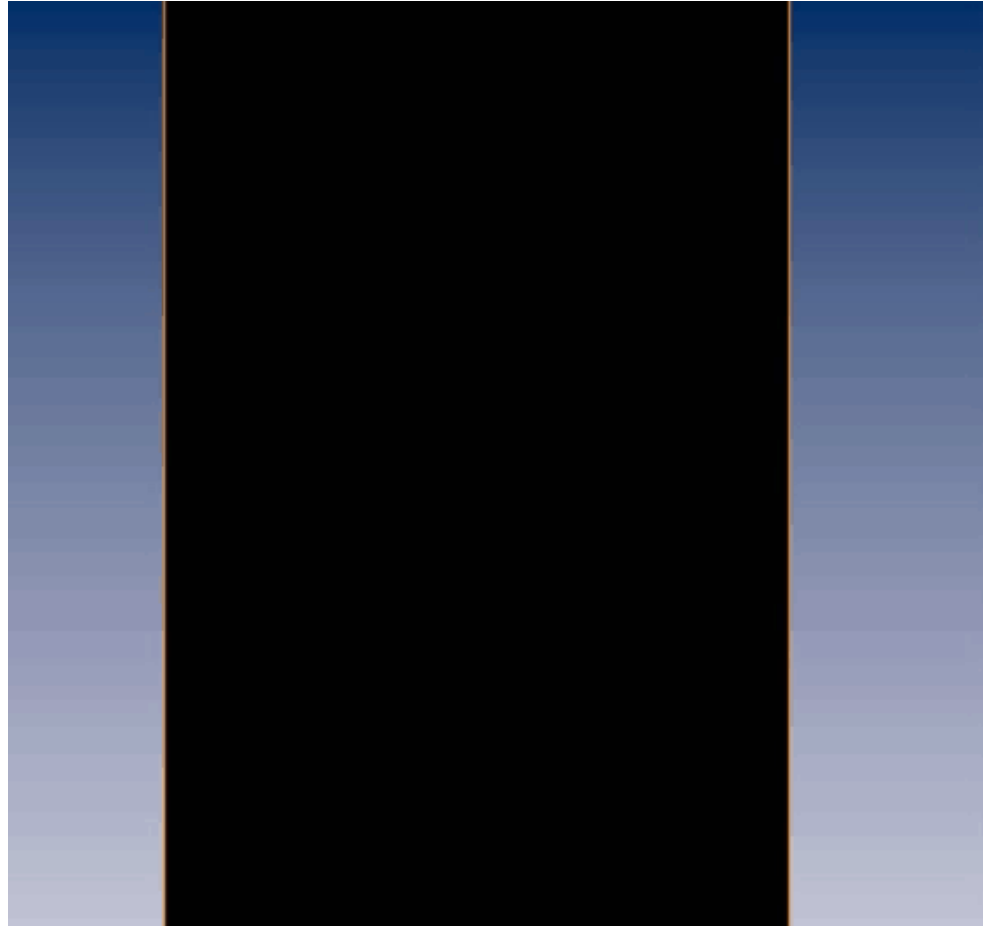
g

Saccharomyces cerevisiae (yeast cells)

C.A. Larabell & M. A. Le Gros (2004). Molecular Biology of the Cell, 15(3), 956-962



Projection images
(60 nm gold balls as fiducial markers,
45 images, collected at 4° interval)

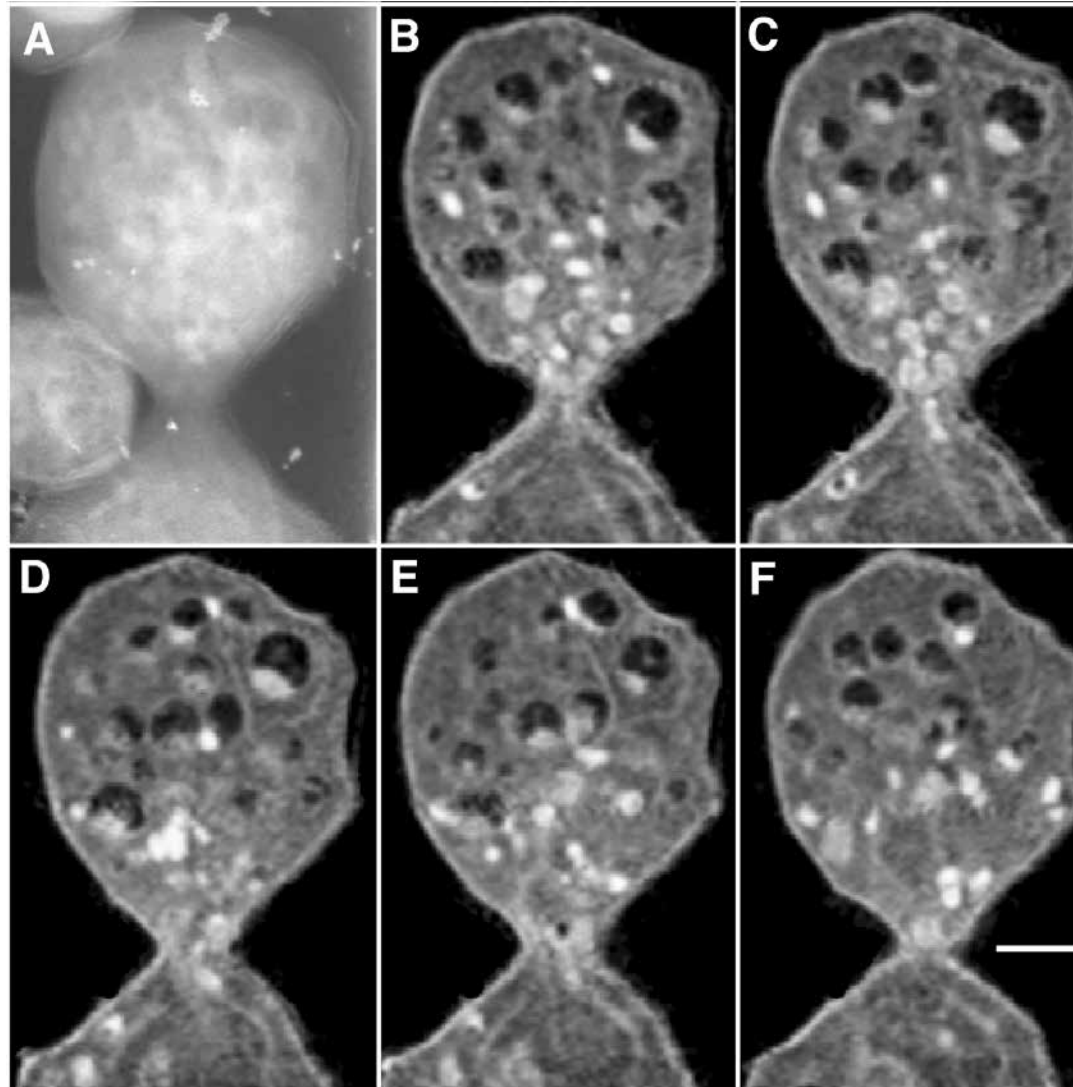


Sagittal orthoslicing

Animation courtesy of C. Larabell, UCSF

Saccharomyces cerevisiae

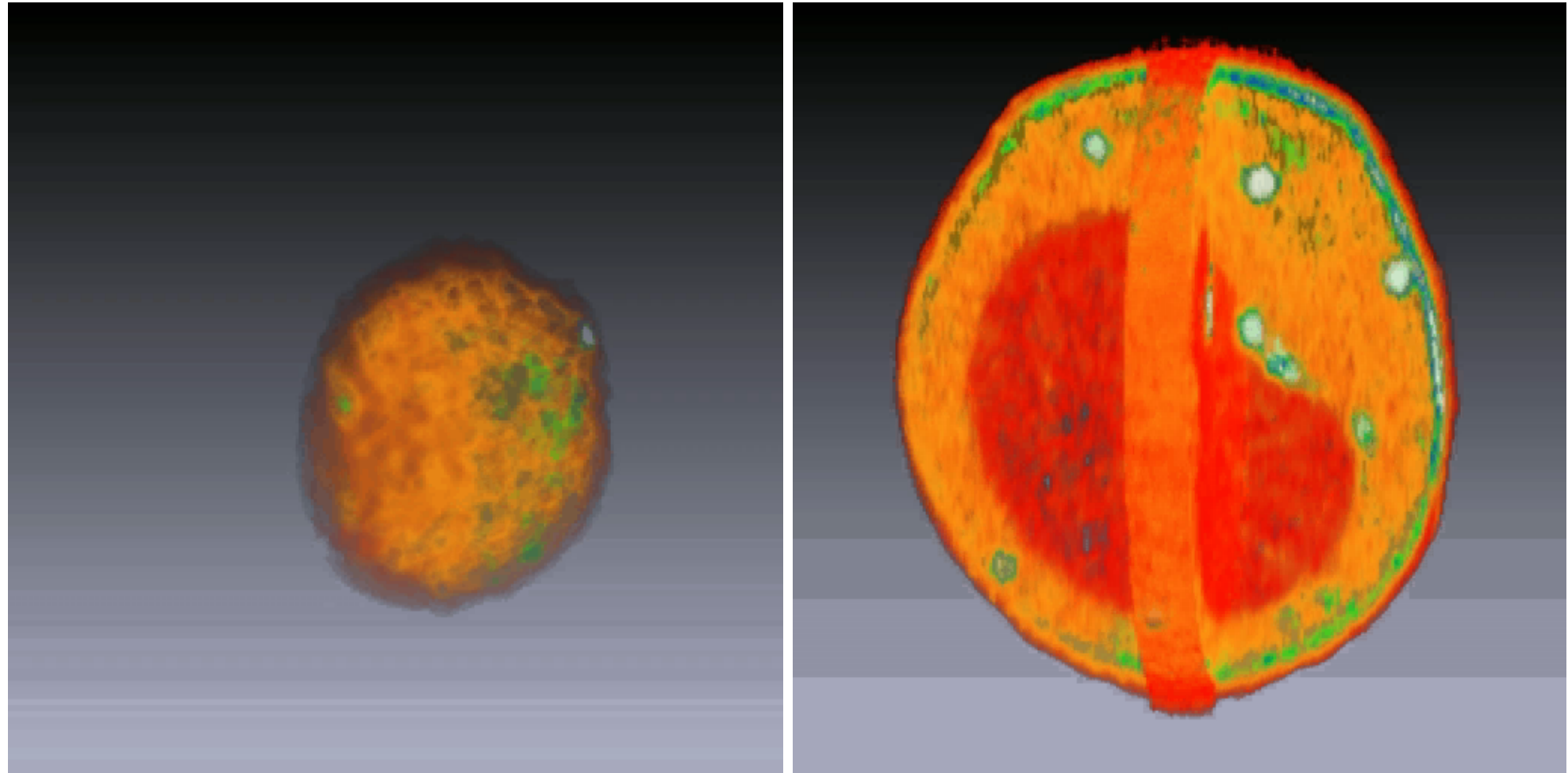
C.A. Larabell & M.A. Le Gros (2004). Molecular Biology of the Cell, 15(3), 956-962



High-magnification view of a budding yeast. (A) Projection image showing numerous superimposed organelles. (B–F) Computer generated sections through the yeast reveals numerous organelles after tomographic reconstruction; the most dense (bright white circles) are filled with lipid. Bar: 0.5 microns

Saccharomyces cerevisiae

C.A. Larabell & M. A. Le Gros (2004). Molecular Biology of the Cell, 15(3), 956-962

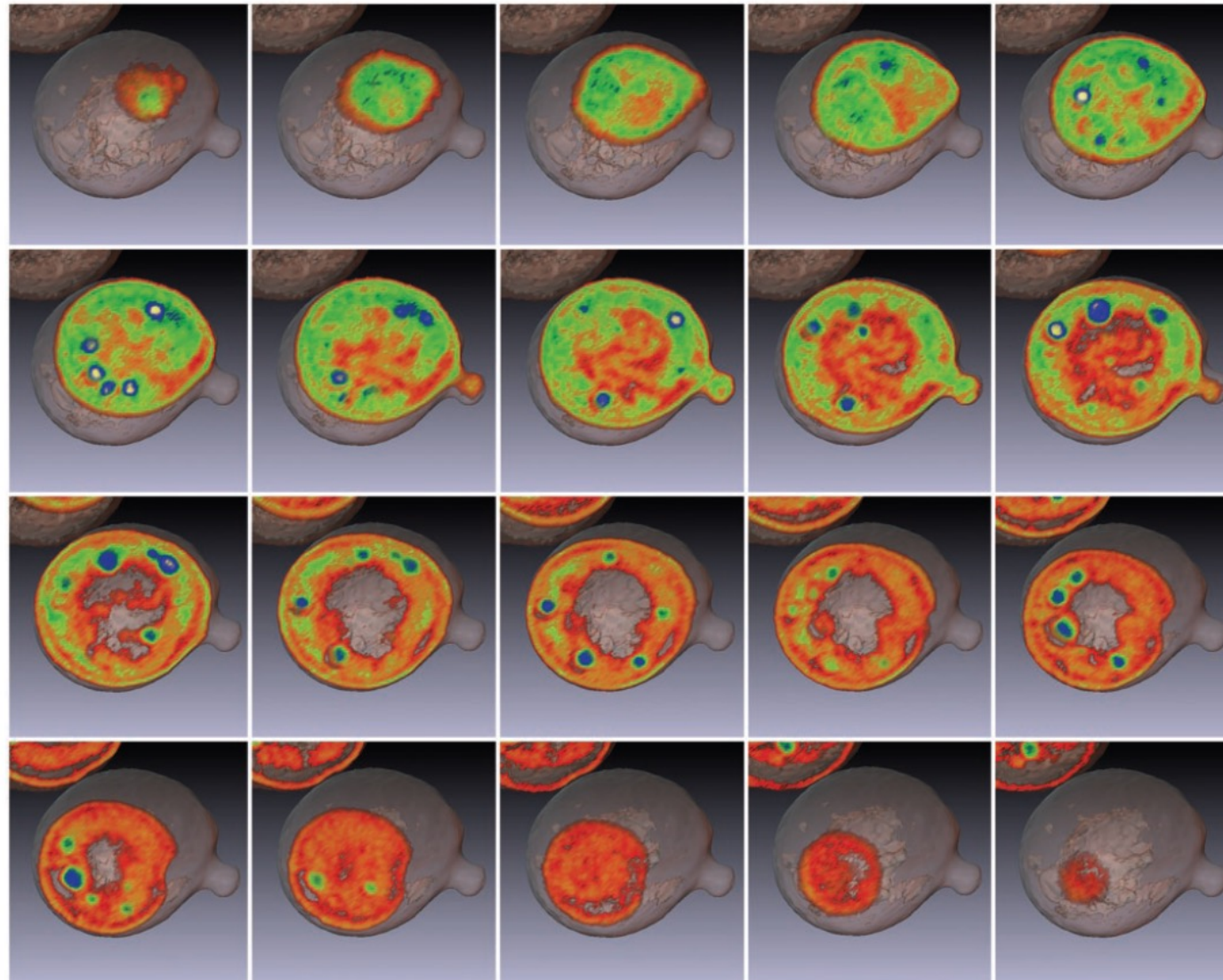


Volume rendering, color-coded using x-ray absorption coefficient:
white = dense lipid droplets, gray = less dense vacuoles, red = nucleus,
green, orange = structures of varying densities

Animation courtesy of C. Larabell, UCSF

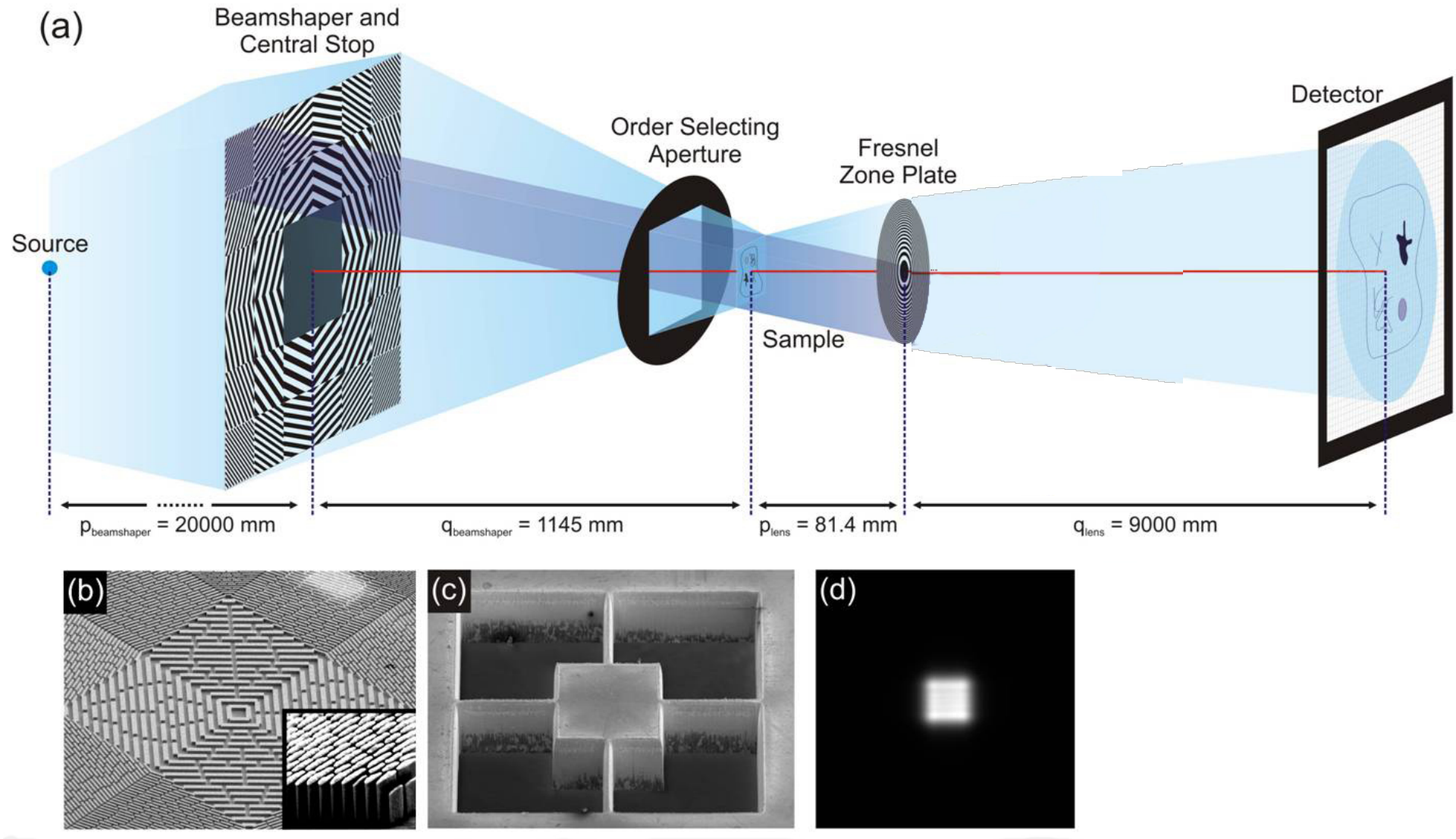
Saccharomyces cerevisiae

C.A. Larabell & M. A. Le Gros (2004). Molecular Biology of the Cell, 15(3), 956-962



Virtual sections through the tomographic reconstruction of an early budding yeast. Structures have been assigned different colors, which indicate degree of X-ray absorption. Dense lipid droplets appear white and other cell structures are colored shades of blue, green, and orange with decreasing density. Yeast cell, 5 microns diameter.

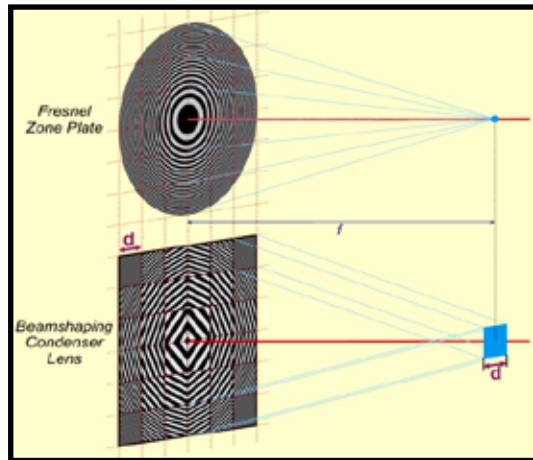
Nanoimaging at TOMCAT (operate at 150-200nm)



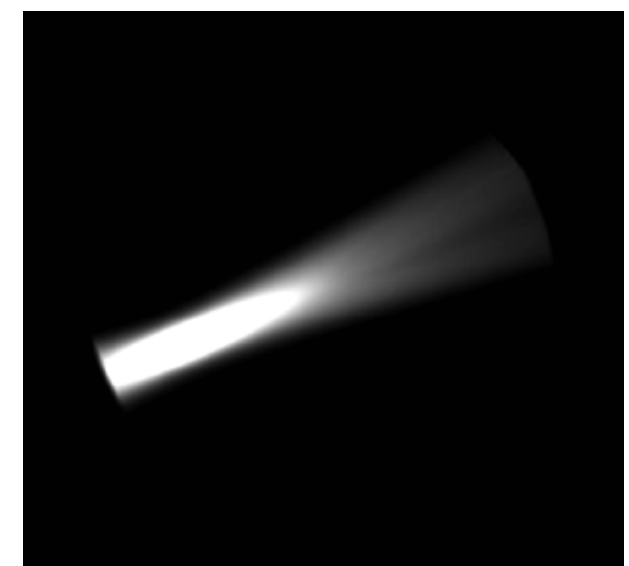
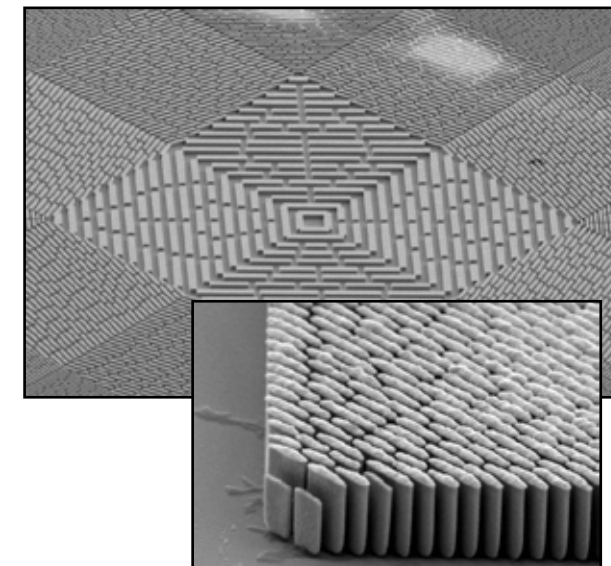
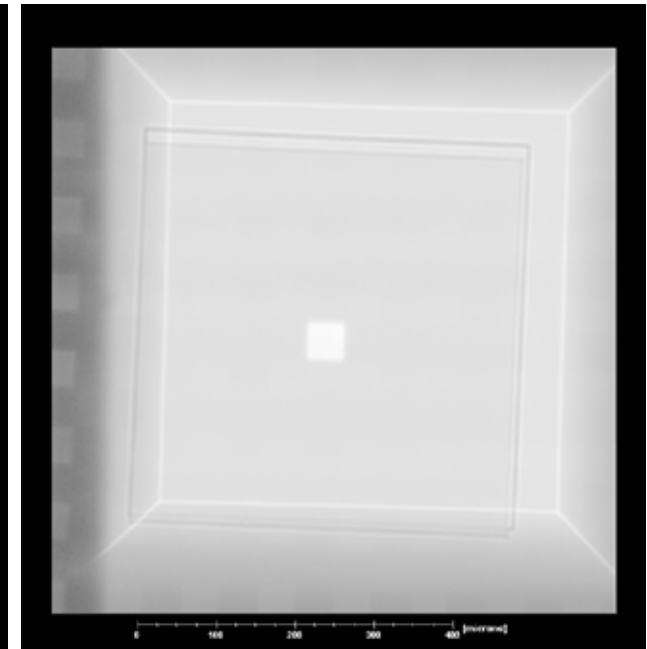
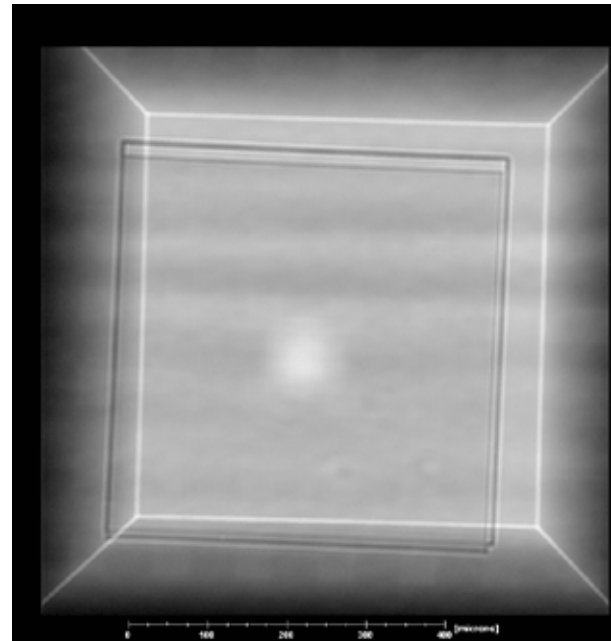
Microscope is operated at 10 keV

M. Stampanoni et al., PRB2010

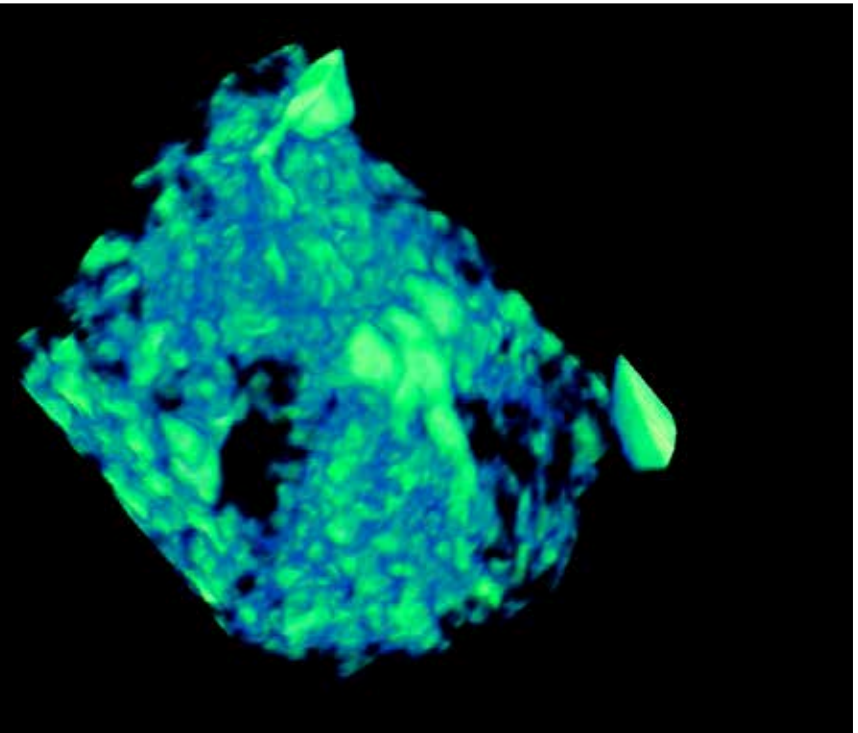
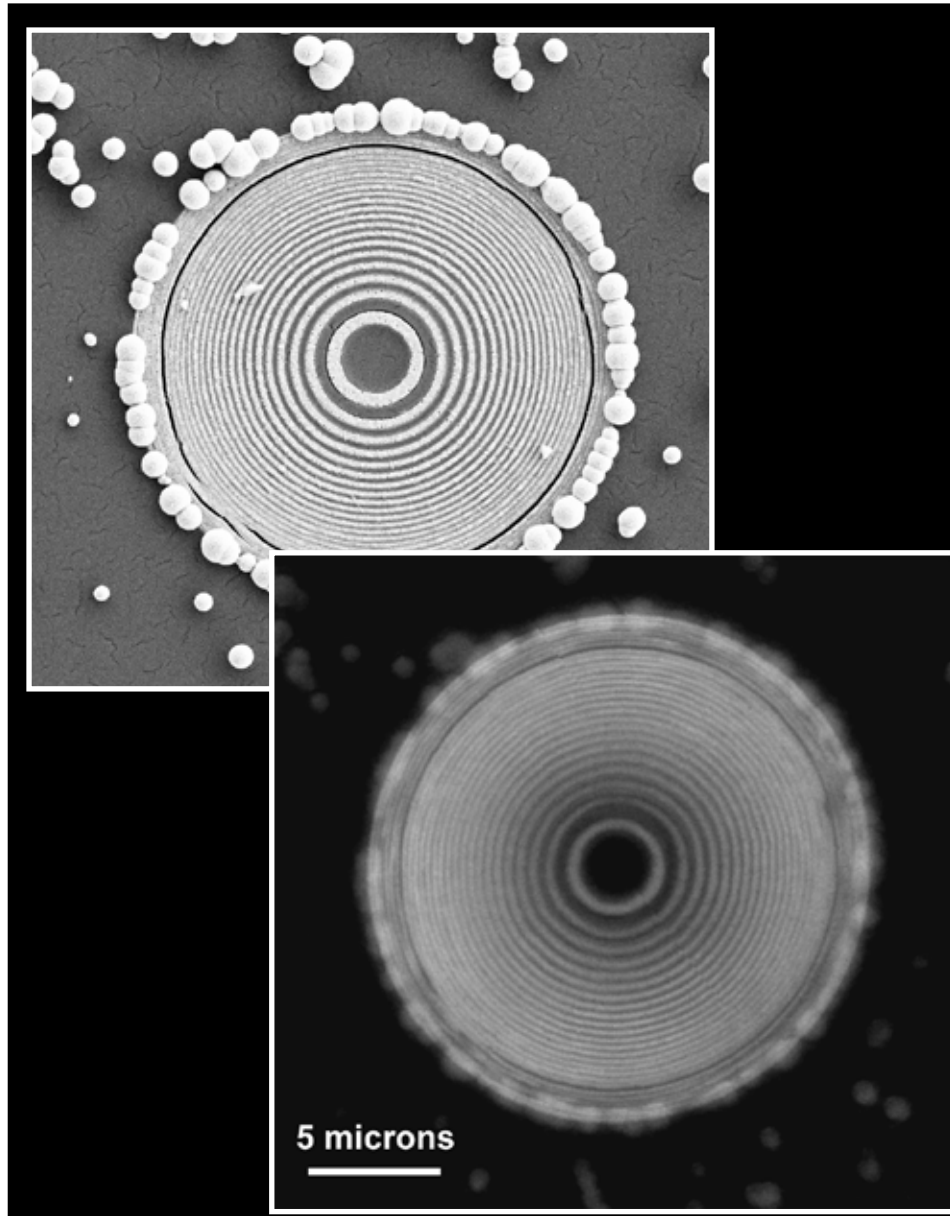
Beamshaper as condenser



Au beamshaper @ 8 keV	
Substrate	~Si 2 microns
Substrate Transmission	> 97 %
Structure height	from 0.7 to 1 micron
“Diameter”	1500µm
Outer zone width	70 nm
Spot size	50 µm x 50 µm
Theoretical Efficiency	20 % each zone
Gain Factor	200
Focal length	1360 (!) mm
Depth of focus	200 µm
Central stop size	~ 500 µm



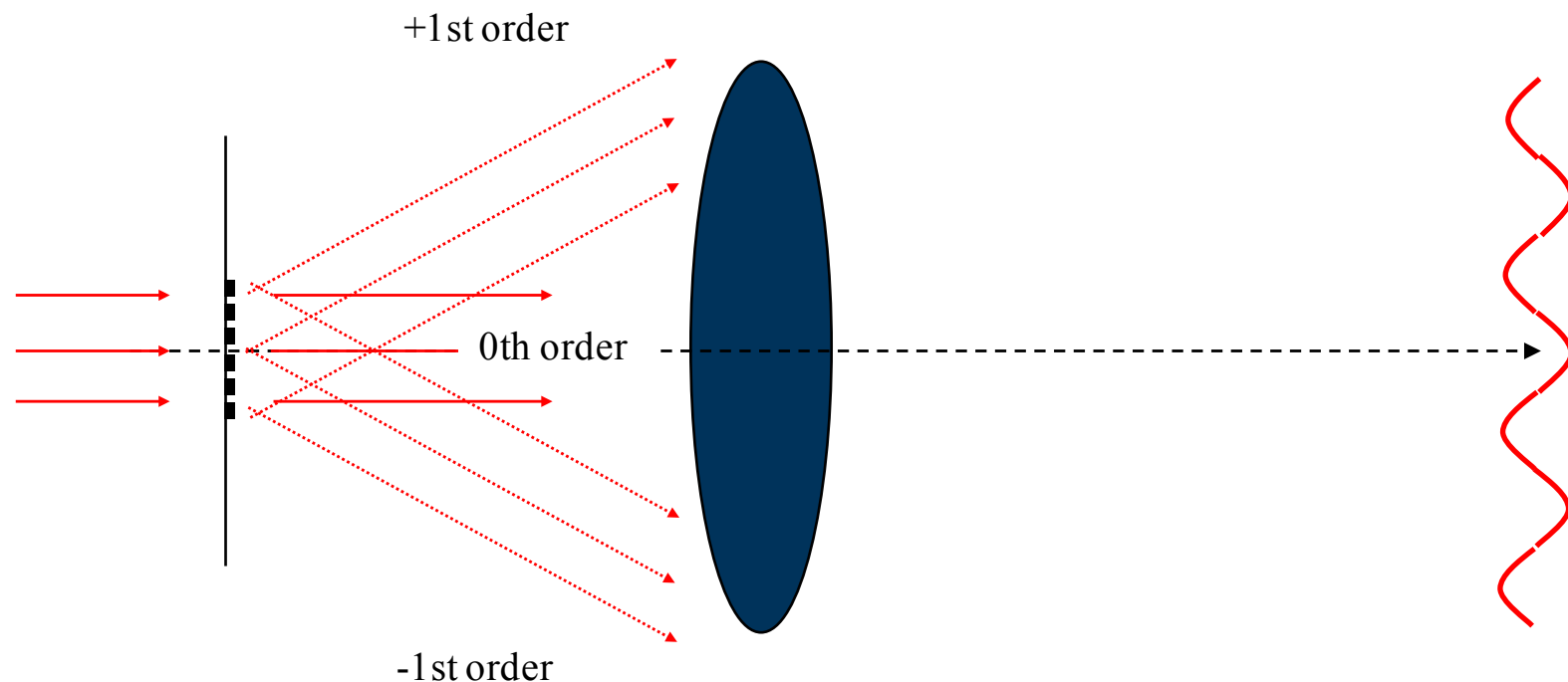
2D and 3D (absorption) nanoimaging



- Voltex view of a 25 um large cement sample
(sample courtesy P. Trtik, EMPA, Switzerland)
 - Porosity filled with Woods metal
- Pixelsize 72 nm – Estimated Resolution 200 nm

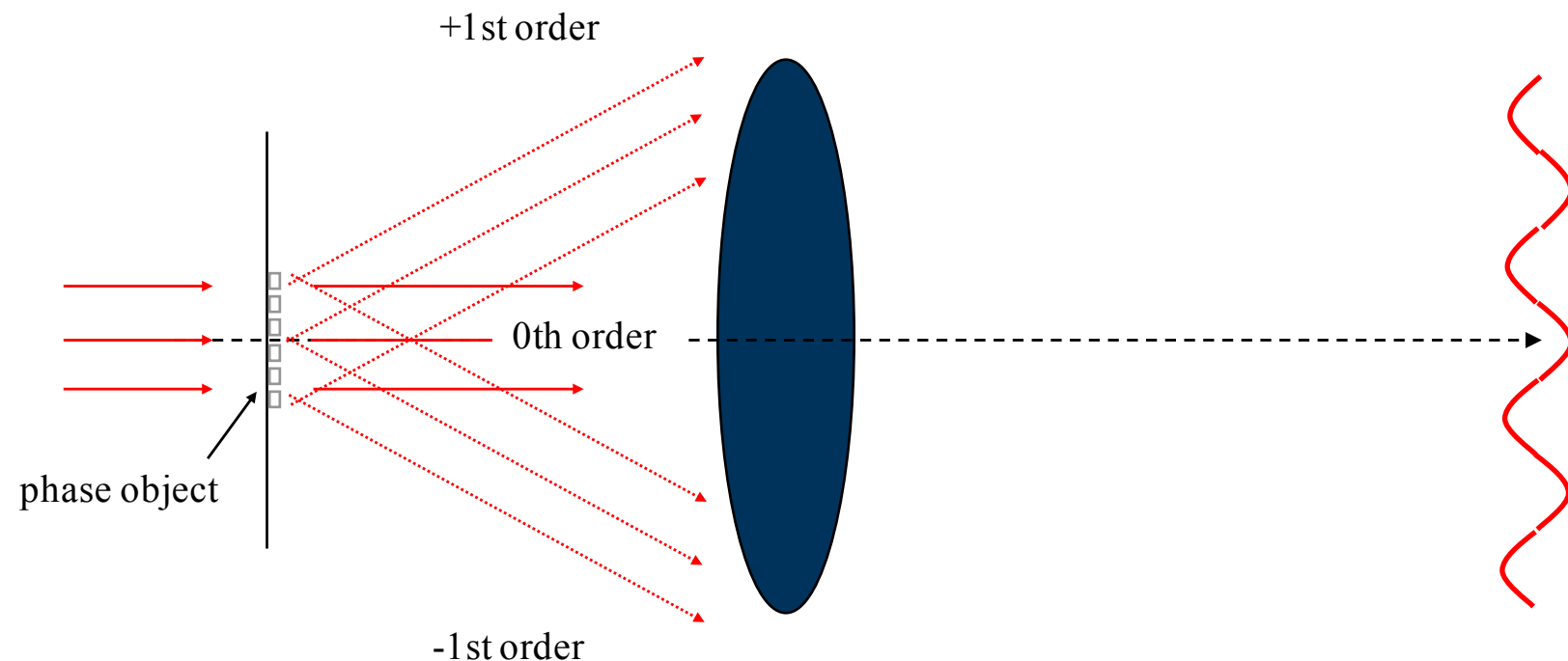
M. Stampanoni et al., Development of X-ray Tomography VI, SPIE, Vol. 7078, Aug. 2008

Imaging of absorption vs phase objects



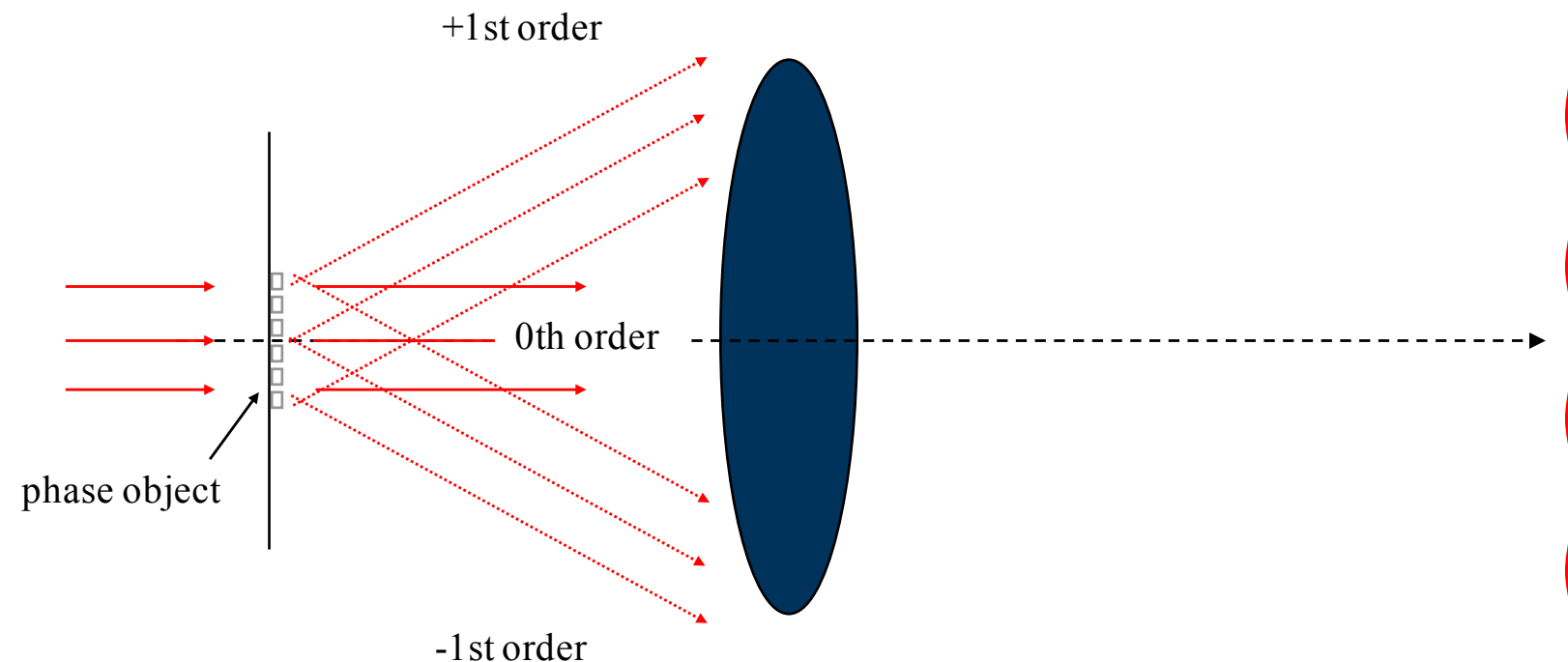
Slide courtesy C. David, PSI

Imaging of absorption vs phase objects



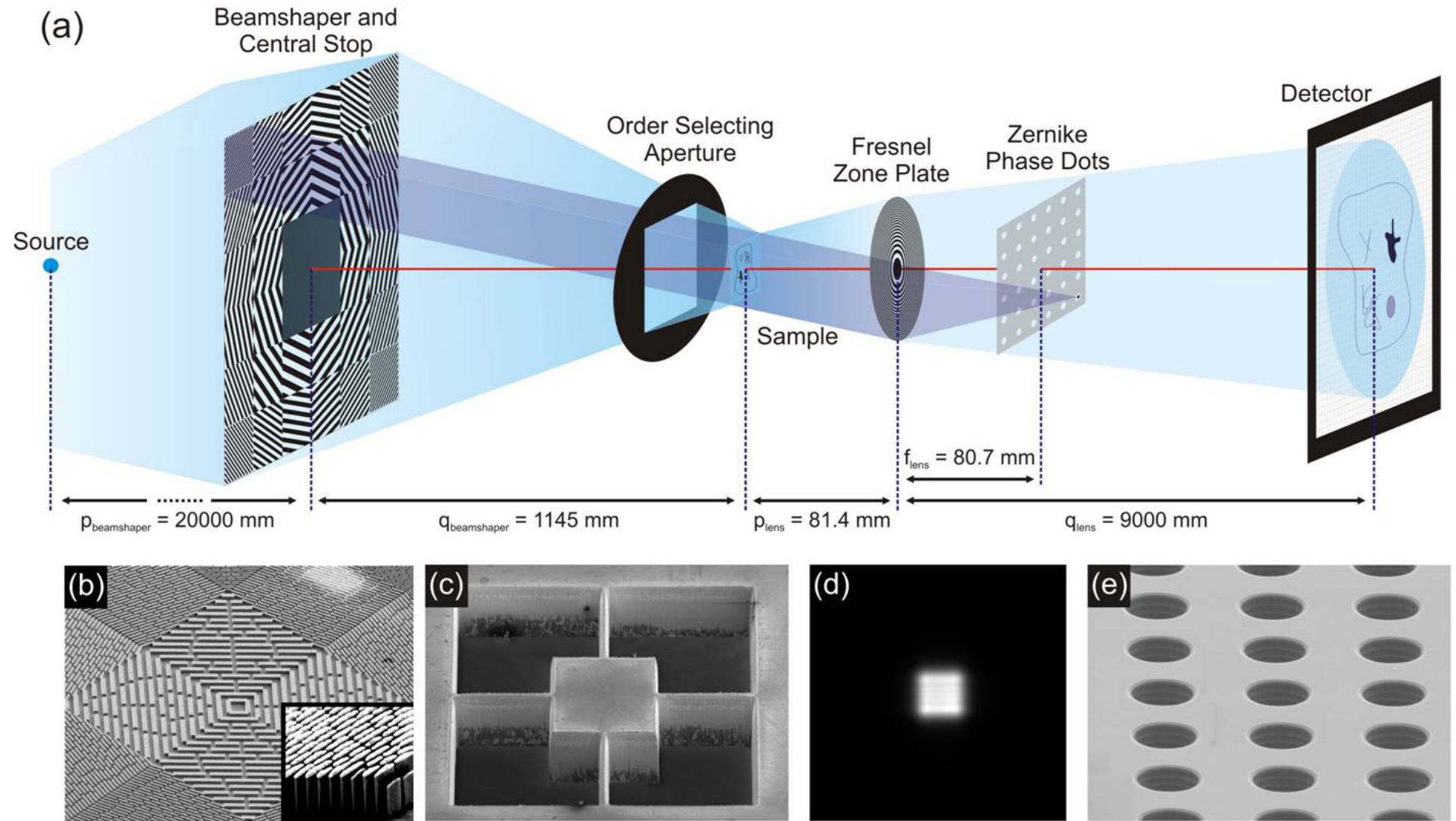
Slide courtesy C. David, PSI

Imaging of absorption vs phase objects



Slide courtesy C. David, PSI

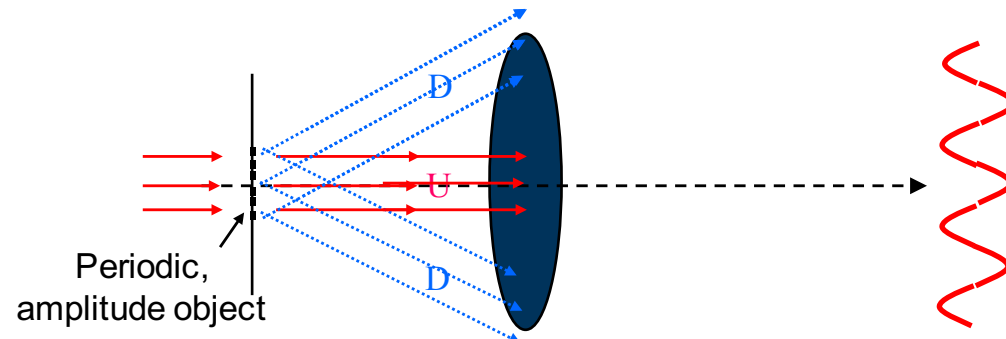
How to switch on phase contrast ?



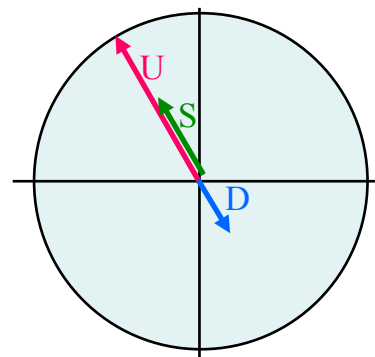
Microscope is operated at 10 keV

M. Stampanoni et al., PRB2010

Zernike phase contrast



$$\vec{S} = \vec{U} + \vec{D}$$



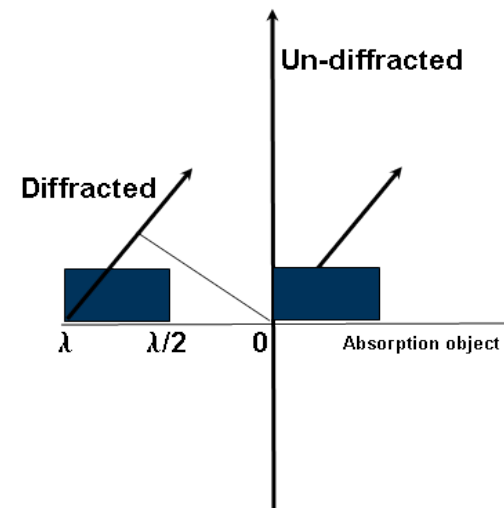
amplitude object

Image formation involves

- collecting diffracted light
- superimposing it with the right phase.

For amplitude objects, U and D are „counter phase“, i.e. the object itself affects the way U and D superimpose.

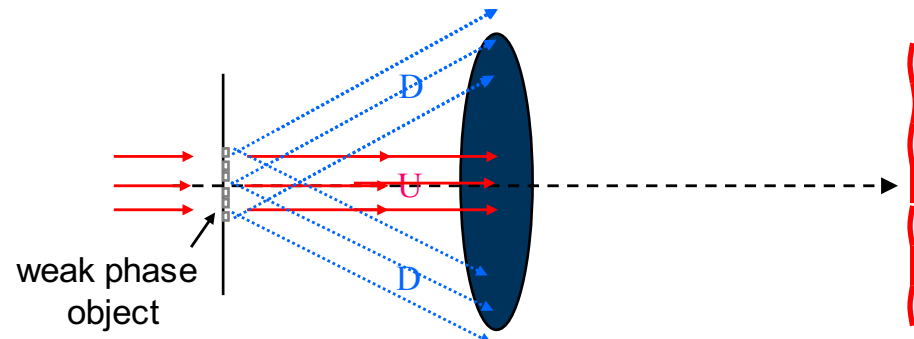
→ Therefore U and S have different amplitudes (i.e. high contrast)



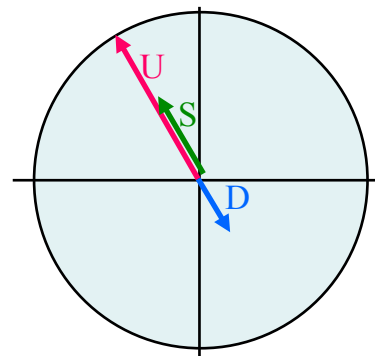
U=undiffracted light, D=diffracted light, S=superposition

Slide courtesy C. David, PSI

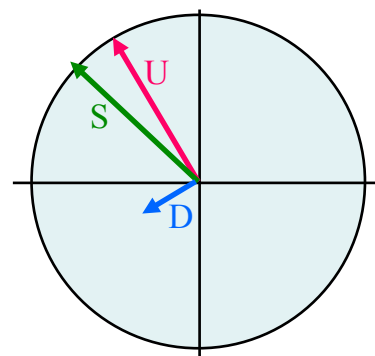
Zernike phase contrast



$$\vec{S} = \vec{U} + \vec{D}$$



amplitude object



weak phase object

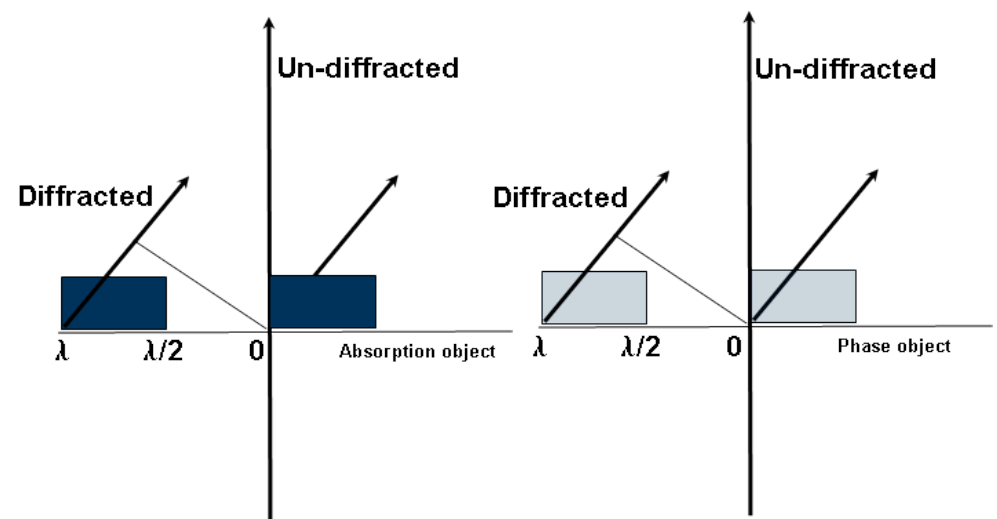
U=undiffracted light, D=diffracted light, S=superposition

Image formation involves

- collecting diffracted light
- superimposing it with the right phase.

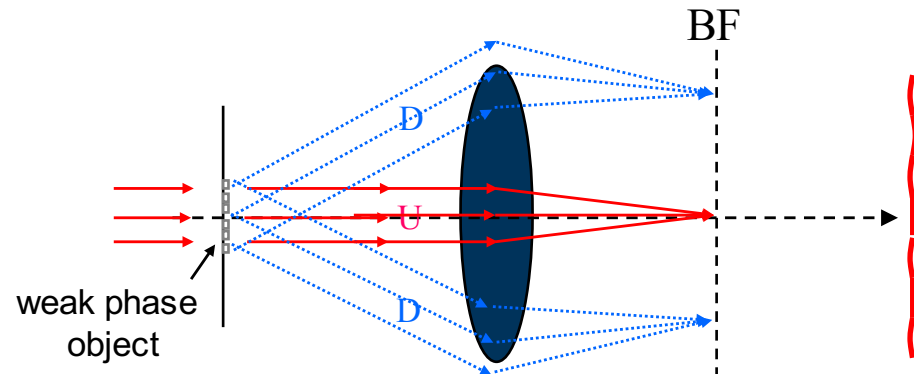
For a weak phase object, U and D are shifted by 90° , i.e the object itself affects only minimally the superposition process.

→ S and U almost have the same amplitude



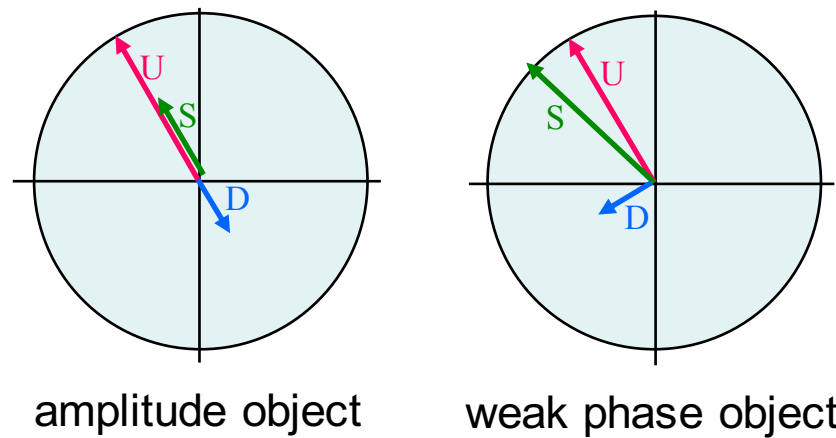
Slide courtesy C. David, PSI

Zernike phase contrast



In the back focal plane, the different diffraction orders can be manipulated in phase (or amplitude)

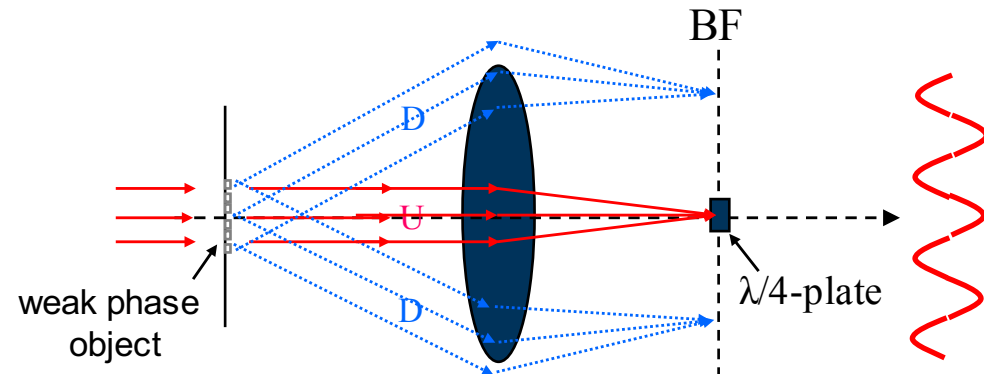
$$\vec{S} = \vec{U} + \vec{D}$$



U=undiffracted light, D=diffracted light, S=superposition

Slide courtesy C. David, PSI

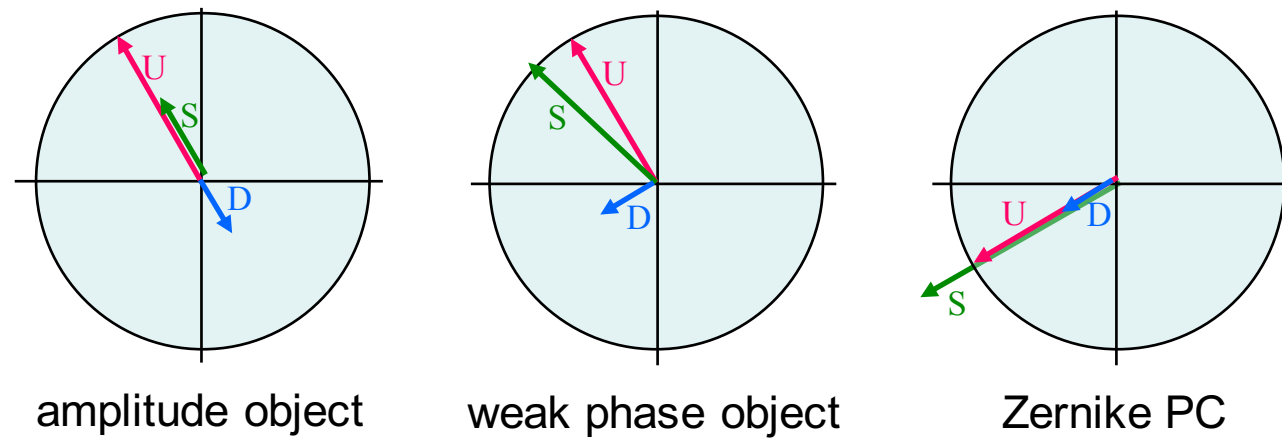
Zernike phase contrast



$$\vec{S} = \vec{U} + \vec{D}$$

In the back focal plane, the different diffraction orders can be manipulated in phase (or amplitude)

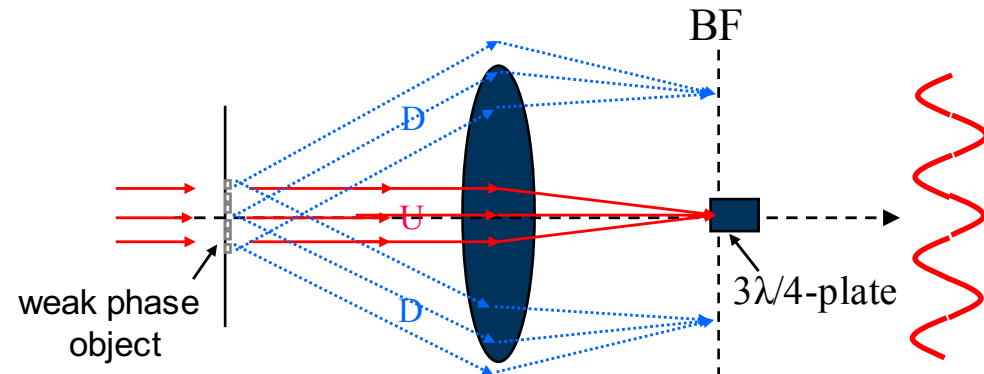
In Zernike PC, U is shifted in phase using a phase plate in the BF-plane



U=undiffracted light, D=diffracted light, S=superposition

Slide courtesy C. David, PSI

Zernike phase contrast

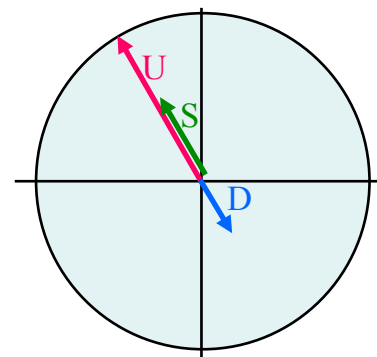


$$\vec{S} = \vec{U} + \vec{D}$$

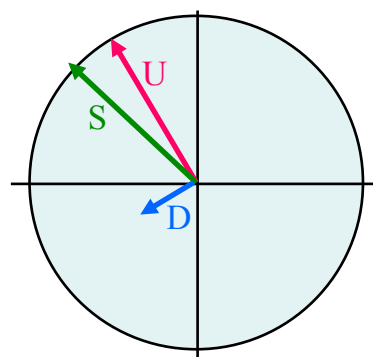
In the back focal plane, the different diffraction orders can be manipulated in phase (or amplitude)

In Zernike PC, U is shifted in phase using a phase plate in the BF-lane

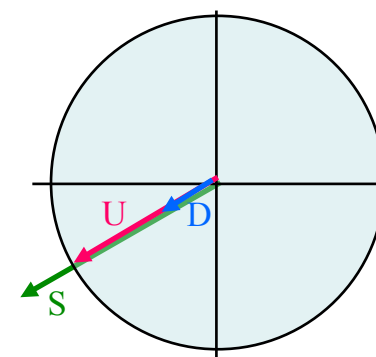
The phase plate can be 90° or 270°



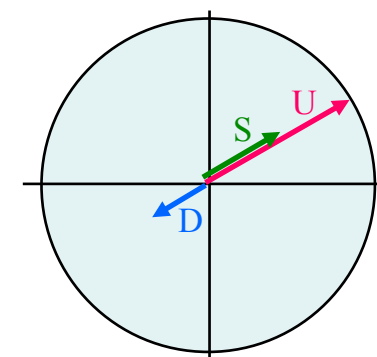
amplitude object



weak phase object



Zernike PC



Zernike PC 270°

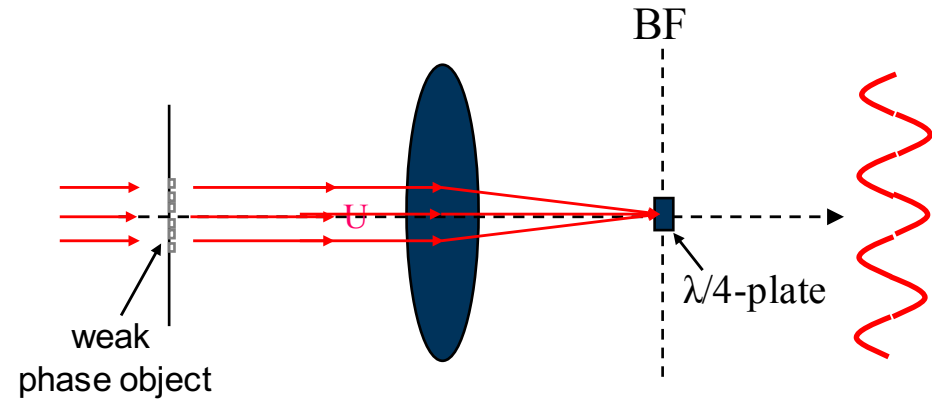
U=undiffracted light, D=diffracted light, S=superposition

Slide courtesy C. David, PSI

Principles of Zernike phase contrast imaging

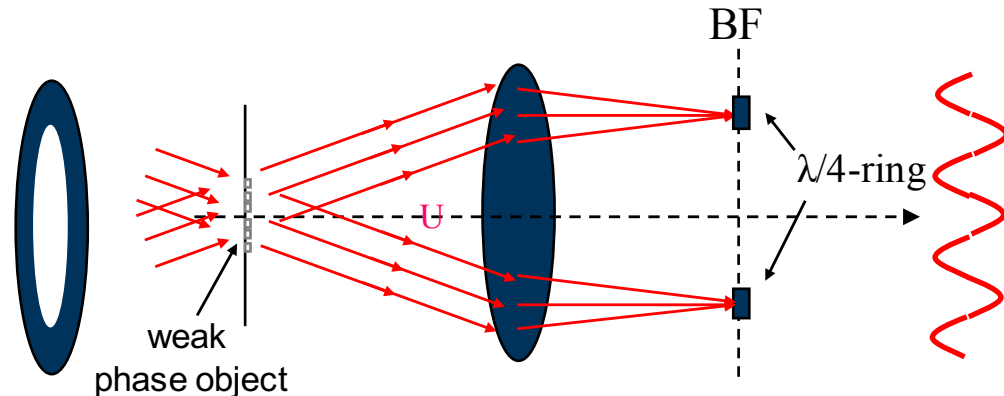
- The interaction of x-rays with structures in a sample leads to the generation of diffracted light besides the direct (undiffracted) radiation passing through the sample.
- According to Abbe theory, diffracted light from an object is required for image formation in a microscope. For an absorption sample, the phase shift between undiffracted (U) and diffracted (D) light is 180° , resulting in a high absorption contrast when superimposing the wave vectors of U and D.
- However, the condition is different for a phase sample where the phase relation between direct and diffracted light is in good approximation 90° (assuming a phase shift δ much smaller than the wavelength, which is met for kiloelectronvolt radiation and sample thickness of the sample under study) resulting in a sum wave vector (S) in the image plane having almost the same amount as the direct light vector thus showing very weak contrast for the sample structure.
- To use the phase information to generate a visible intensity modulation (i.e. contrast) in the image plane, it is required according to Zernike to phase shift the undiffracted light.
- This can be accomplished with a phase shifting optical element in the back focal plane of the objective that is matched in its geometry to the distribution of the undiffracted light
- By these means, the undiffracted light (U) can be phase shifted either by 90° or 270° in respect to the diffracted light (D) and U is in addition reduced in its amplitude by absorption in the phase ring material, thus better matching the intensity level of D. Consequently, U and D can be superimposed in the image plane as parallel or antiparallel vectors, giving high contrast.

Zernike phase contrast: practical aspects



Slide courtesy C. David, PSI

Zernike phase contrast: practical aspects



Problem: condenser illuminates from all kinds of angles

- Phase ring needs to be broad to cover all U-light
- Phase ring also shifts some D-light → Halo-effects!!
- Ring condenser required

Practical realization

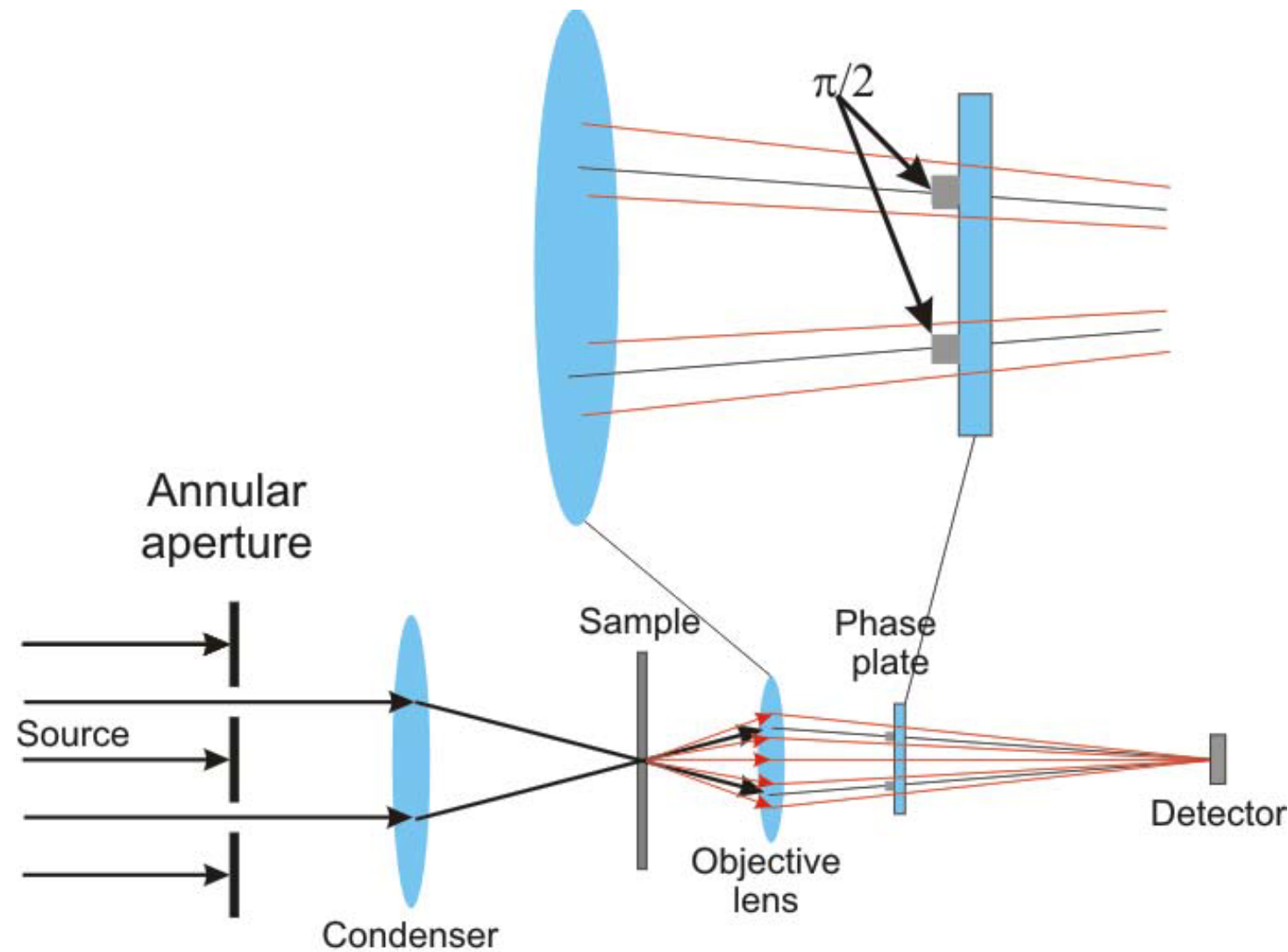
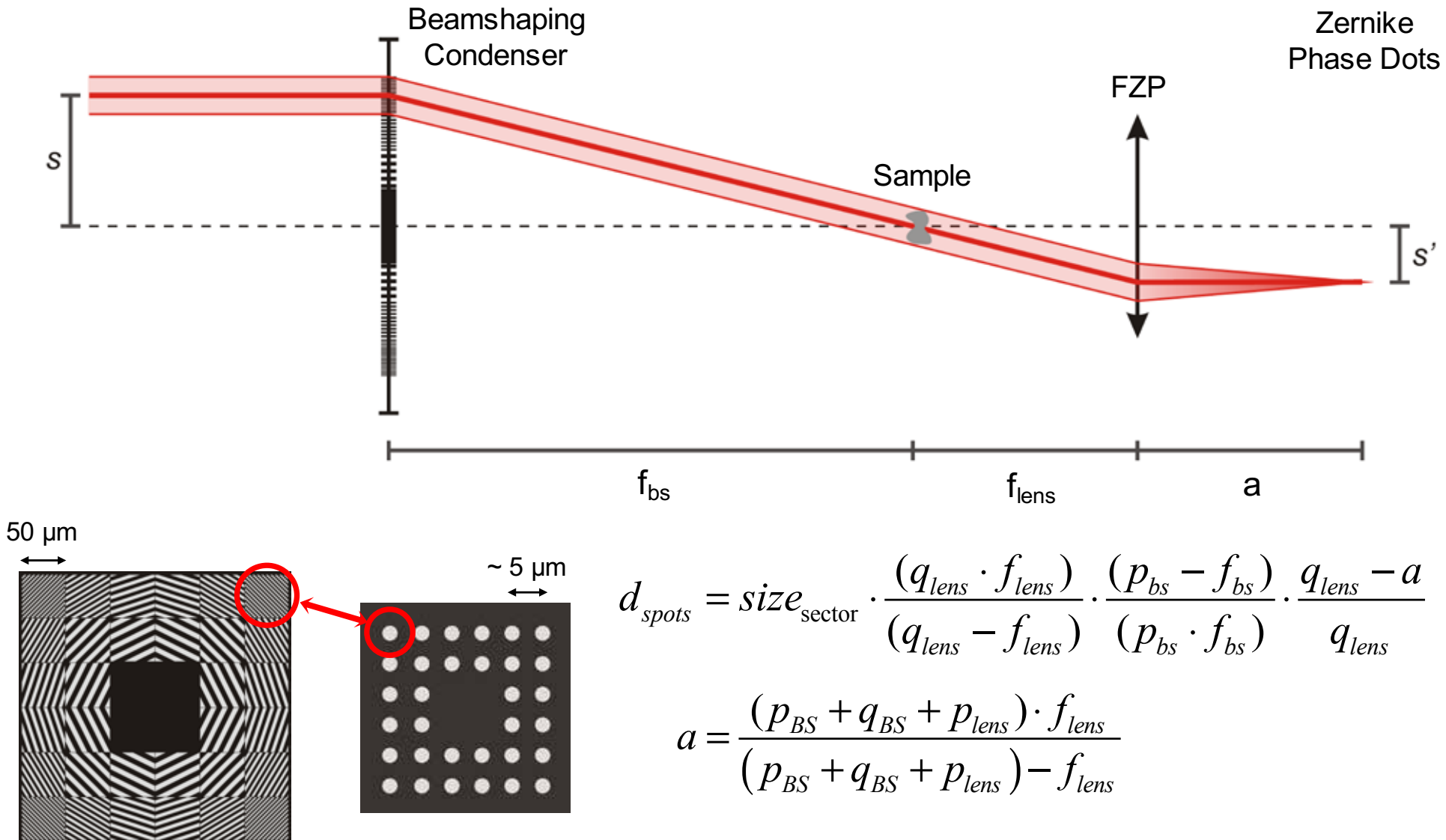


Image courtesy of Ismo Vartiainen

Zernike phase contrast microscopy



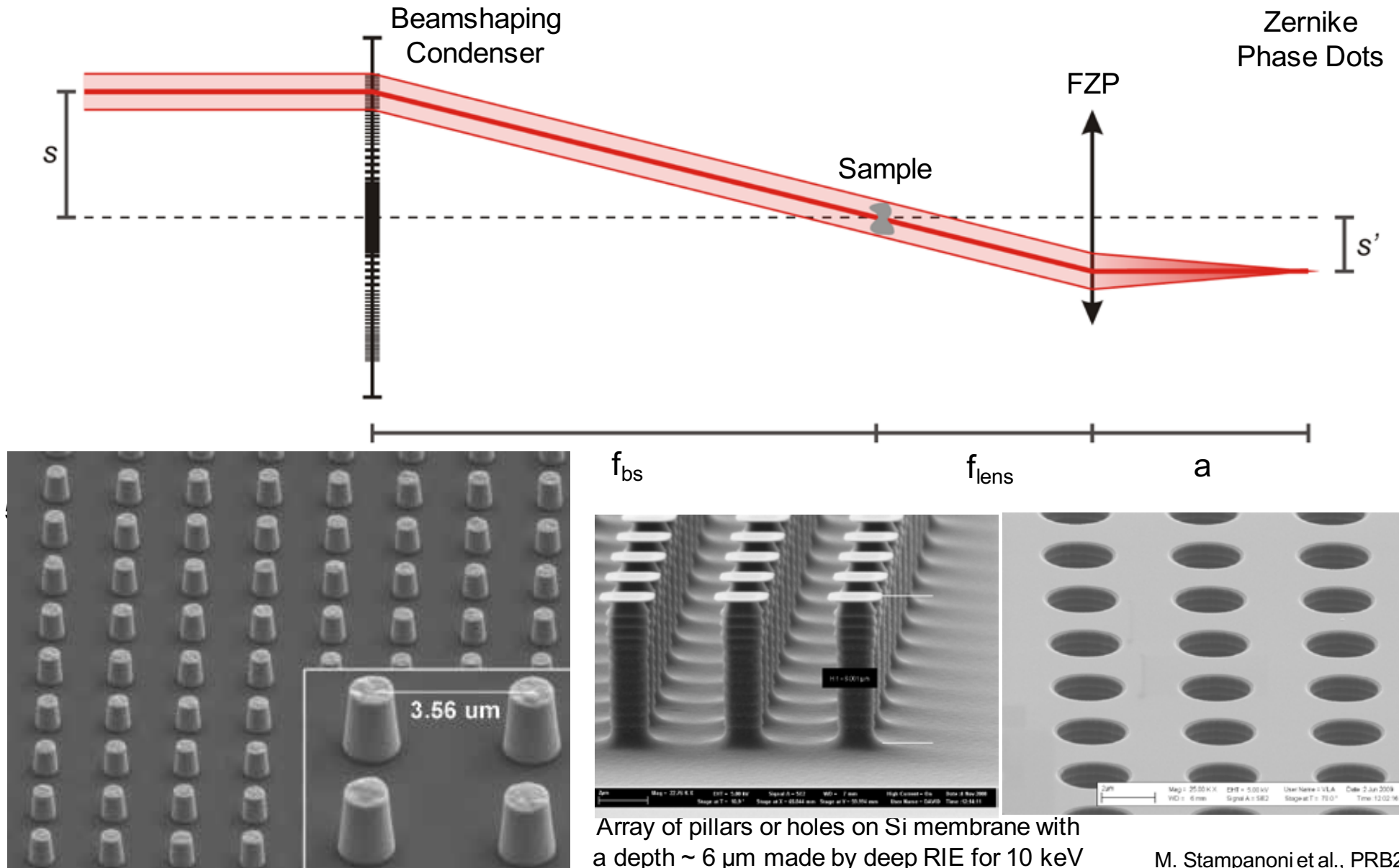
$$d_{spots} = size_{sector} \cdot \frac{(q_{lens} \cdot f_{lens})}{(q_{lens} - f_{lens})} \cdot \frac{(p_{bs} - f_{bs})}{(p_{bs} \cdot f_{bs})} \cdot \frac{q_{lens} - a}{q_{lens}}$$

$$a = \frac{(p_{BS} + q_{BS} + p_{lens}) \cdot f_{lens}}{(p_{BS} + q_{BS} + p_{lens}) - f_{lens}}$$

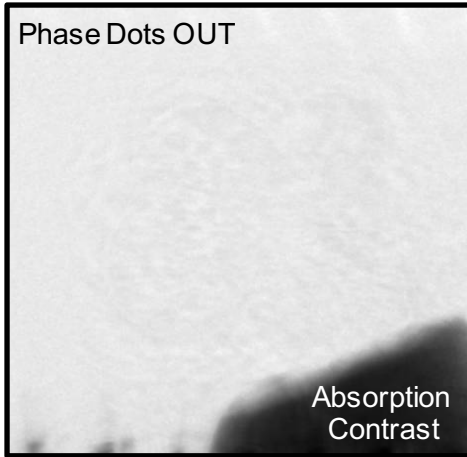
Array of pillars or holes on Si membrane with a depth $\sim 6 \mu\text{m}$ made by deep RIE for 10 keV

M. Stampanoni et al., PRB2010

Zernike phase contrast microscopy



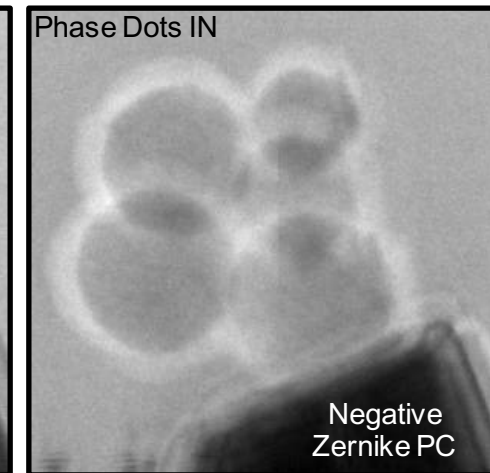
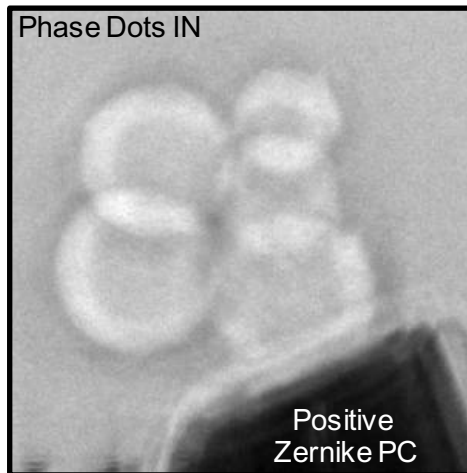
Phase dots in action



Pure phase object:
 $F(x, y) = \exp(i\phi(x, y))$

Transmission of 0th-order:
 $A = a \exp(i\alpha)$

Intensity at image plane:
 $I(x, y) = |C|^2 [a^2 - 2a\phi(x, y)\sin(\alpha)]$

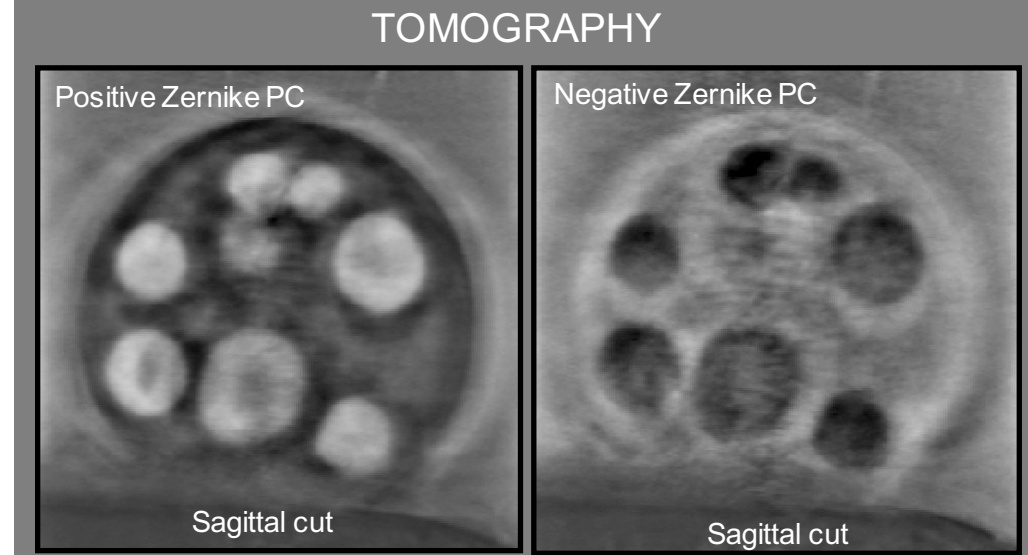
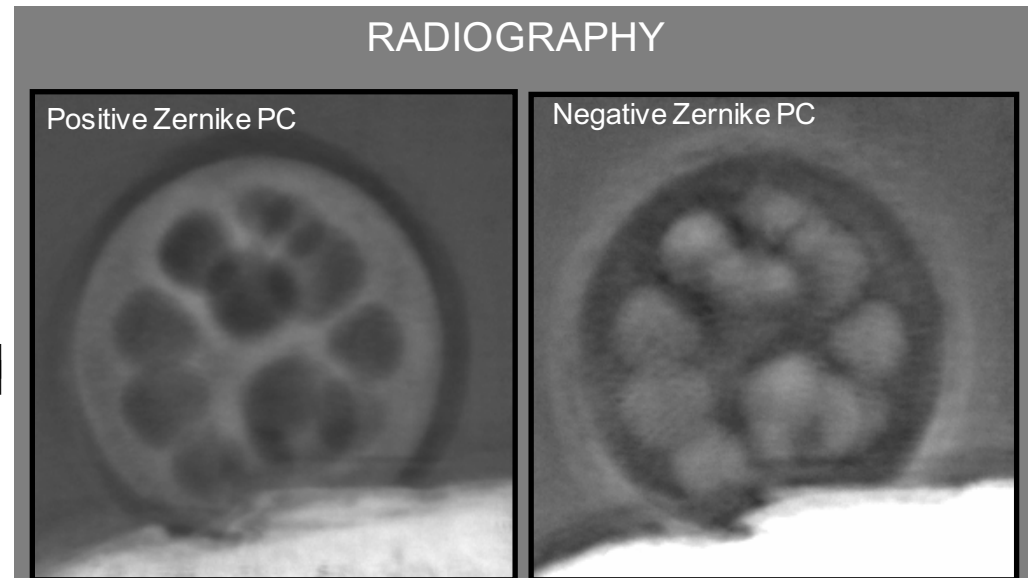


Intensity with non-absorbing $\pi/2$ -phase shifters:

$$I_{\pm\pi/2}(x, y) = |C|^2 [a^2 \pm 2a\phi(x, y)]$$

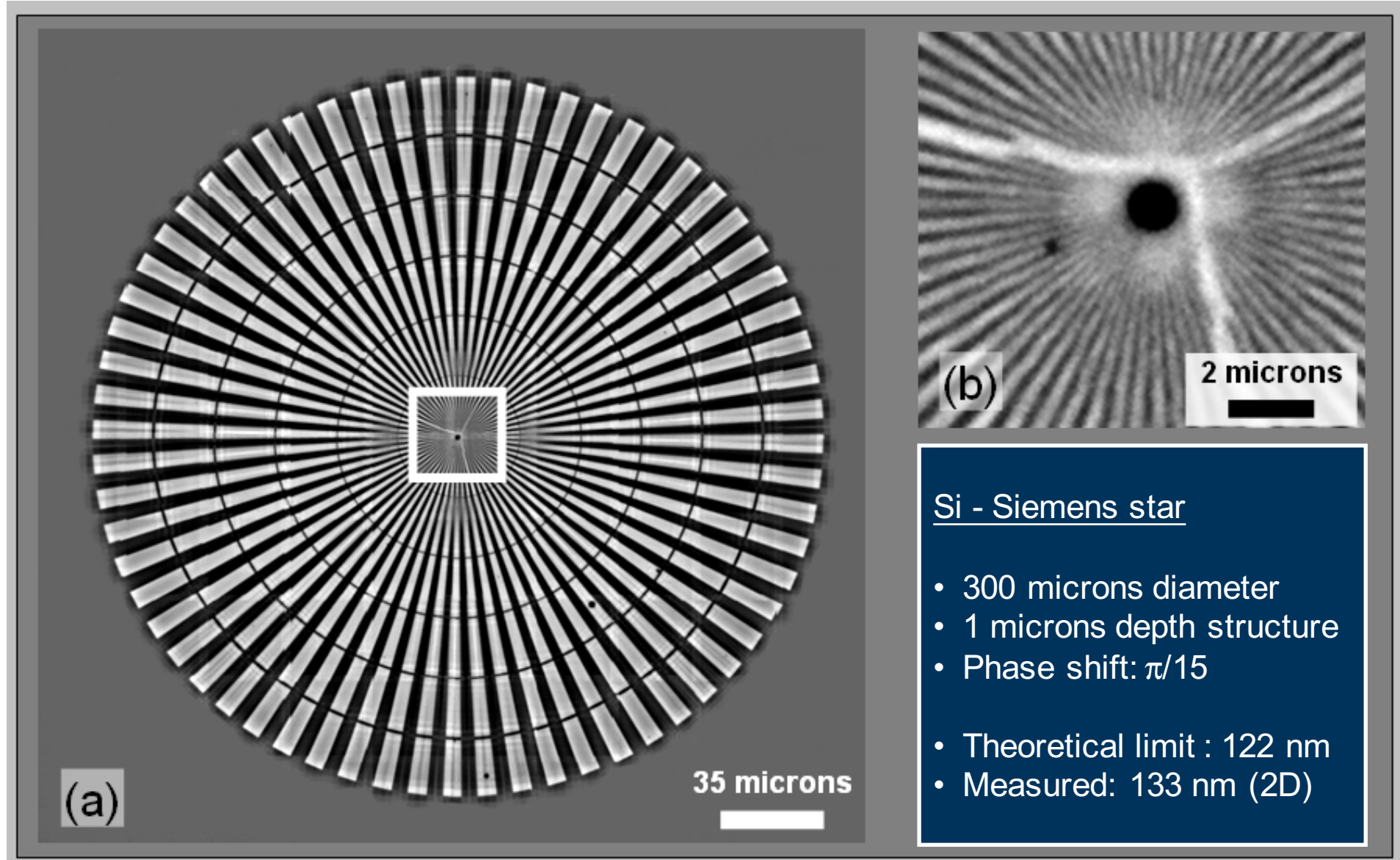
Remove "C" with measurement of (+,-) images:

$$\phi(x, y) = \frac{I_{\pi/2}(x, y) - I_{-\pi/2}(x, y)}{2[I_{\pi/2}(x, y) + I_{-\pi/2}(x, y)]}$$



I. Vartiainen unpublished

Resolution measurement (phase contrast mode)



M. Stampanoni et al., PRB2010

Porcine aortic endothelial (PAE) cells

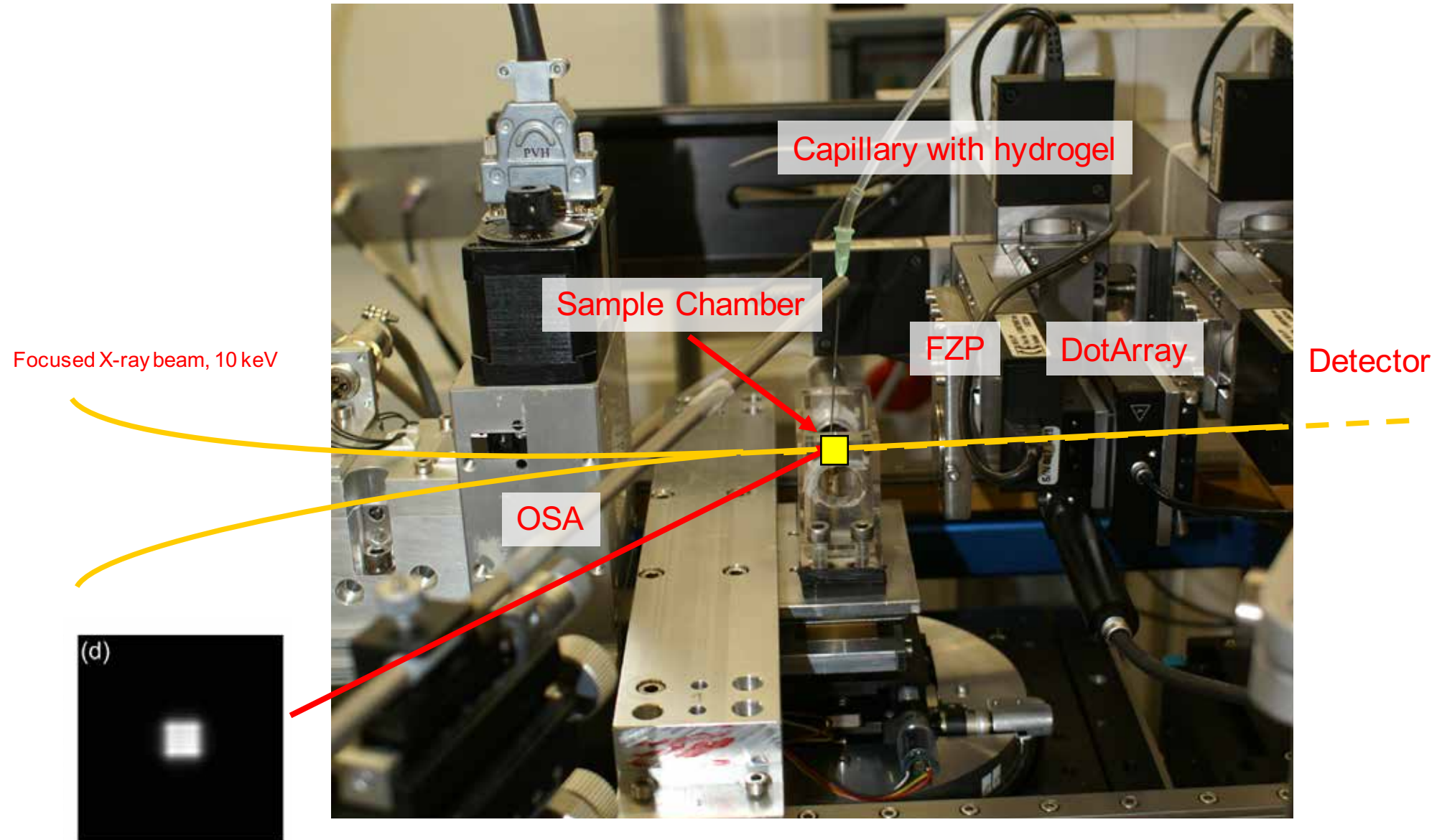
Mitosis ongoing...

- Fixed (not stained) cells on a 1 um Si_3Ni_4 membrane
- Zernike Phase contrast at 10 keV
- 30x30 um single shots
- Mesh scan over 1x1 mm

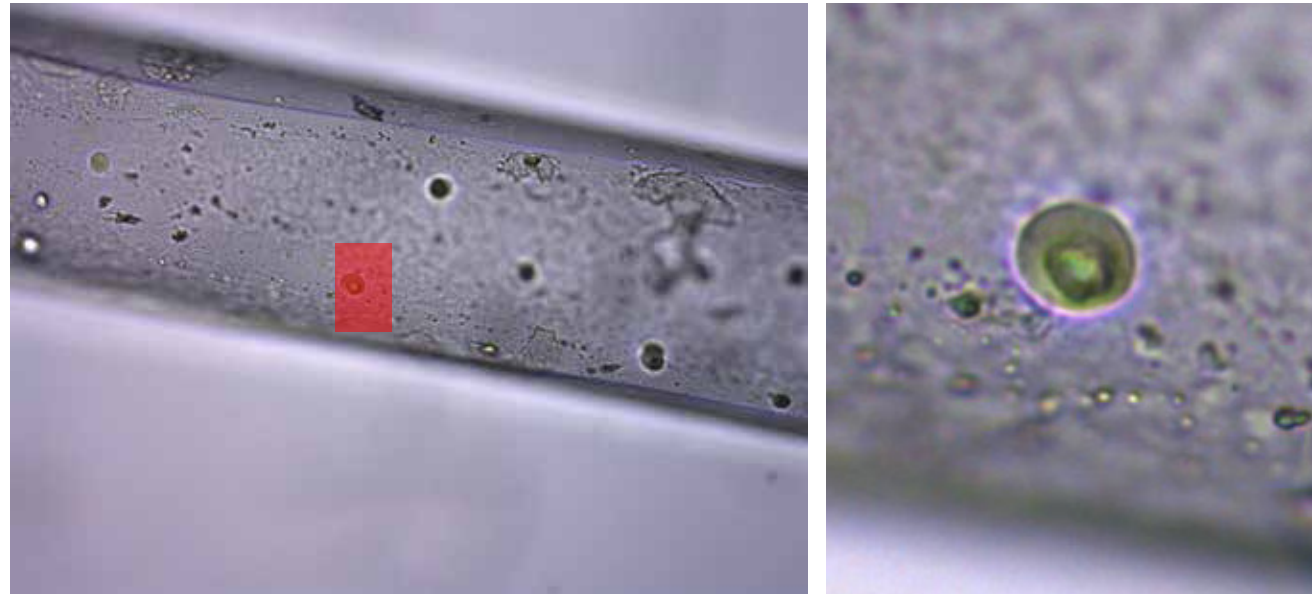
Mitosis just finished



Tomographic nanoimaging of MC3-preosteoblast cell

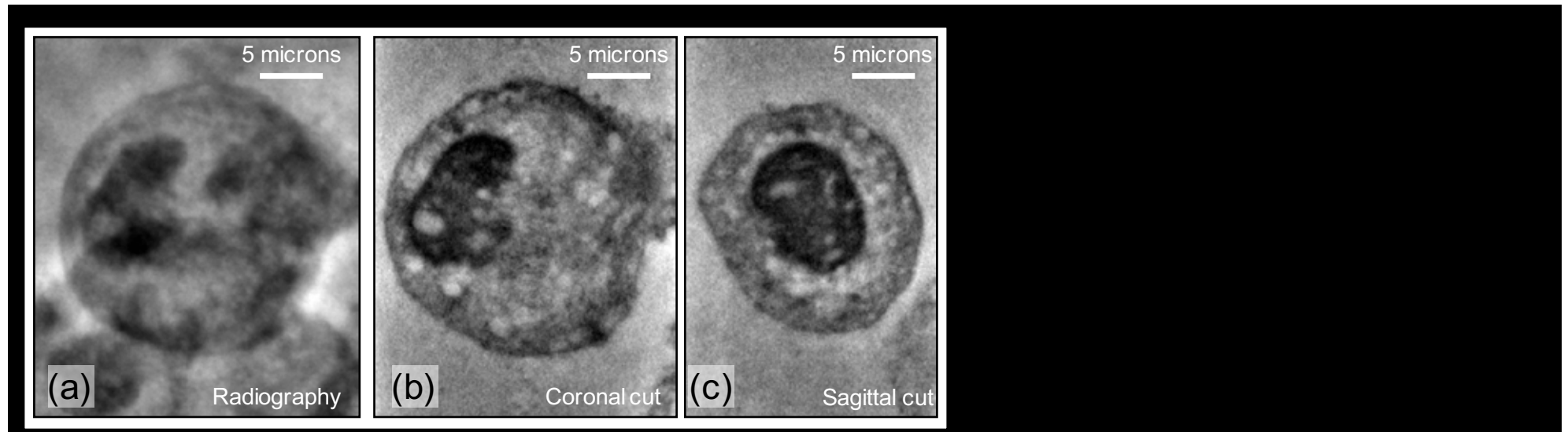


Nanotomography of a MC3-preosteoblast cell



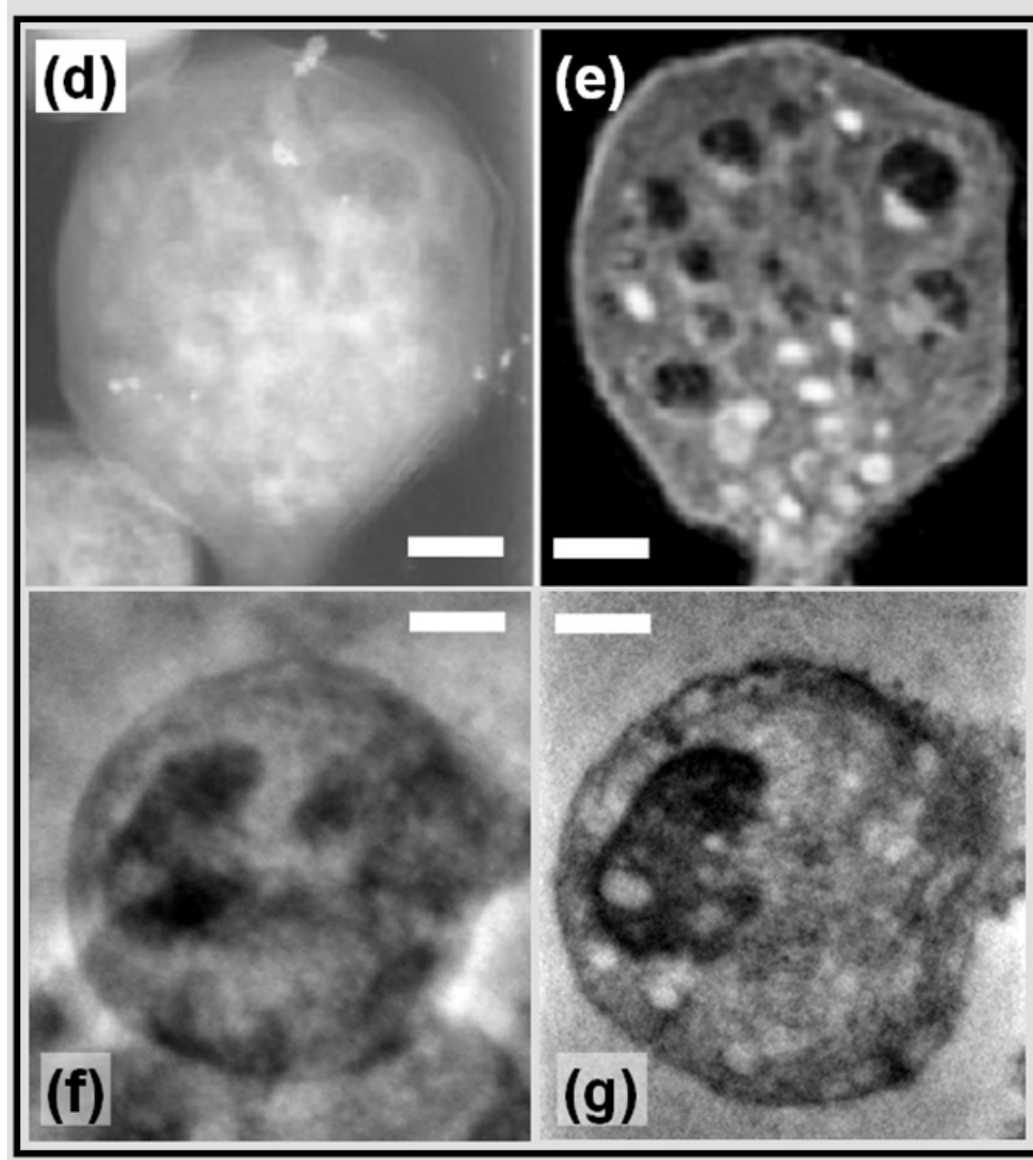
TOMCAT Nanoscope

- 10 keV (!)
- Pixel size: 70 nm
- True 3D res: ~ 200 nm
- High penetration power !
- High depth of focus !



M. Stampanoni et al., PRB2010

Soft vs Hard X-ray *tomographic* imaging of cells



ALS: XM-1 Microscope

- Water window operation
- Pixel size: 50 nm
- True resolution: >100 nm
- Optics in vacuum
- Sample cryo-cooled
- Single cells in 20 microns capillary

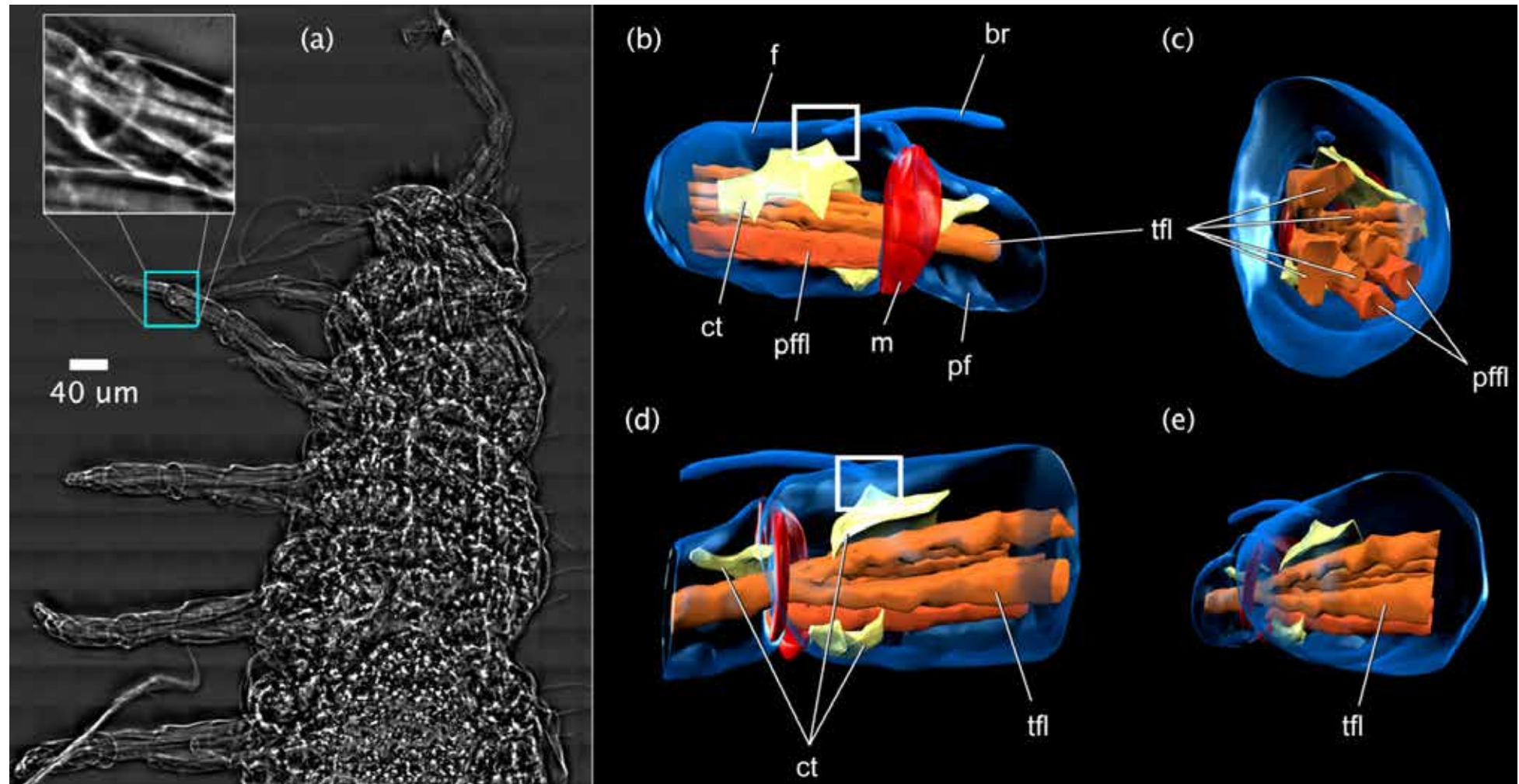
C.A. Larabell et al., Molecular Biology of the Cell, 15(3), 956-962, 2004

TOMCAT Nanoscope

- 10 keV
- Pixel Size 70 nm
- True 3D res: ~ 200 nm
- High penetration power !
- High depth of focus !
- No cooling
- Sample in large capillary
- Lower dose-deposition (?)

M. Stampanoni et al., PRB2010

Soil-dwelling micro-arthropod (*Pauropoda* sp.)



(a) Stiched 2D projection of *Pauropus* species.

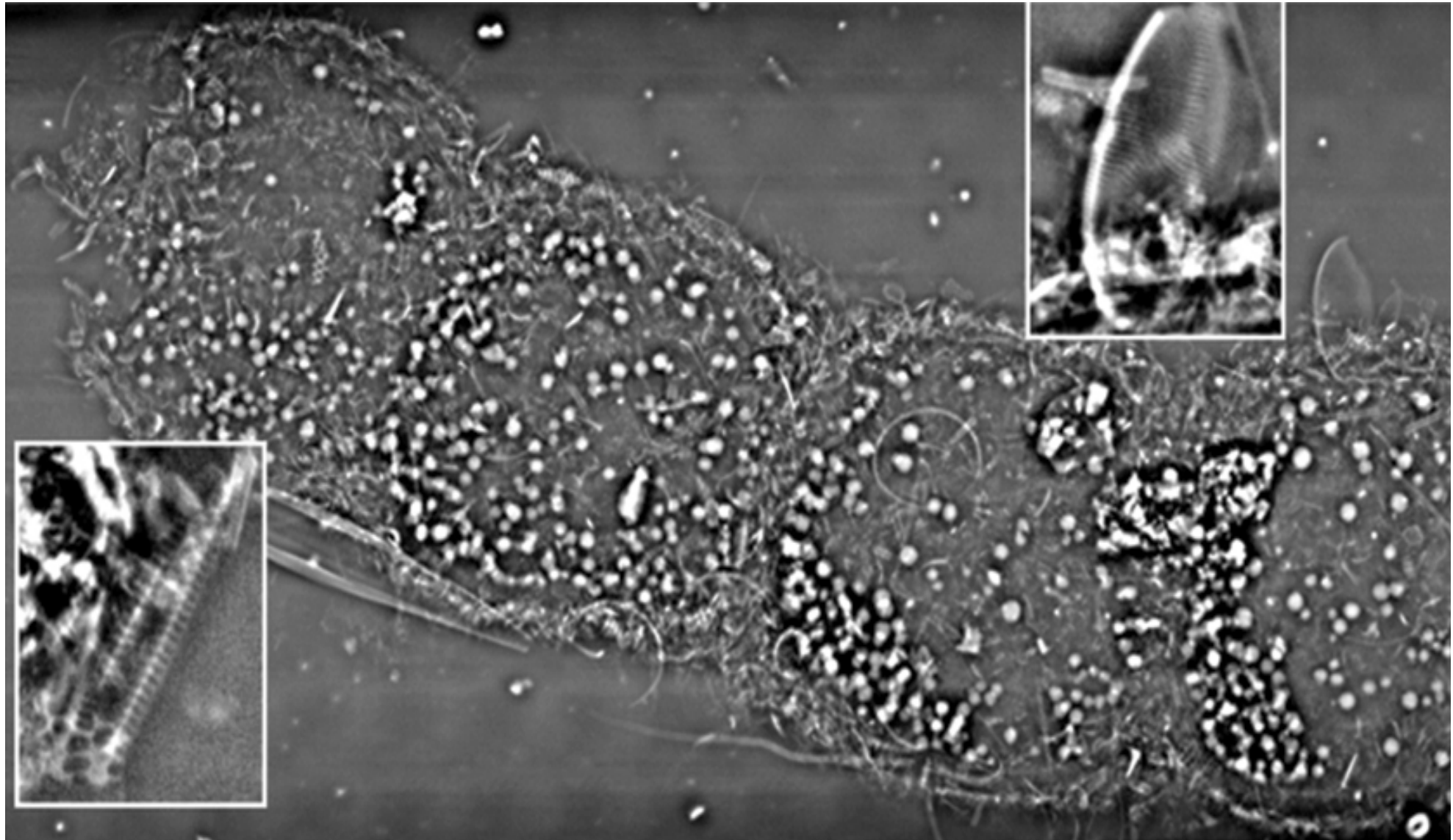
(b-e) Volume rendering of the tomographic reconstruction of the femur-postfemur articulation and muscle groups.

The colormap highlights the cuticle (blue, partly transparent), muscles (orange), connective tissue (yellow), and membranes (red)

(b), anterior view; (c), mesolateral view; (d), posteroir view; (e), mesoanterad view.

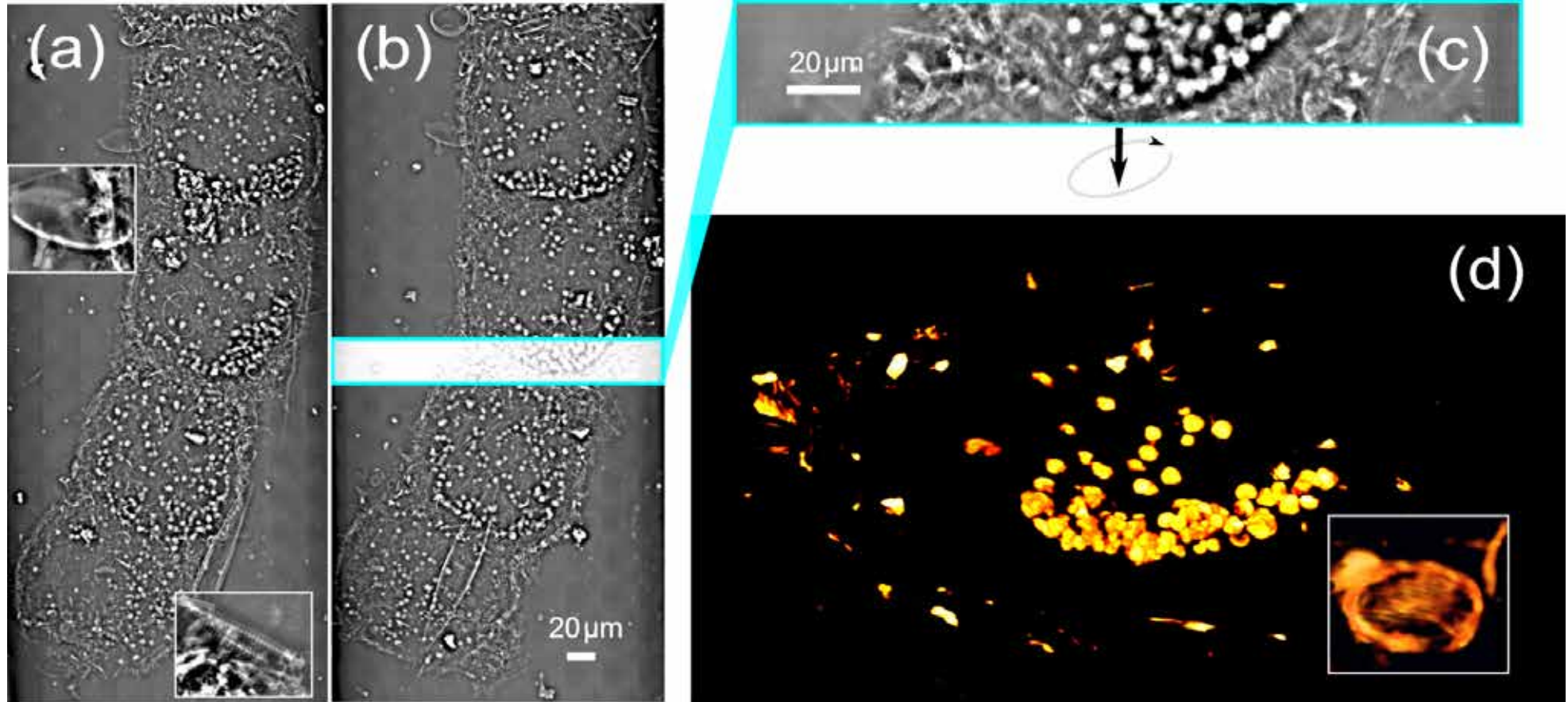
R. Mokso et al., JSB2012

Thiomargarita namibiensis



→ Solution: mosaic nano-radiography and nano-tomography

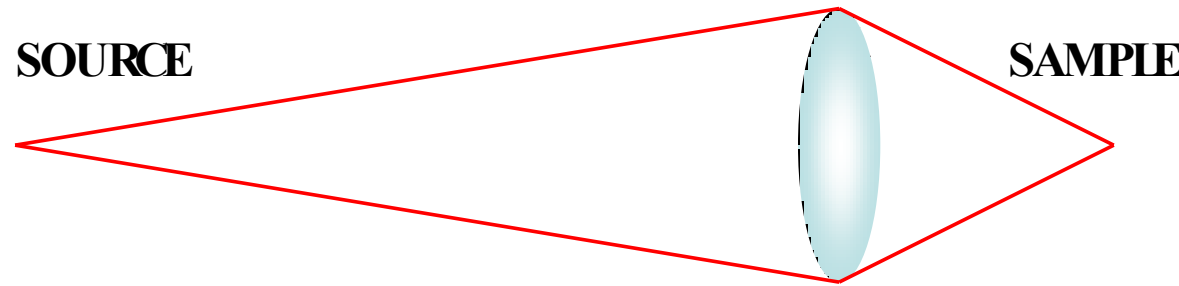
Nano-mosaic (3D): *Thiomargarita namibiensis*



- (a) and (b) 2D mosaic images, at 0° and 45° respectively, consisting of 9×20 radiographic images obtained through raster scanning the sample in full-field microscopy mode.
- (c) shows a row of 1×6 images used for the tomography by combining 73 angular positions.
- (d) 3D rendering of the inclusions.

→ First time determination of accurate 3D distribution of the sulfur inclusions at the periphery of the cell (including volumetric distribution)

X-ray optics



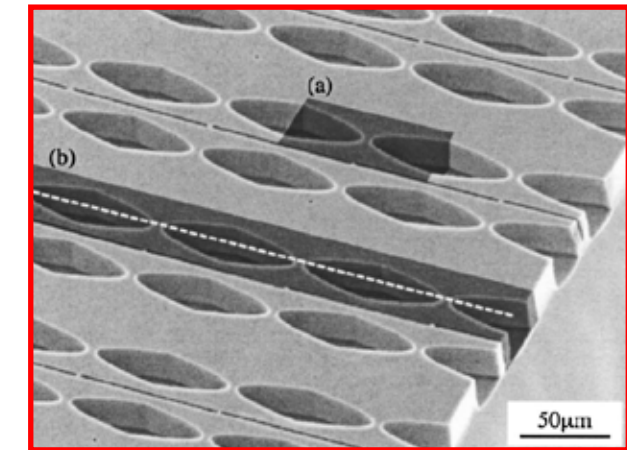
Diffractive lenses

Fresnel Zone plates
Crystals
Multilayers



Mirrors

KB-systems
Wolter mirrors
Capillary optics
Microchannels



Refractive lenses

Compound refractive lenses

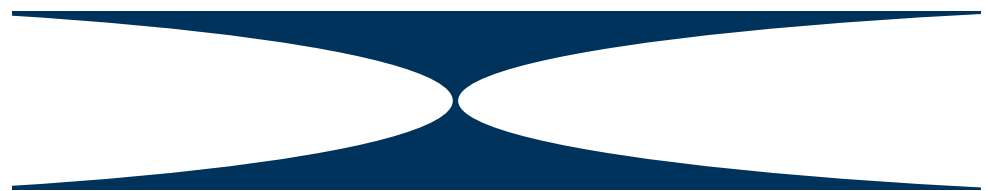
Refractive lenses



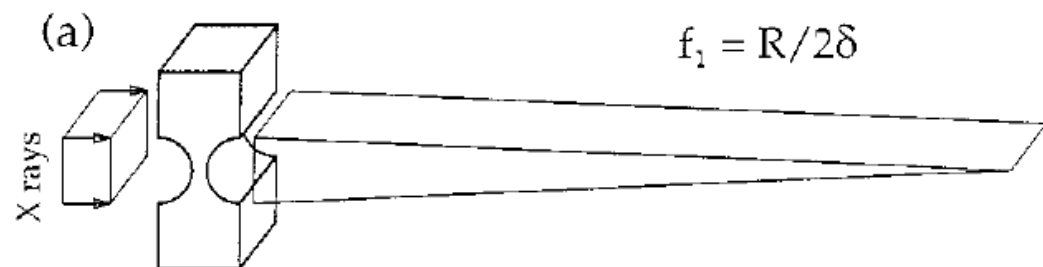
Focusing lens
for $n > 1$



Focusing lens
for $n < 1$

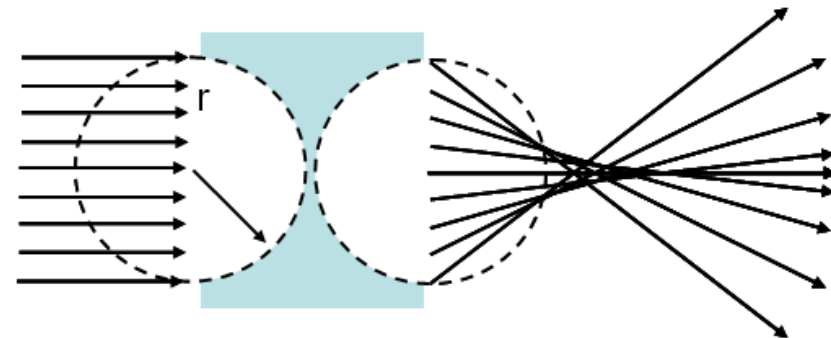


Focusing lens
for small δ

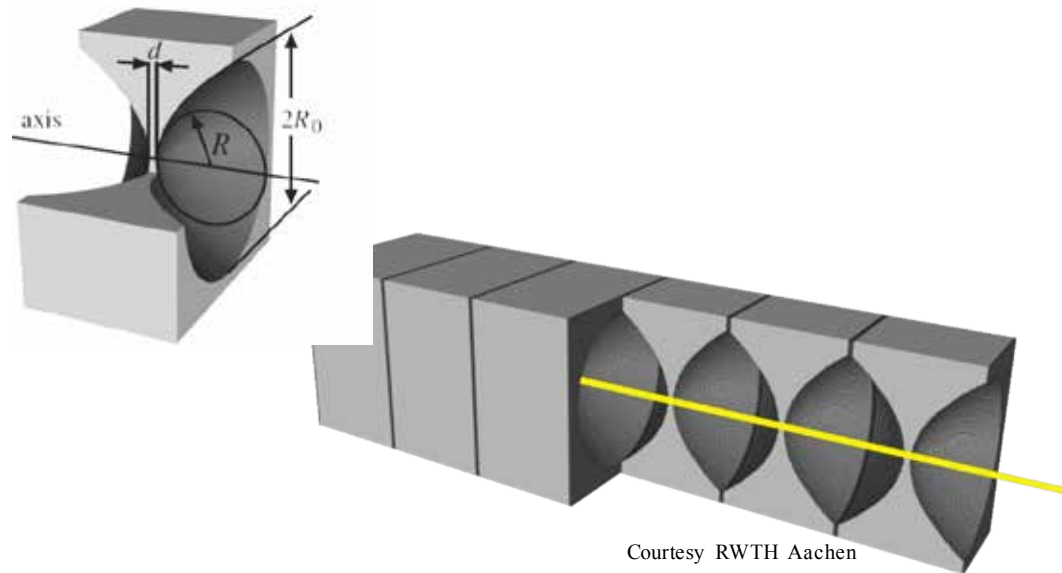


A. Snigirev et al., Applied Optics 37 (4), 653, 1998
A. Snigirev et al., Nature 384, 49, 1996

Refractive lenses



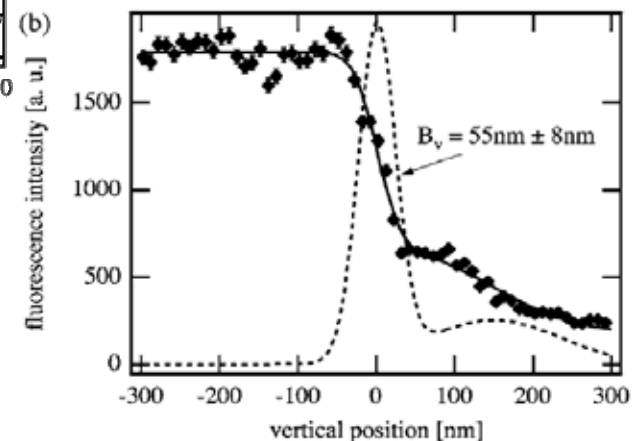
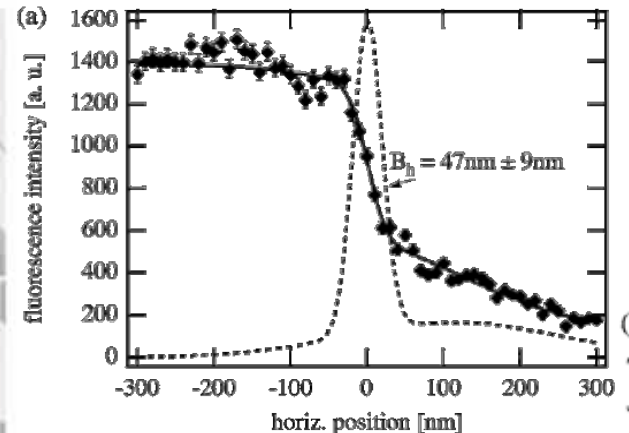
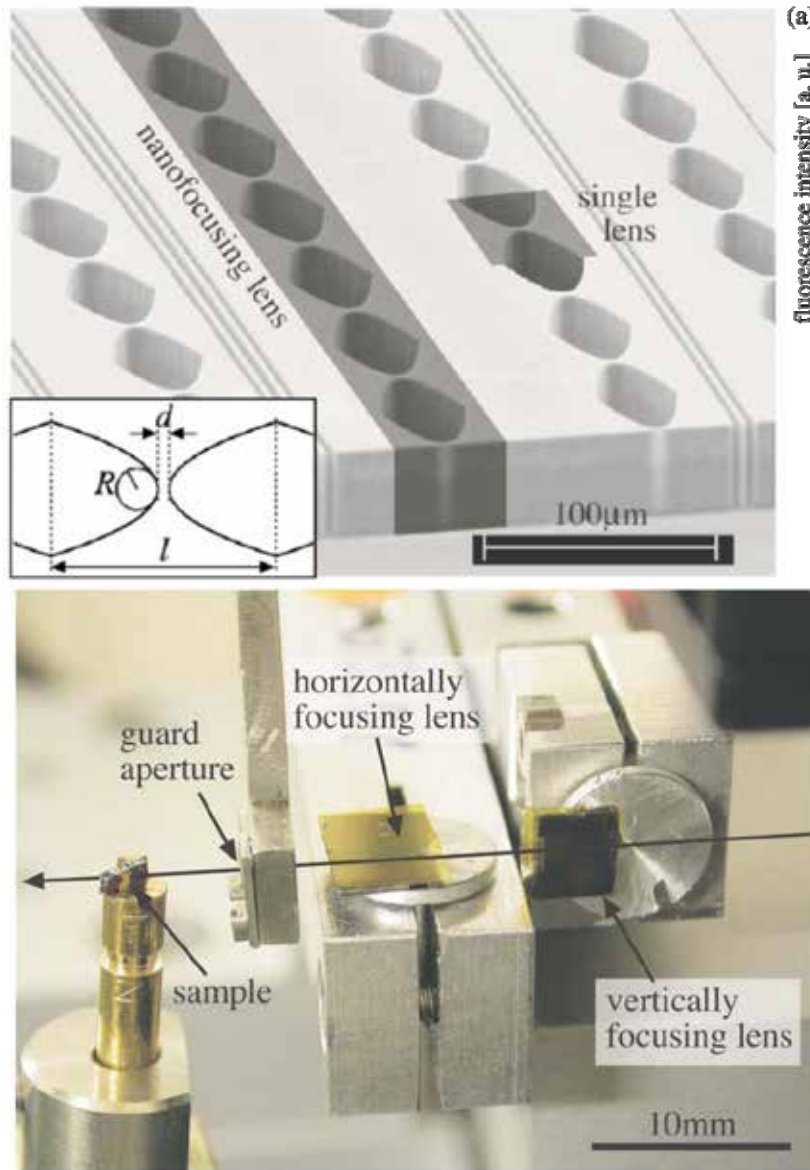
spherical lens
=> spherical aberrations



- Useful, very robust devices
- Resolution limited by shape errors to $\sim 1\mu\text{m}$
- Only efficient for hard x-rays
- Very chromatic: $f \sim E^2$

B. Lengeler et al., J. Phys. D: Appl. Phys. 38 (2005) A218–A222

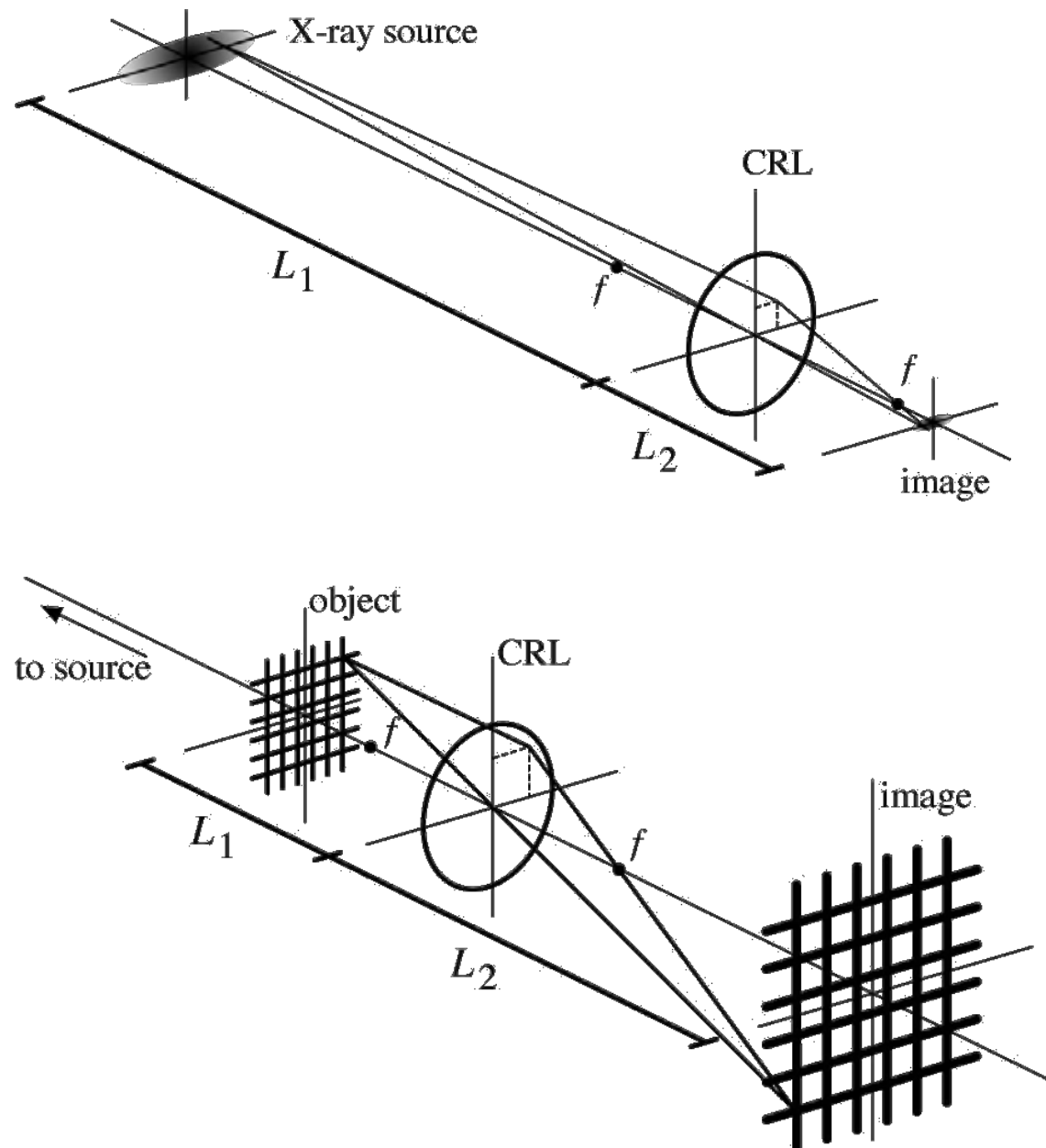
Silicon planar refractive lenses



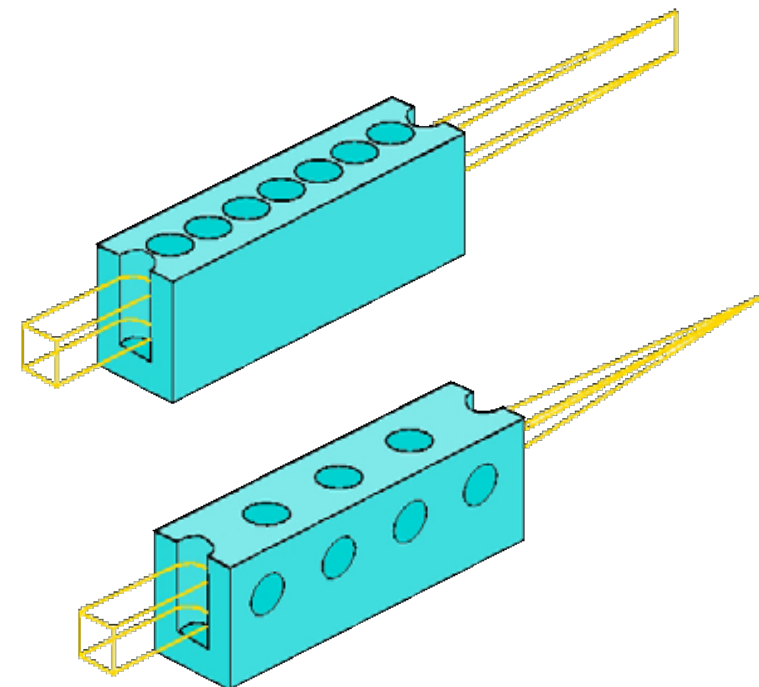
- Planar refractive lenses etched into silicon
- Small dimensions allow for high precision
- Close to diffraction limited resolution
- About **50nm x 50nm** measured @ 20keV for two orthogonal sets of lenses
- Called Nanofocusing lenses (NFLs)

C. Schroer et al., APL 87, 124103, (2005)

CRL in action...

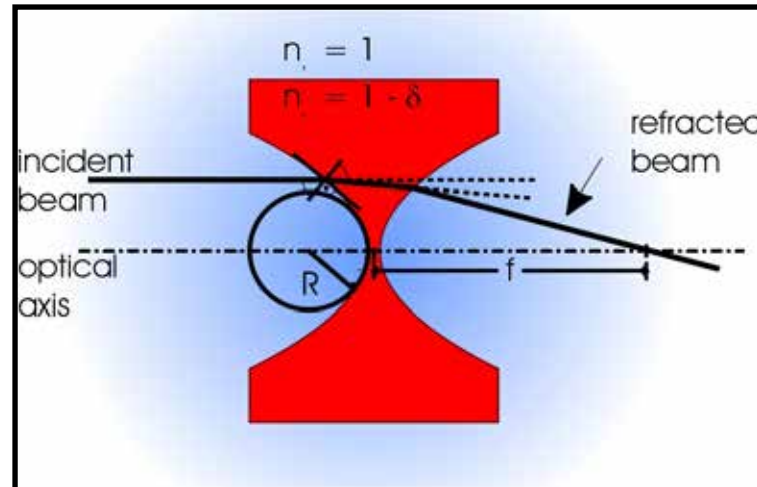


An X-ray source (undulator) with elliptical profile can be imaged through a compound refractive lens to obtain a small focal spot.

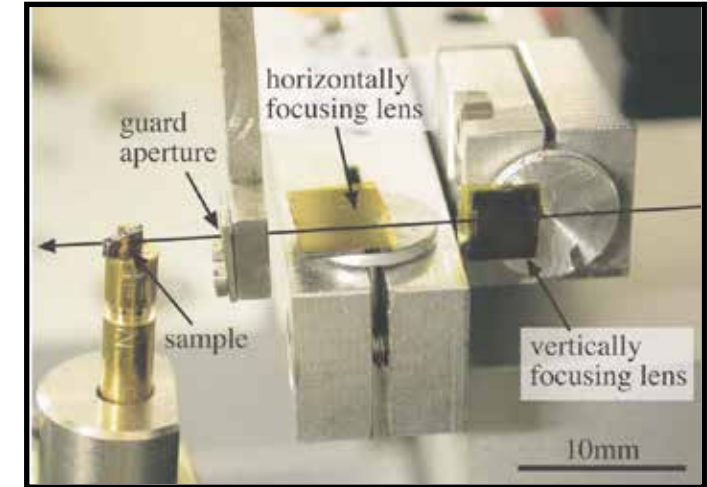


With CRL that have parabolic shape and rotational symmetry around the optical axis it is possible to image an object illuminated by hard X-rays onto a position sensitive detector

Take home message CRL



$$f = \frac{R}{2N\delta}$$

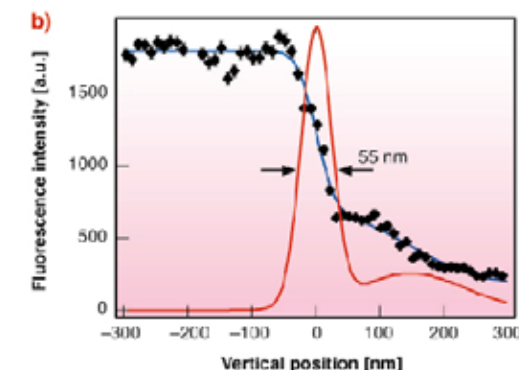
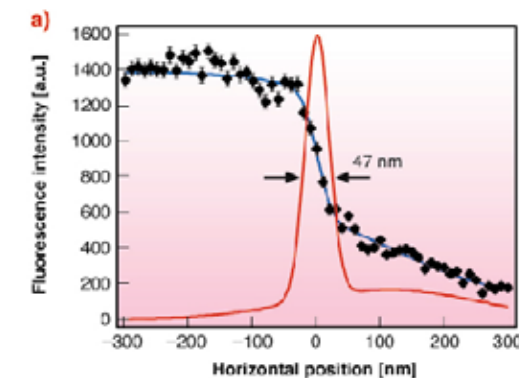


■ Advantages:

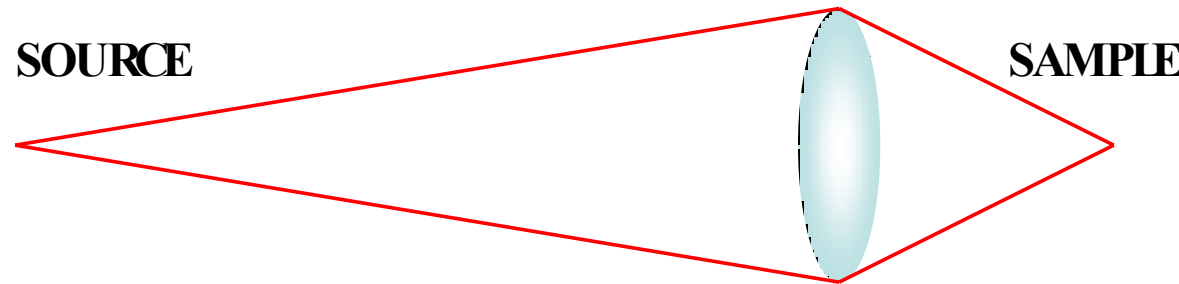
- CRL can produce nm focused beam
- Manufacture is simple and low cost
- Low sensitivity to heat load

■ Disadvantages:

- Efficiency is limited by absorption
- Small numerical aperture
- Strong chromatic aberration

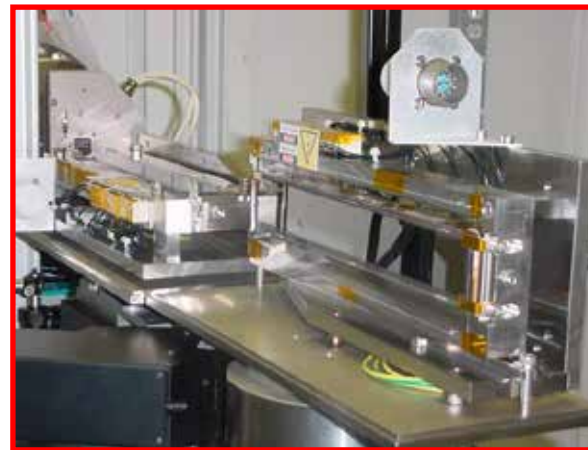


X-ray optics



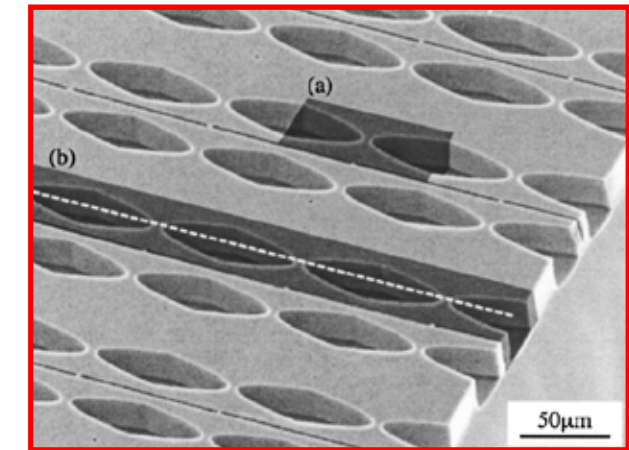
Diffractive lenses

Fresnel Zone plates
Crystals
Multilayers



Mirrors

KB-systems
Wolter mirrors
Capillary optics
Microchannels

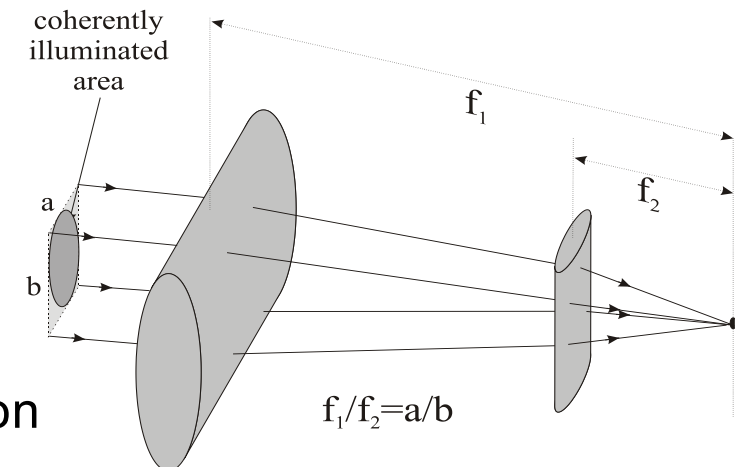
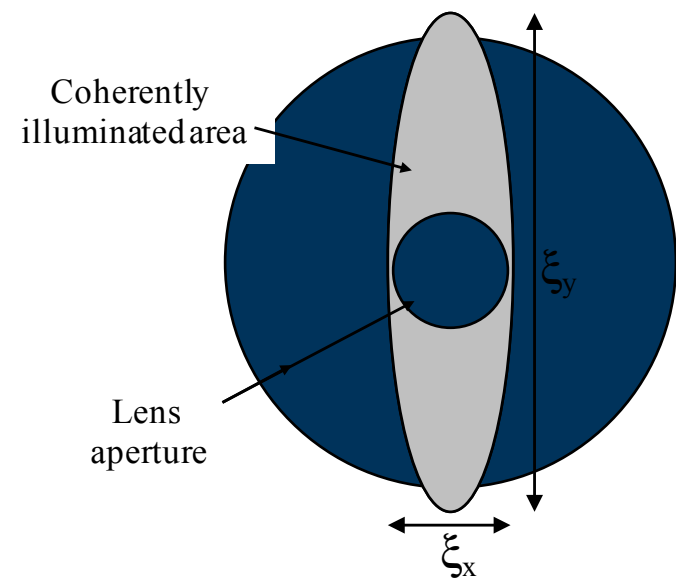


Refractive lenses

Compound refractive lenses

2-dimensional focusing

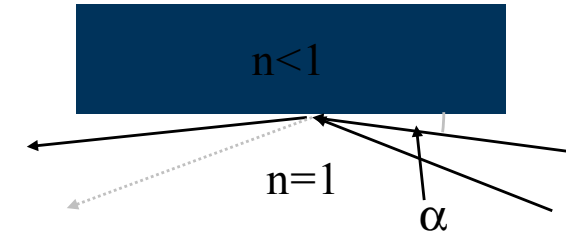
- On a synchrotron the hor. source size is usually larger than the vert. source size
 $\Rightarrow \xi_x < \xi_y$
- How can I collect all the coherent photons and focus in a small (diffraction limited) spot?
- For a lens aperture $D \approx \xi_x$ diffraction limited focusing is possible, but most coherent photons are lost
- For a lens aperture $D \approx \xi_y$ all coherent photons are collected, but also incoherent photons.
 \Rightarrow horizontal resolution goes down
- Solution: separate focusing in hor. and vert. direction



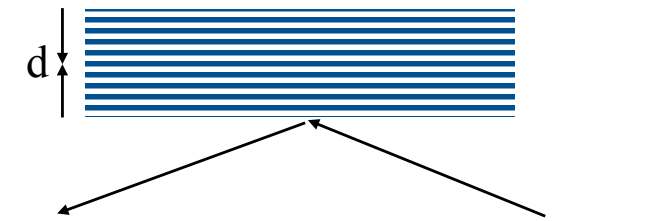
Slide courtesy C. David, PSI

Focusing mirrors

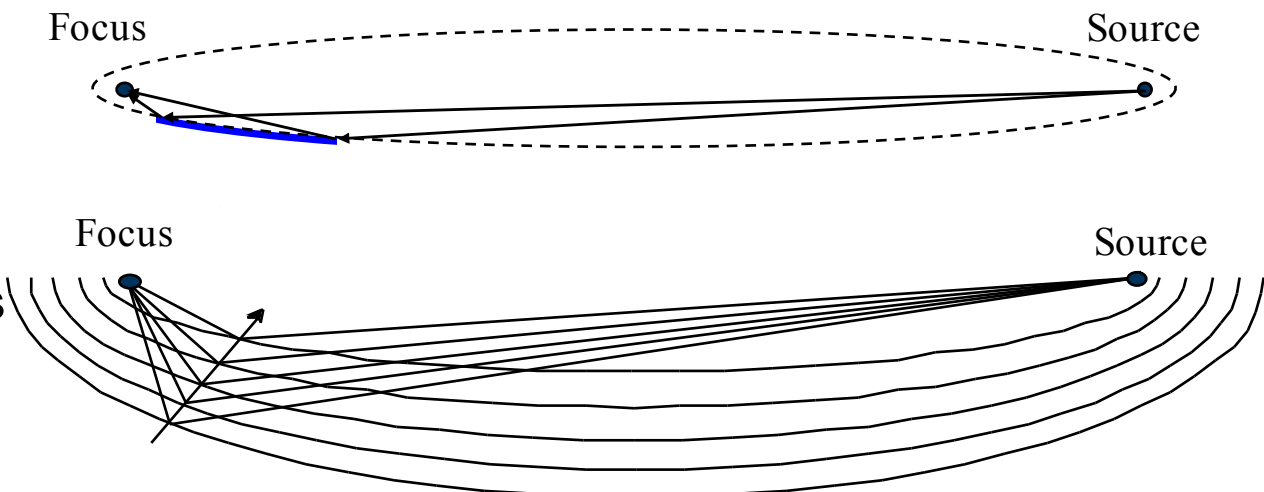
- For x-rays, $n = 1 - \delta - i\beta$ with $\text{Re}(n) < 1$
→ Reflection on a surface only in *total reflection* for $\alpha \leq \alpha_{\text{crit}}$, i.e. at *grazing incidence* (e.g. Rh, $\lambda=1 \text{ \AA}$, $\alpha_{\text{crit}} \approx 0.3^\circ$)



- Larger reflection angles can be obtained by multilayer mirrors with $\lambda = 2d \sin \alpha$
- Focusing mirrors surfaces are paraboloids



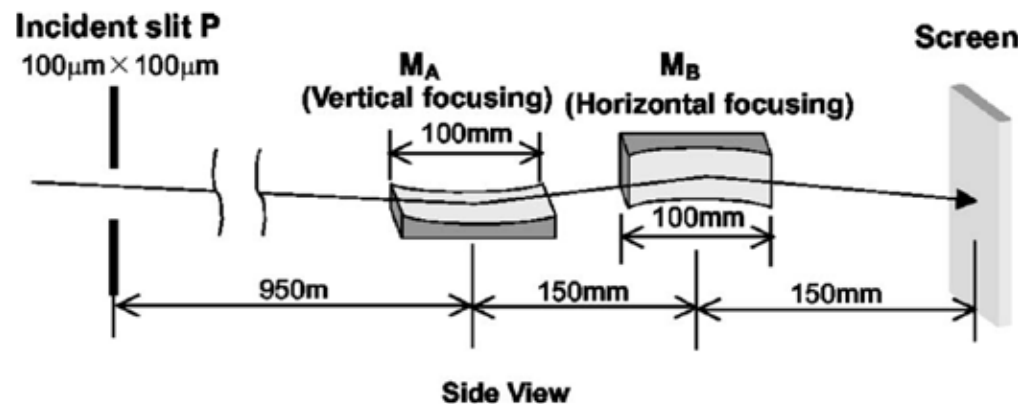
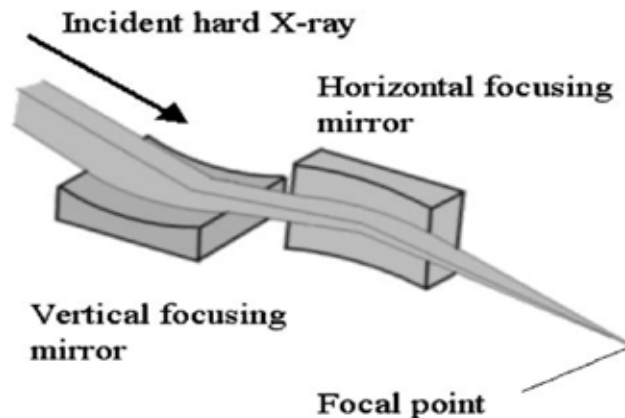
- Focusing multilayer mirrors require graded MLs



Slide courtesy C. David, PSI

Focusing mirrors

- Grazing incidence requires long footprints (many centimeters)
 - extremely difficult to make 2D-focusing mirror surfaces
 - all high resolution hard x-ray mirrors are KB-systems



KB mirror system for at 15 keV by H. Mimura et al. (Univ. of Tokyo)

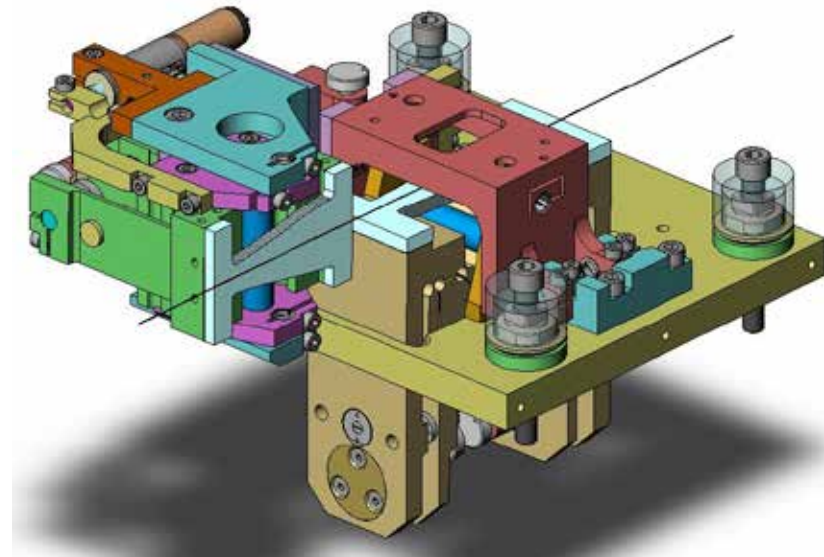
Involves various advanced polishing and metrology techniques to achieve a figure error of **below 2nm!**

World record:

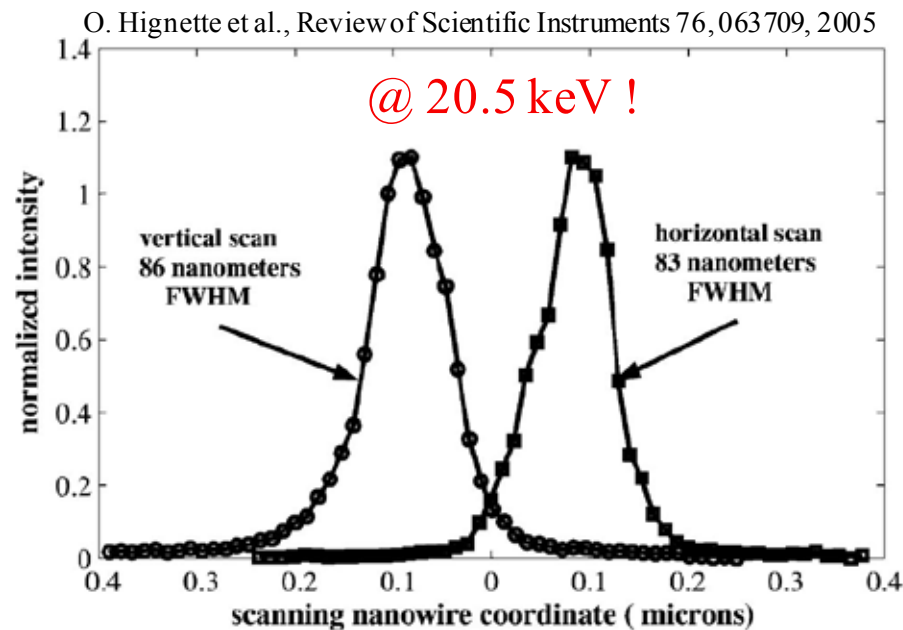
36nm x 48nm FWHM resolution for 100 μm x 100 μm aperture

Slide courtesy C. David, PSI

Focusing with multilayer KB-system

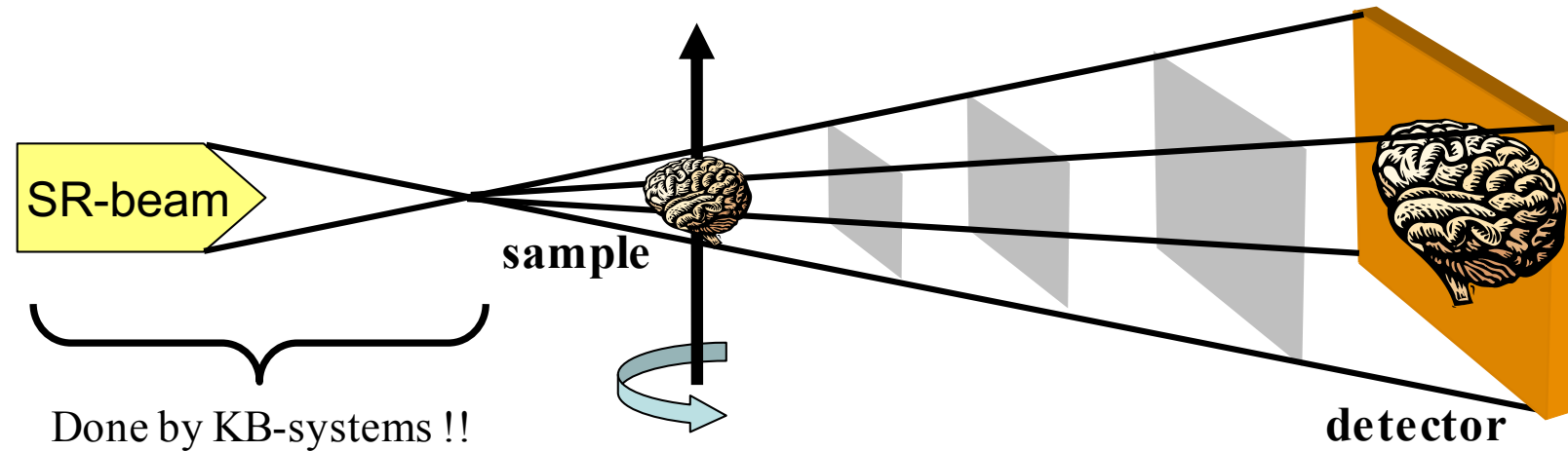


- Two orthogonal mirrors for successive horizontal and vertical focus
- Static system, with mirrors optimized for a given incidence angle and focus.
- Dynamic system, with actuators bending flat mirrors into the elliptic shapes required by the experiment.



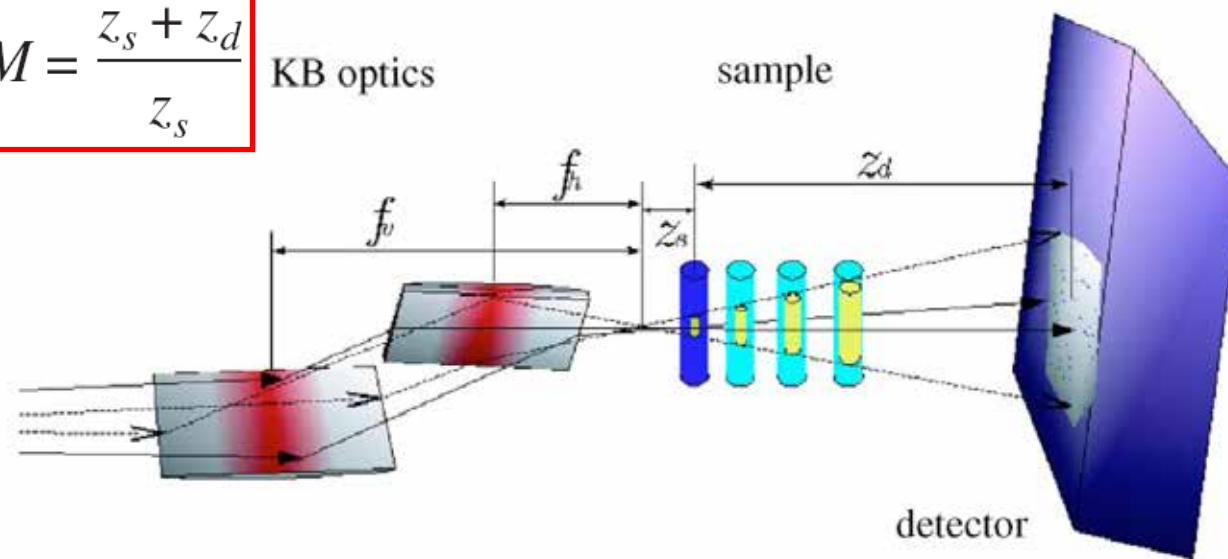
- Achromatic reflection: a wide range of X-ray wavelengths are reflected.
- Experiments requiring energy tuning can be performed without any readjustment of the optics.
- A combination of different metal and multilayer coatings makes it possible to cover the range from 2 keV to 90 keV.

Projection microscopy



$$M = \frac{z_s + z_d}{z_s}$$

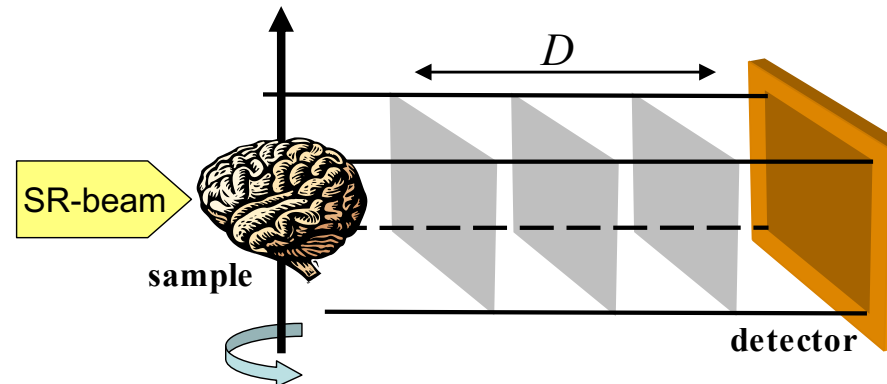
KB optics



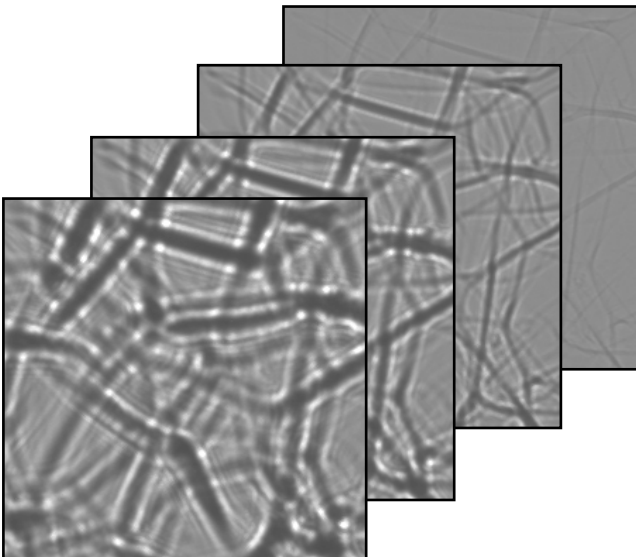
Mokso et al., Applied Physics Letters 90, 144104 2007

Remember: phase retrieval in the near field

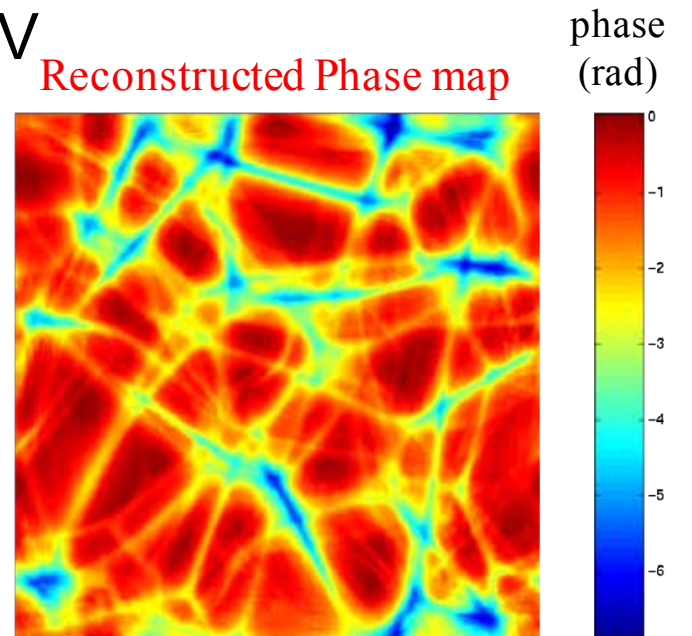
- Acquire images at multiple detector distances
- Retrieve the phase considering free-space propagation



- Example: non-absorbing foam @ 18 keV

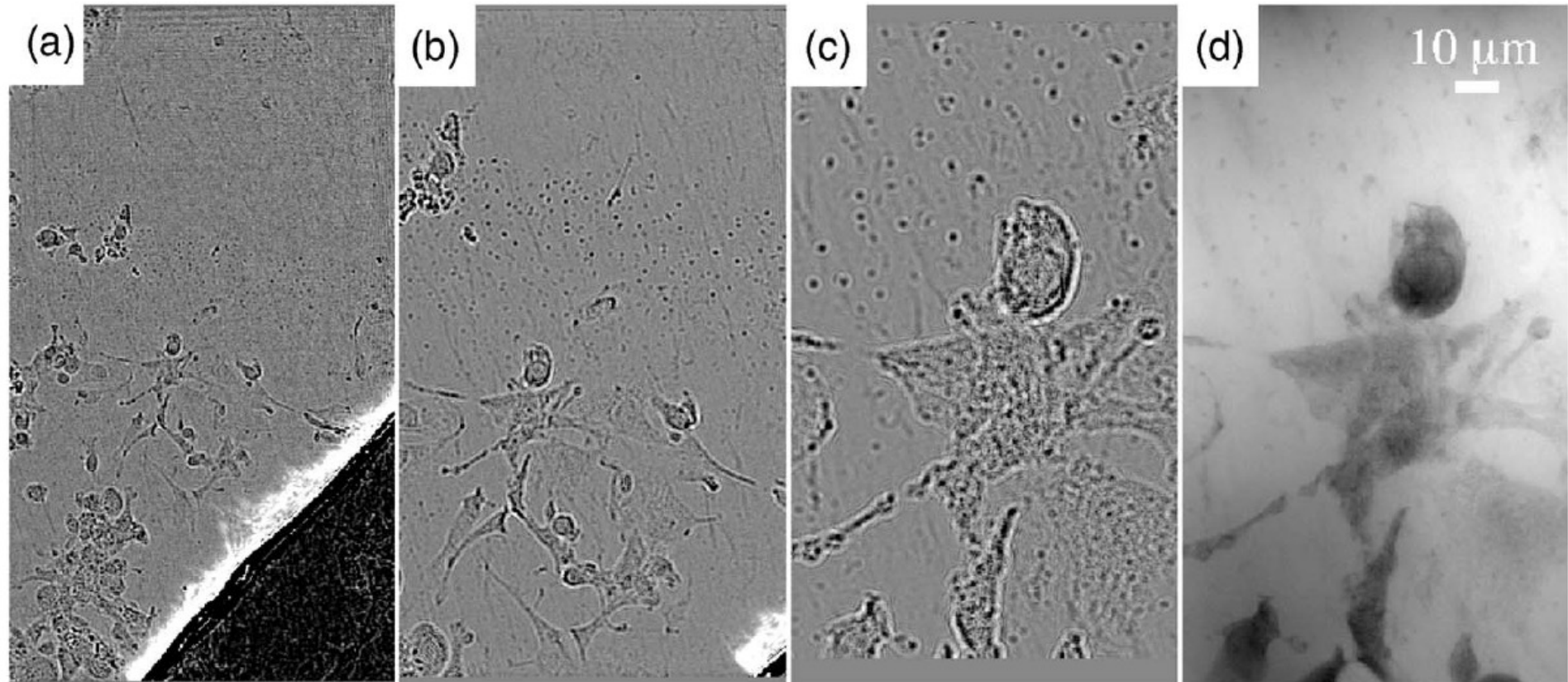


(Phase retrieval algorithm
Cloetens et al., Applied Physics
Letter 75, 2912, 1999)



Fixed neuron

Mokso et al., Applied Physics Letters 90, 144104 2007

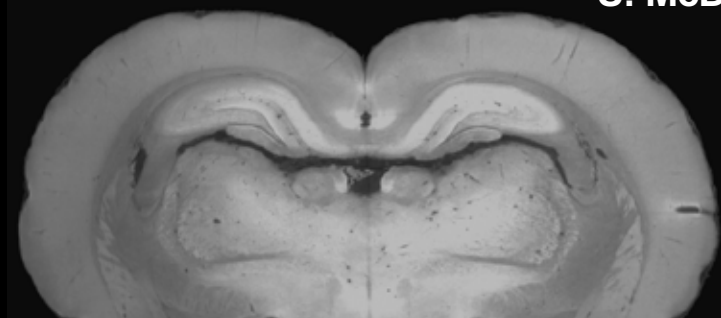


Magnified radiography of a fixed neuron cell demonstrating the effect of the sample-to-focus distance z_s on the magnification M and equivalent propagation distance D . The radiographs were recorded at z_s of (a) 225 mm, 175 mm, (b) 125 mm, 75 mm and (c) 45 mm.

Combining numerically five radiographs a phase map d with a pixel size of 85 nm is retrieved (see phase contrast imaging...)

Let push the resolution further...

S. McDonald, M. Stampanoni et al., JSR 2010
→ Grating interferometry



E.M. Friis, M. Stampanoni et al., Nature 2007

→ Modified Transport of Intensity

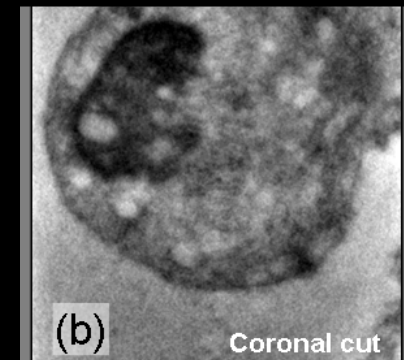
Pushing the limits !
Going below 10 nm...

10 microns

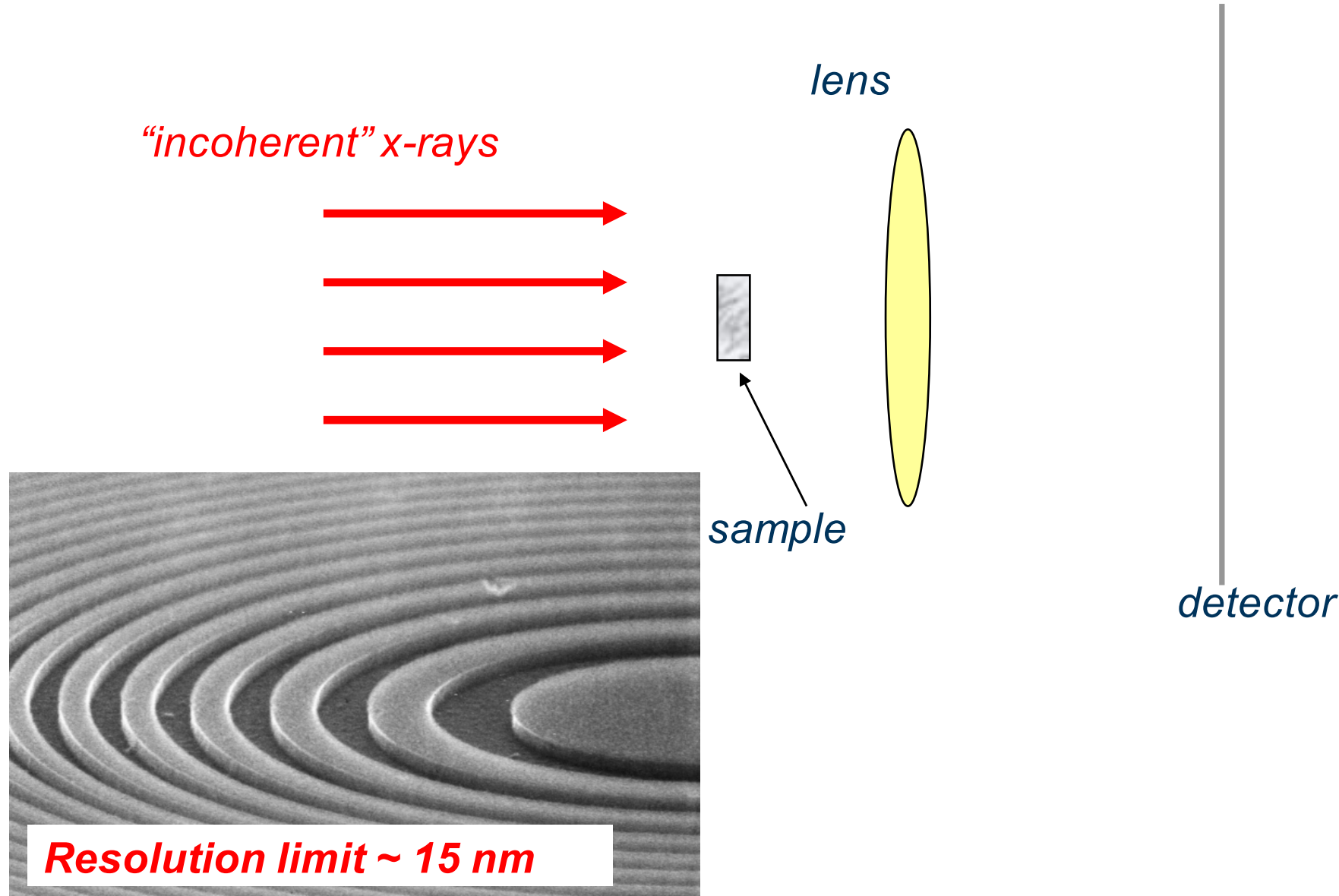
1 micron

0.1 micron

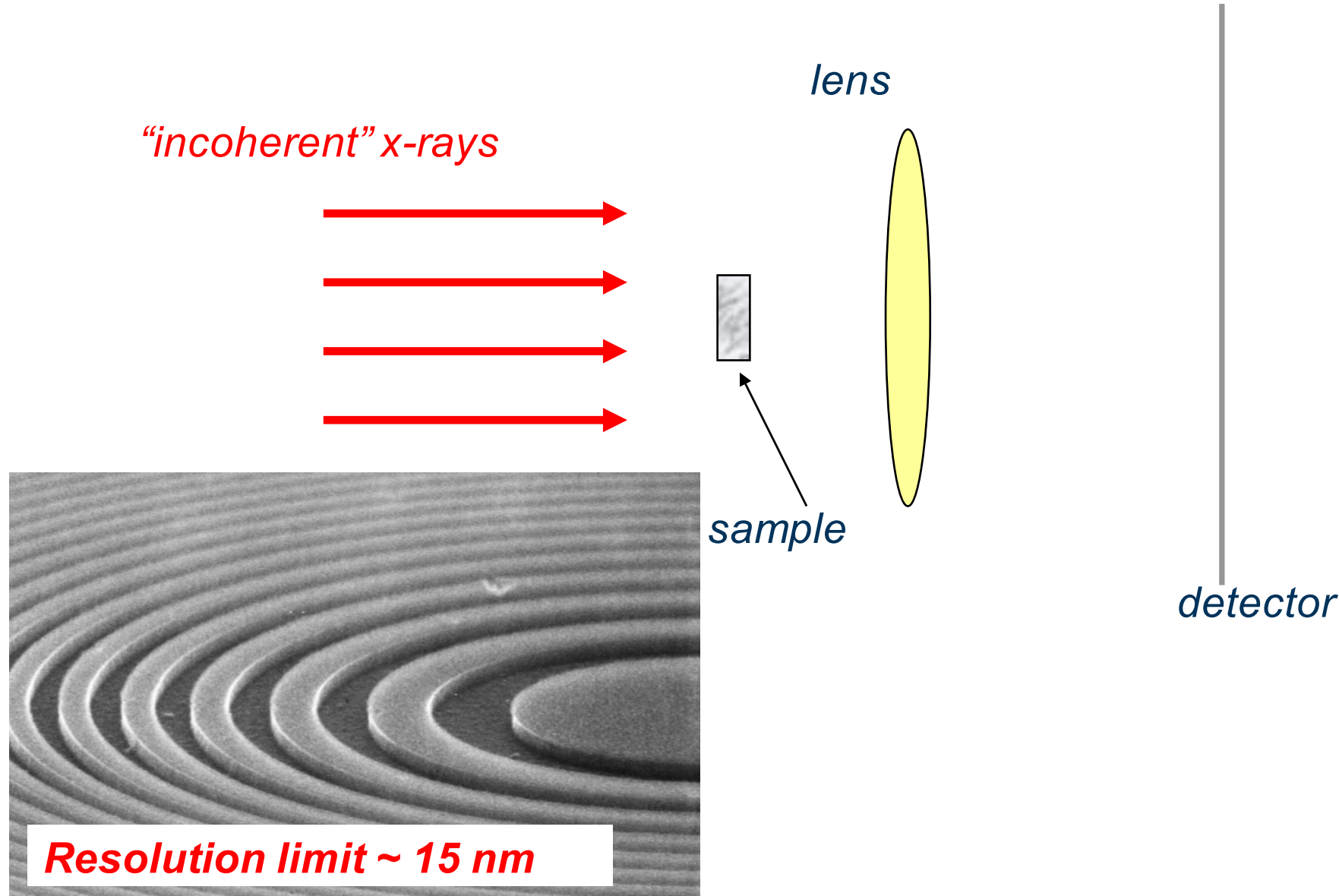
M. Stampanoni et al., PRB 2010
→ Hard X-ray Microscopy Phase contrast



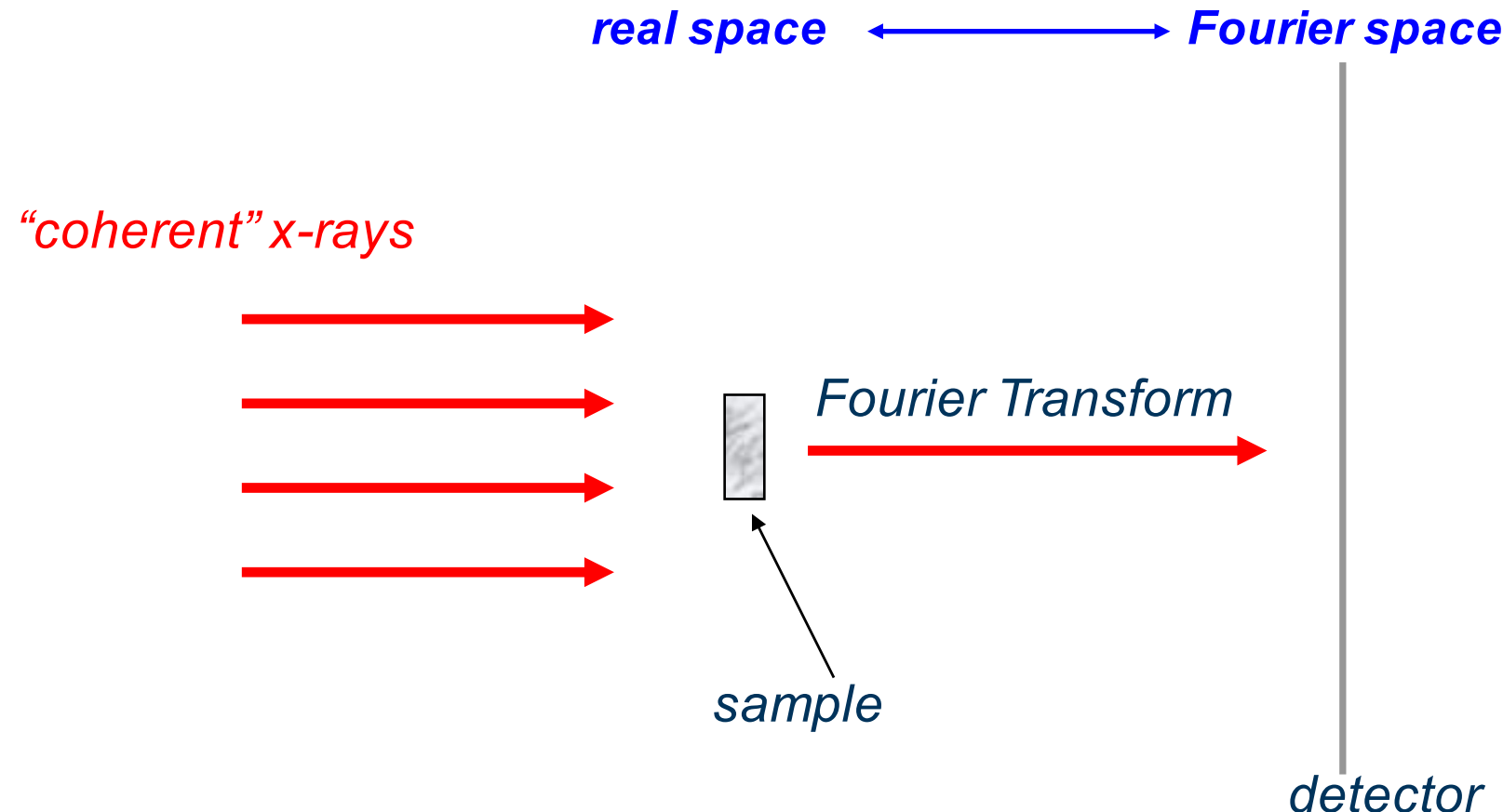
Classical bright-field X-ray microscopy



Coherent Diffractive Imaging

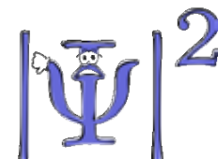


Coherent Diffractive Imaging



Coherence:

allows the interpretation of observations based on modeling of propagation and interaction with matter.

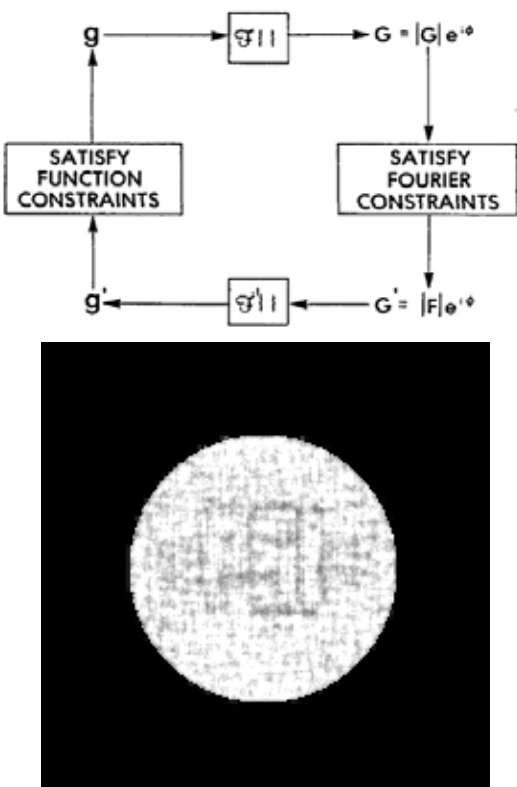
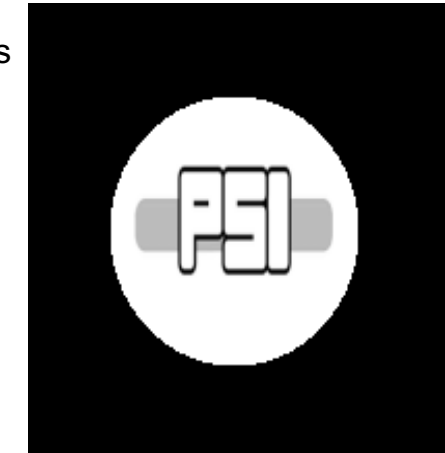


Measurement:

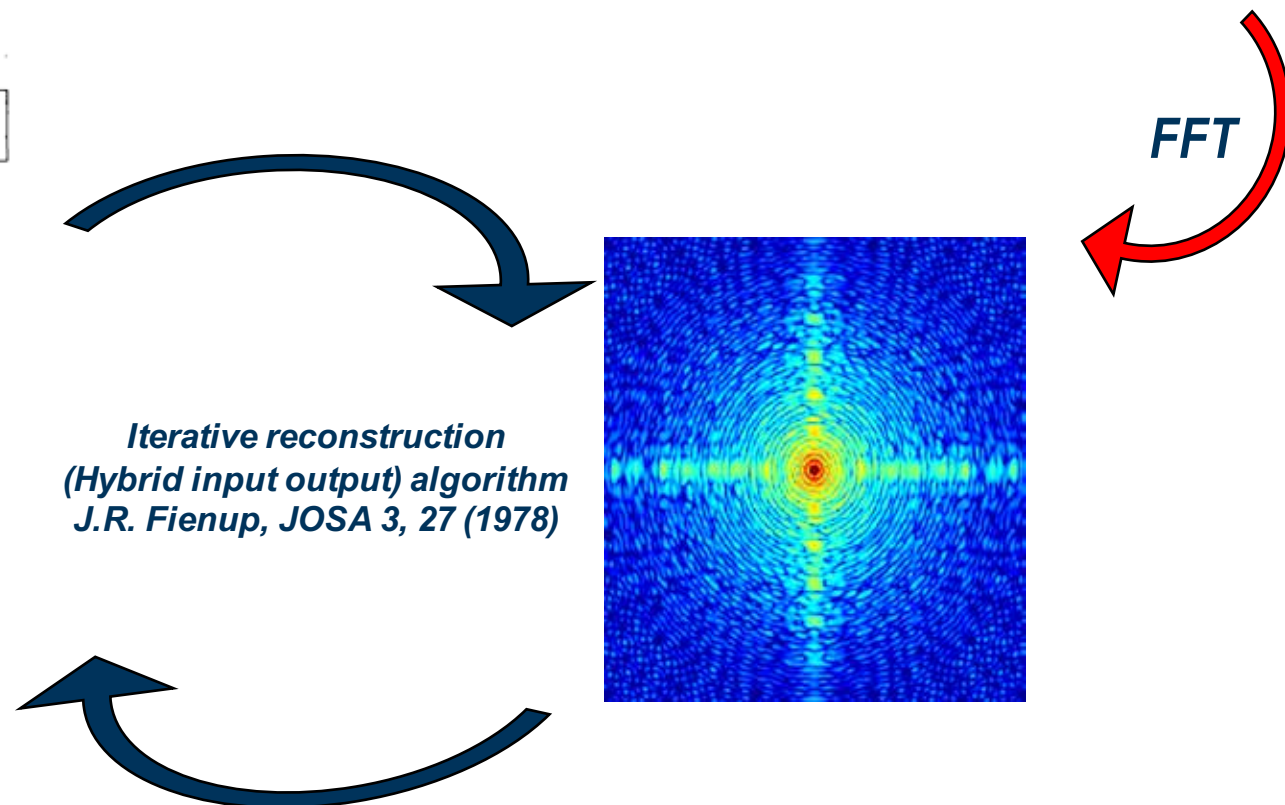
leads to the loss of a part of the information. This is the **phase** problem.

Diffraction Microscopy (simulation)

- Determining the phases of a diffraction pattern is crucial since the diffraction pattern of an object is its Fourier transform.
- Phase problem:
 - In order to properly inverse transform the diffraction pattern the phases must be known.
 - The amplitude however, can be measured from the intensity of the diffraction pattern and can thus be known experimentally.
- The HIO algorithm uses negative feedback in fourier space in order to progressively force the solution to conform to the fourier domain constraints (support).**

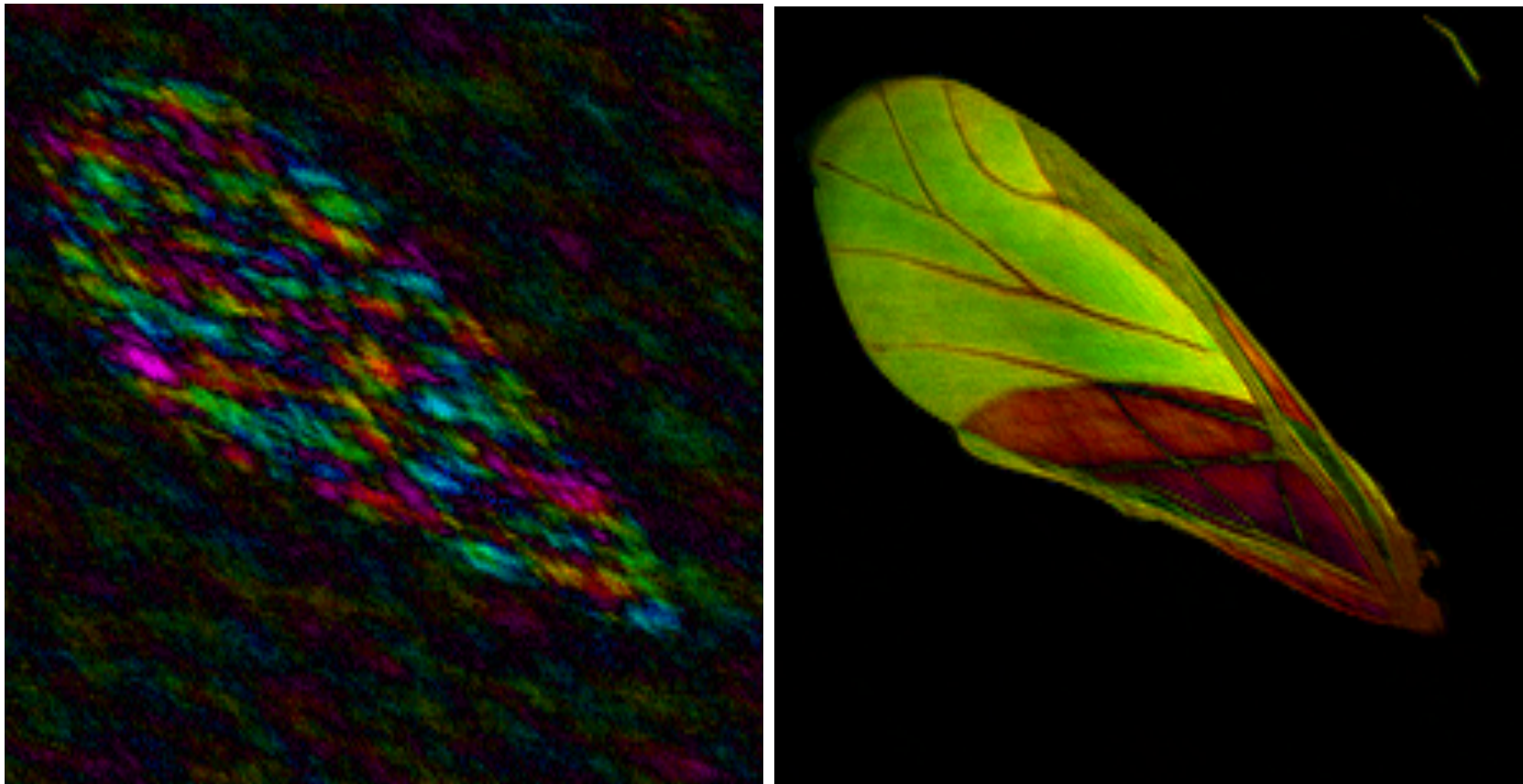


*Iterative reconstruction
(Hybrid input output) algorithm
J.R. Fienup, JOSA 3, 27 (1978)*



Diffraction microscopy (visible light)

Iterative reconstruction algorithm



Seminal Work: Fienup (1982), Appl. Opt. 21, 2758-2769, HIO

Elser (2003), J. Opt. Soc. Am. A20, 40-55

Slide courtesy of P. Thibault, PSI

First experimental demonstration of X-ray CDI

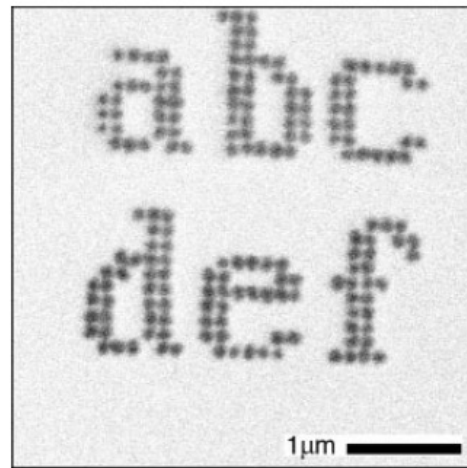


Figure 1 A scanning electron microscope image of the specimen. The specimen was fabricated by depositing gold dots, each ~ 100 nm in diameter and 80 nm thick, on a silicon nitride membrane.

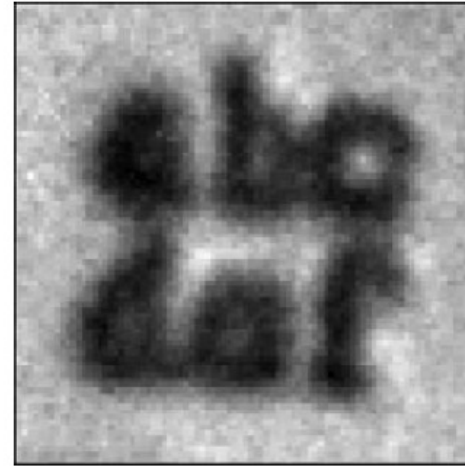


Figure 3 An optical microscope image of the specimen.

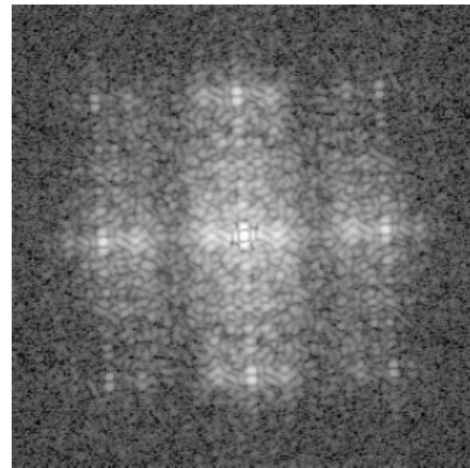


Figure 2 A diffraction pattern of the specimen (using a logarithmic intensity scale). The central 15-pixel-radius circular area is supplied by the squared magnitude of the Fourier transform of the optical microscope image (Fig. 3).

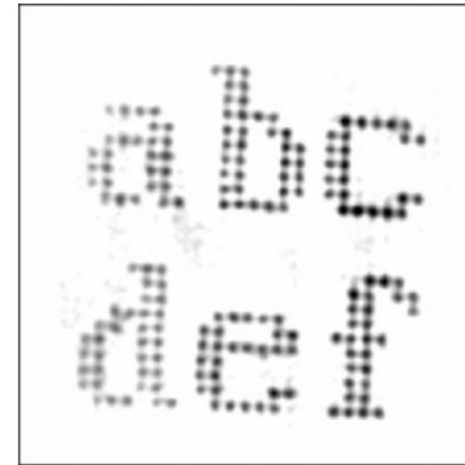


Figure 4 The specimen image as reconstructed from the diffraction pattern of Fig. 2.

J. Miao et al., Nature 400, Jul. 22, 1999

CDI on biological sample (soft X-rays)

PNAS

Biological imaging by soft x-ray diffraction microscopy

David Shapiro*, Pierre Thibault†, Tobias Beetz*‡, Veit Elser†, Malcolm Howells§, Chris Jacobsen*‡¶, Janos Kirz*, Enju Lima*, Huijie Miao*, Aaron M. Neiman¶, and David Sayre*

*Department of Physics and Astronomy, Stony Brook University, Stony Brook, NY 11794-3800; †Department of Physics, Cornell University, Ithaca, NY 14853;

§Advanced Light Source, Lawrence Berkeley National Laboratory, Berkeley, CA 94720; ¶Department of Biochemistry and Cell Biology, Stony Brook University, Stony Brook, NY 11794-5215; and ‡Center for Functional Nanomaterials, Brookhaven National Laboratory, Upton, NY 11973

Edited by Margaret M. Murnane, University of Colorado, Boulder, CO, and approved August 24, 2005 (received for review April 21, 2005)

We have used the method of x-ray diffraction microscopy to image the complex-valued exit wave of an intact and unstained yeast cell. The images of the freeze-dried cell, obtained by using 750-eV x-rays from different angular orientations, portray several of the cell's major internal components to 30-nm resolution. The good agreement among the independently recovered structures demonstrates the accuracy of the imaging technique. To obtain the best possible reconstructions, we have implemented procedures for handling noisy and incomplete diffraction data, and we propose a method for determining the reconstructed resolution. This work represents a previously uncharacterized application of x-ray diffraction microscopy to a specimen of this complexity and provides confidence in the feasibility of the ultimate goal of imaging biological specimens at 10-nm resolution in three dimensions.

coherent x-ray diffraction imaging | x-ray microscopy

that it acts as the sole source of scattering. The specimen is illuminated by a coherent beam of x-rays, and the far-field diffraction pattern is recorded on a charge-coupled device (CCD) camera. The intensity measurements are converted to magnitudes and are submitted to an iterative algorithm (16) for retrieval of the phases. In our experiments, the phase retrieval was accomplished by the difference-map algorithm (17). This iterative method is well suited to problems where the object function sought has to satisfy two different constraints. In our particular case, the first constraint is that the magnitude of the Fourier transform of the object should be equal to the magnitude of the measured diffraction pattern. The second constraint is that the object must lie within the support boundary, which must be known or determined by the algorithm. In the current experiment, the sampling of the diffraction pattern is such that the object's "support" (the region within which it is known to be contained) is only 4% of the corresponding real space area,

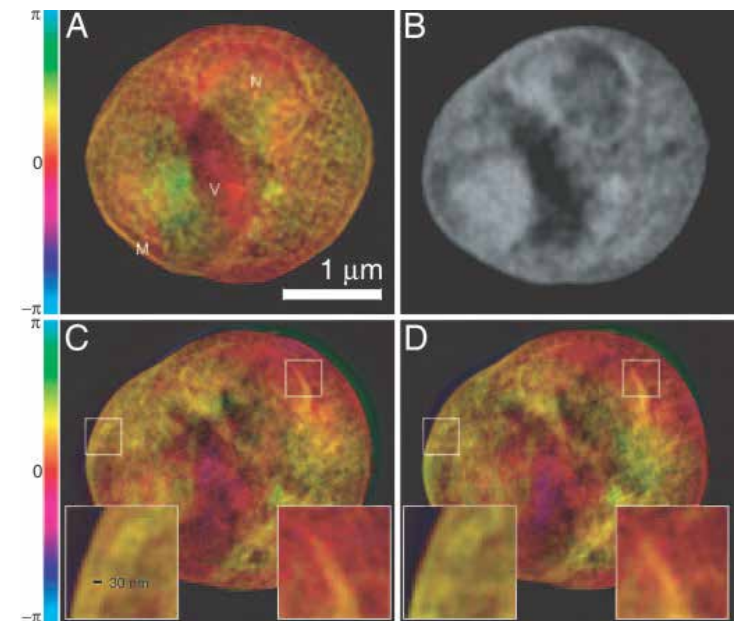
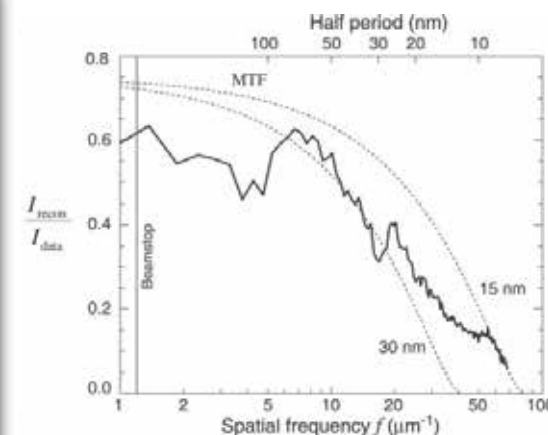
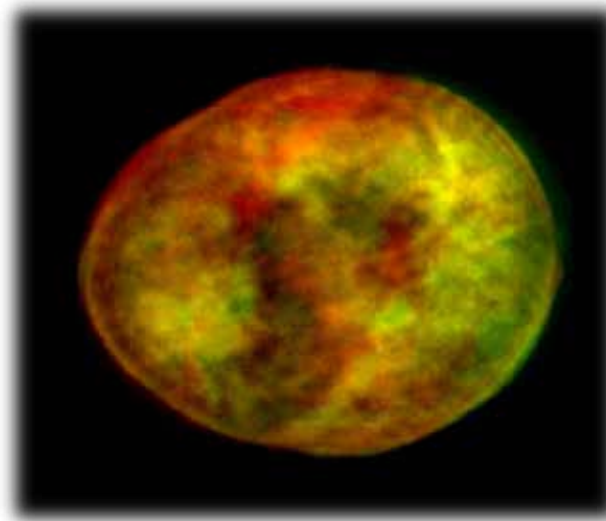


Fig. 3. Images of a freeze-dried yeast cell. *A* was obtained by phasing the diffraction data in Fig. 1, whereas *C* and *D* were obtained from reconstructions of two separate, slightly lower exposure data sets acquired with the cell tilted by 3° (*C*) and 4° (*D*) relative to *A* (Movie 2, which is published as supporting information on the PNAS web site, displays reconstructed images at 1° intervals over a 7° range). Insets in *C* and *D* show ≈30-nm fine features at the cell and nuclear membrane regions that are reproduced consistently in these separate recordings and reconstructions, even though these 2D reconstructions are projections along the beam axis with some blurring as a result of defocus. The renderings of the complex-valued reconstructions use brightness to represent magnitude and hue to represent phase (the color scale indicates reconstructed phase values). *A* is labeled according to a provisional identification of the nucleus (*N*), a storage vacuole (*V*), and the cell membrane (*M*). *B* shows a National Synchrotron Light Source X1A2 STXM (27) image taken of the same cell using 540-eV x-rays and a zone plate with an estimated Rayleigh resolution of 42 nm; this image shows absorption effects only, so it is shown in grayscale. The STXM image is shown here for comparison purposes only; it was taken at a different photon energy and in a different contrast mode (incoherent brightfield) than applies to the reconstructed diffraction data. The information contained in the STXM image was not used in any way in obtaining the diffraction reconstruction.



How to push the resolution even further?

- Key points:

- Coherent illumination → To enable CDI
- Overlapping illumination → To enable *Ptychography*

→ A form of coherent diffractive imaging in which a specimen is stepped through a localized coherent “probe” wavefront, generating a series of diffraction patterns at the plane of a detector. By stepping the specimen such that the illuminated area at each position *overlaps with its neighbors*, redundancy is introduced into ptychographical data that can be exploited during the reconstruction of an image.

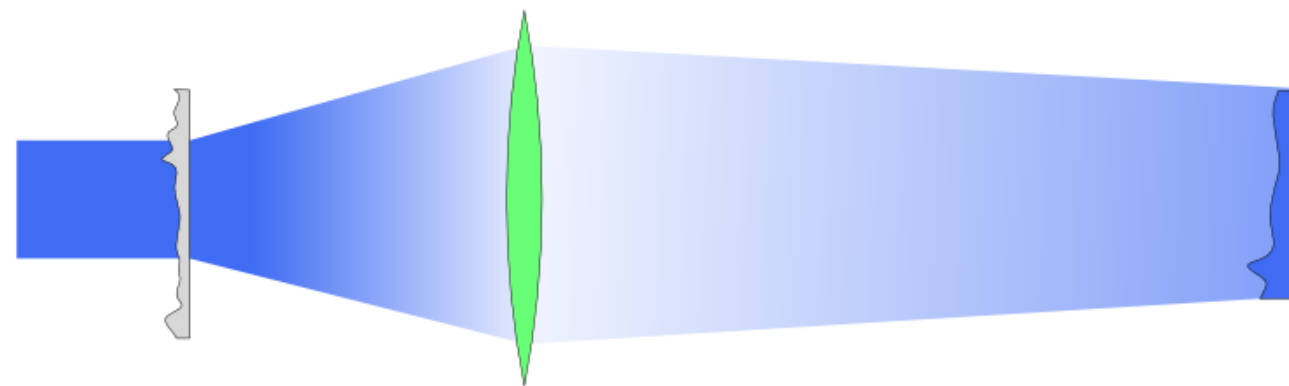
→ The redundancy allows diffraction patterns to be extrapolated beyond the aperture of the recording device, leading to super-resolved images, improving the limit on the finest feature separation

How to collect overlapping diffraction information from samples?

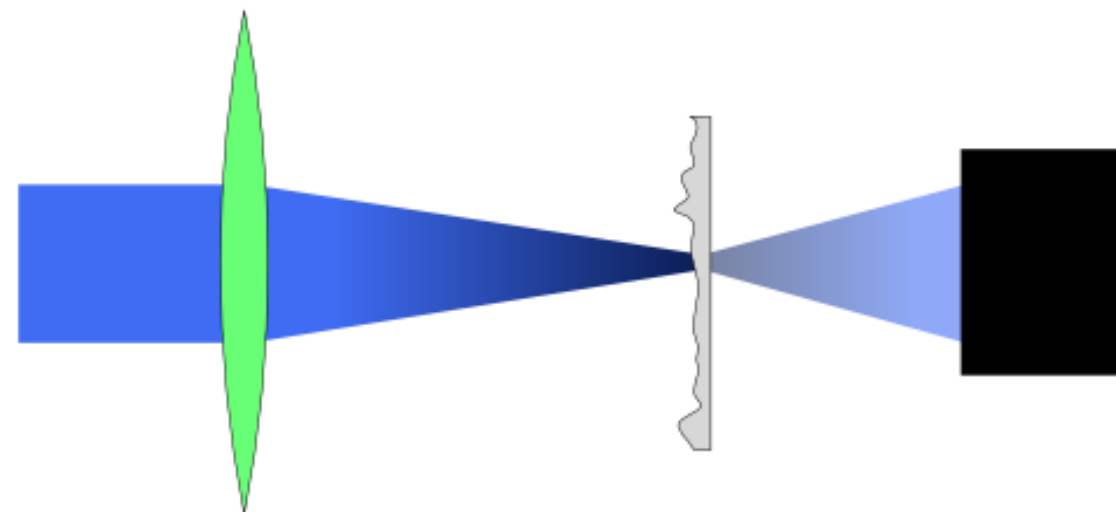
A. Maiden, J. Opt. Soc. Am. A / Vol. 28, No. 4 / April 2011

How to collect information from matter

**Full field
microscopy**

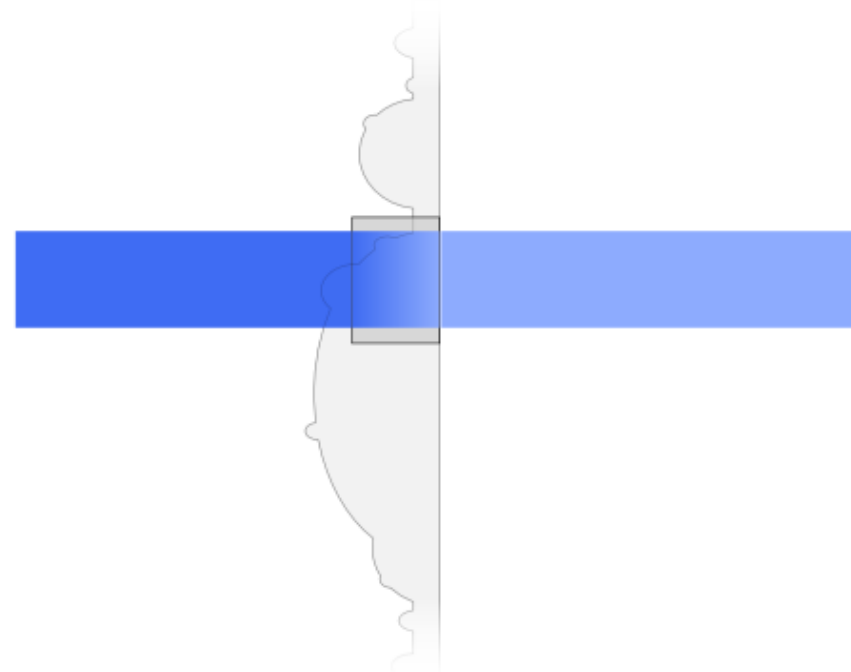


**Scanning
transmission
microscopy
(STXM)**



Slide courtesy of P. Thibault, PSI

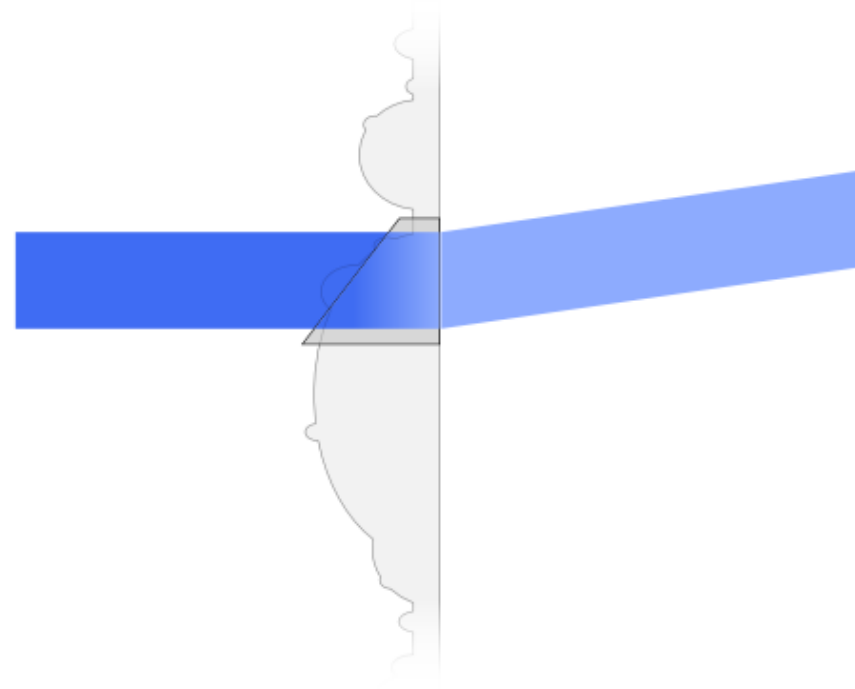
More deeply into SXTM...



beam transmission → specimen absorption

Slide courtesy of P. Thibault, PSI

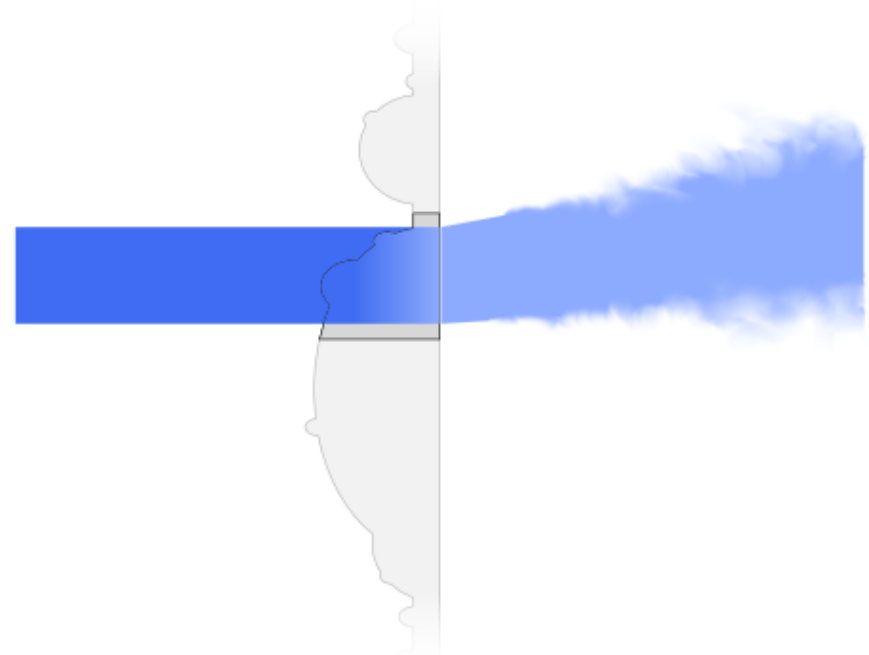
More deeply into SXTM...



beam deflection → phase gradient

Slide courtesy of P. Thibault, PSI

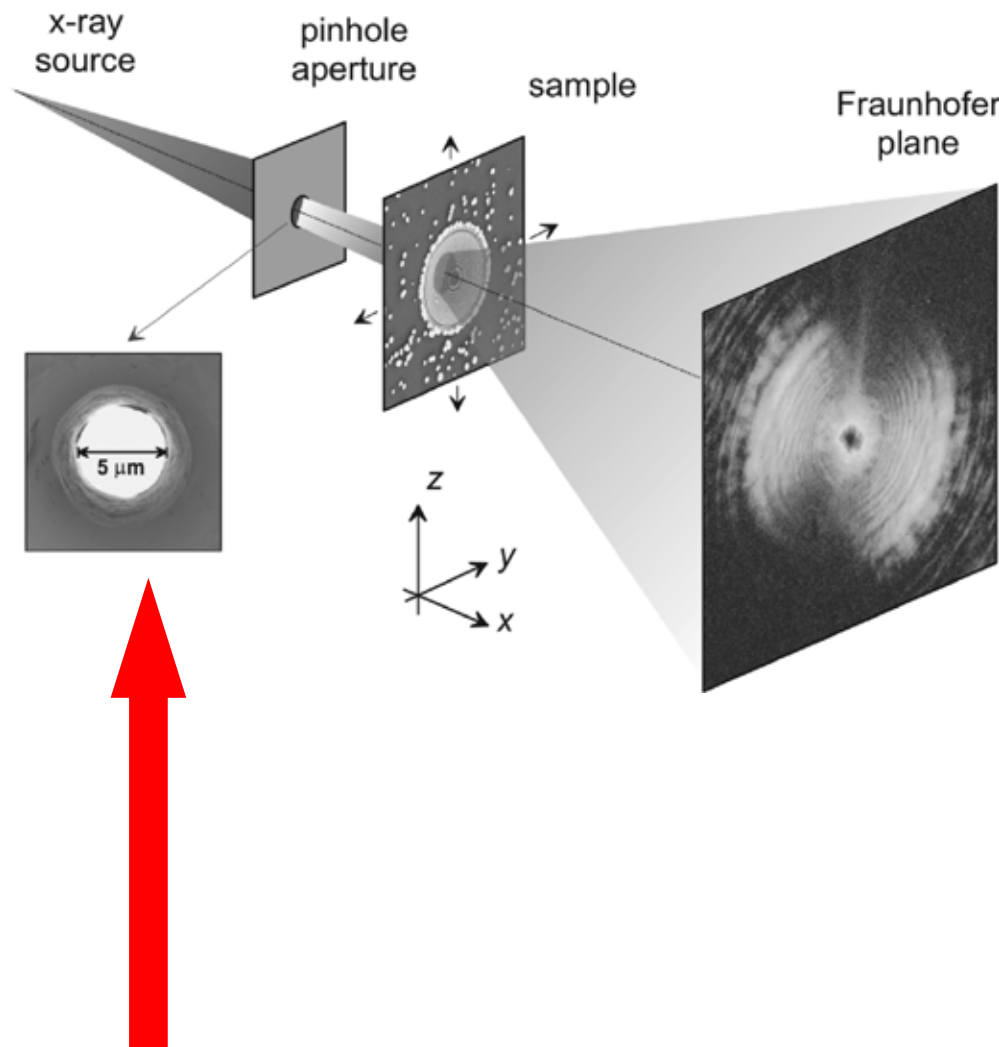
More deeply into SXTM...



scattering → higher resolution information

Slide courtesy of P. Thibault, PSI

Ptychographic 2D X-ray imaging

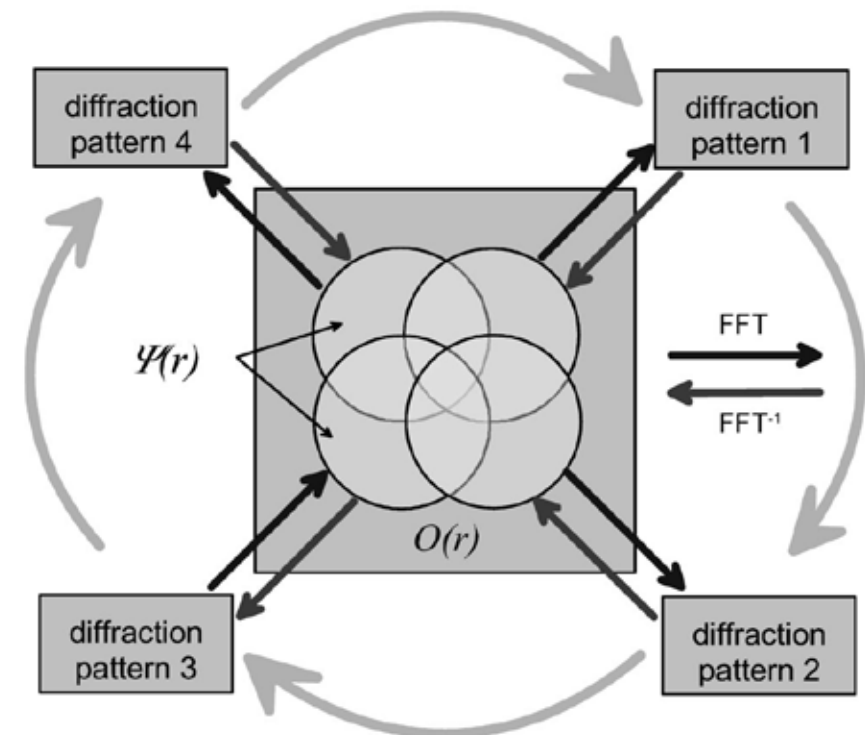


Keep in mind: pinhole 5 microns!

Ptychographical Iterative Engine (PIE)

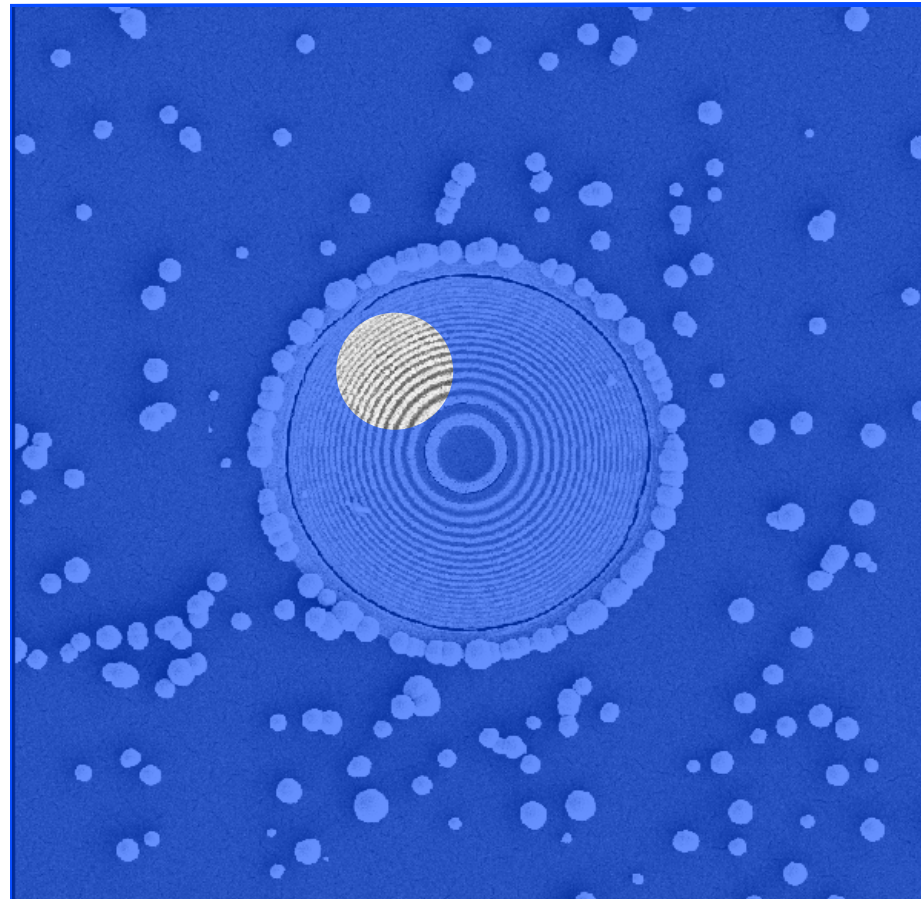
- Initial exit wave calculation (on the basis of a current estimate)
- Propagation to the Fraunhofer plane
- Modulus replaced by recorded data while preserving phase (usual for iterative methods)
- Backpropagation
- Resulting difference used to update the estimate

Note: Subsequent data from adjoining areas are fed into the algorithm to speed up convergence!

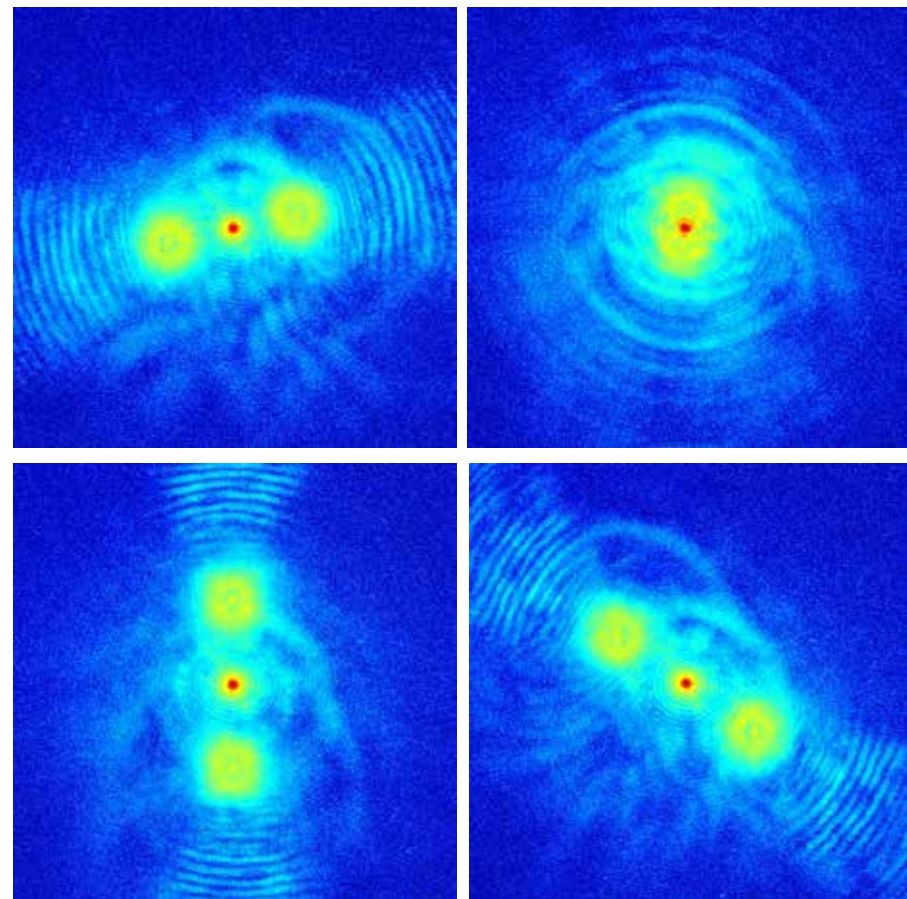


Rodenburg *et al.* (2007), Phys. Rev. Lett., 98, 034801.

Ptychographic 2D X-ray imaging



Fresnel zone plate specimen

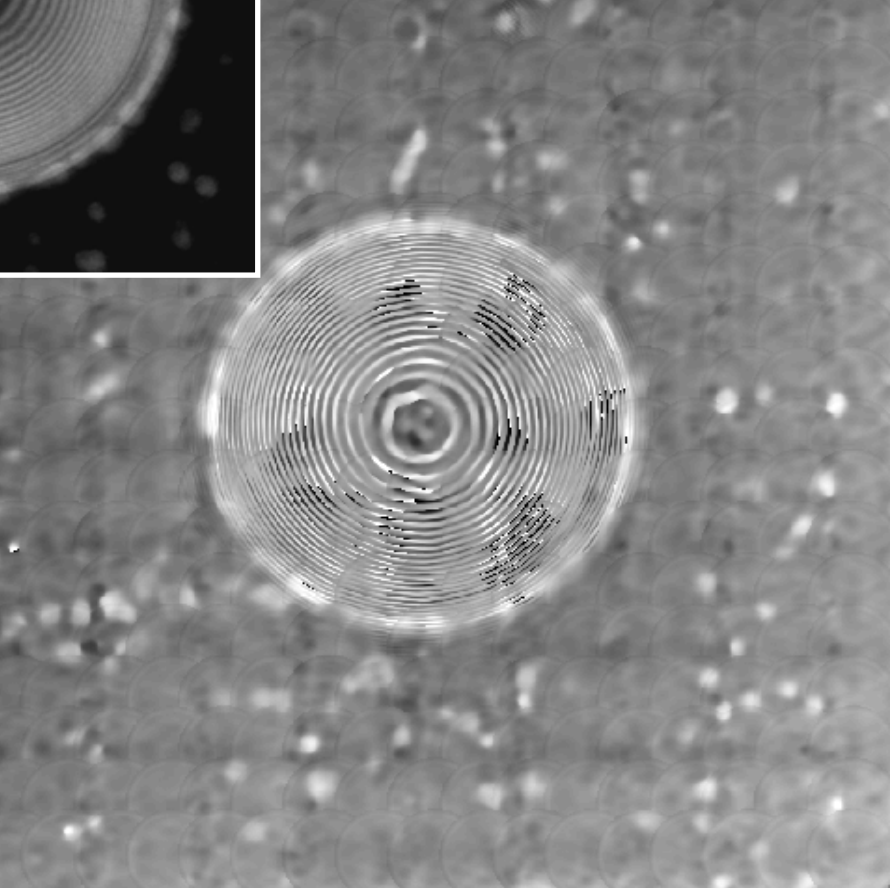
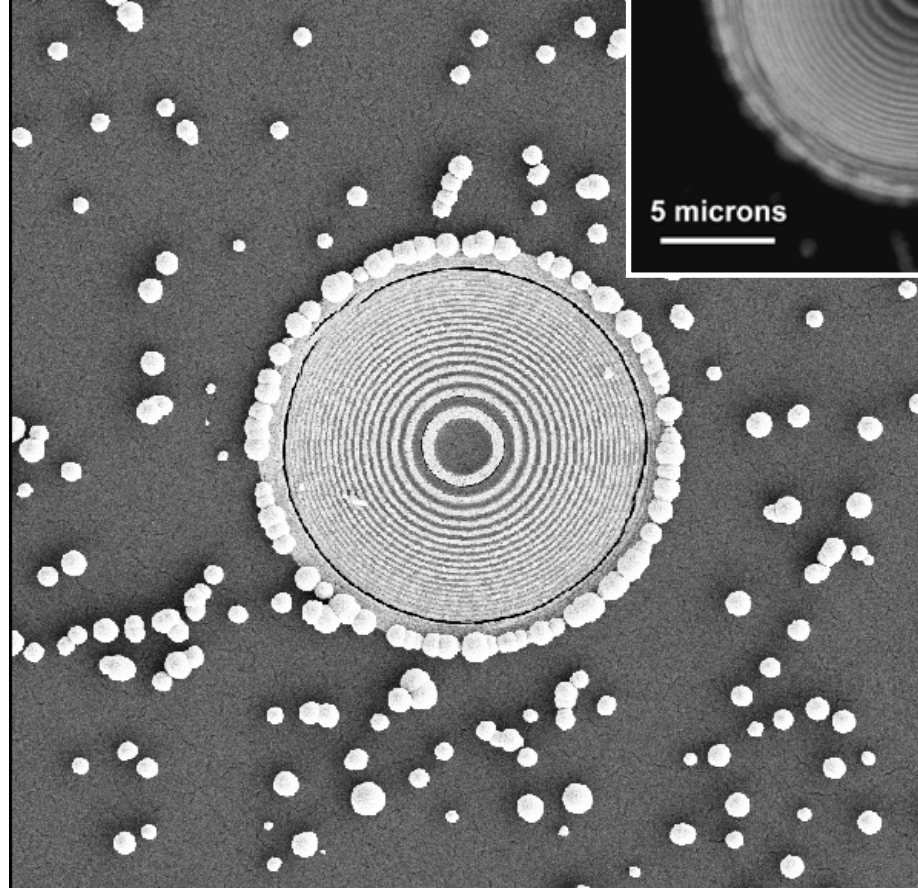
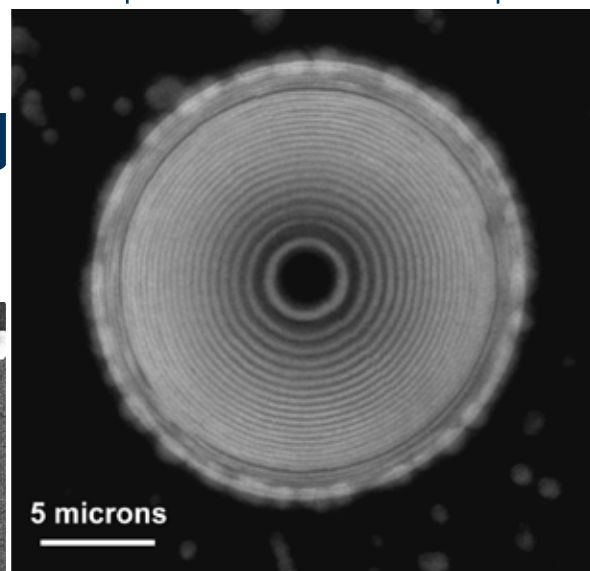


Hard X-ray (8 keV) diffraction patterns

Rodenburg *et al.* (2007), Phys. Rev. Lett., 98, 034801.

Slide courtesy of P. Thibault, PSI

Ptychog imaging



Fresnel zone plate specimen

PIE Result

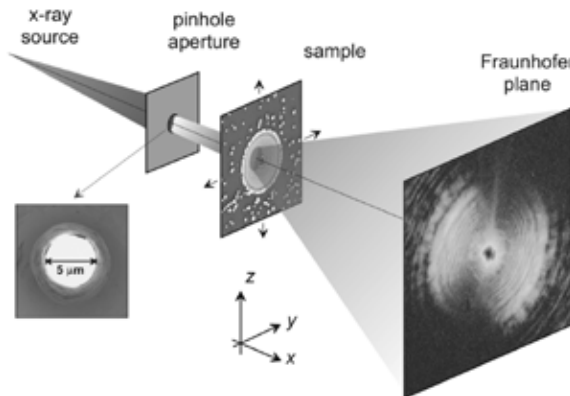
Resolution measured: 50 nm!
Remind: pinhole 5 microns!

Rodenburg *et al.* (2007). Phys. Rev. Lett., 98, 034801.

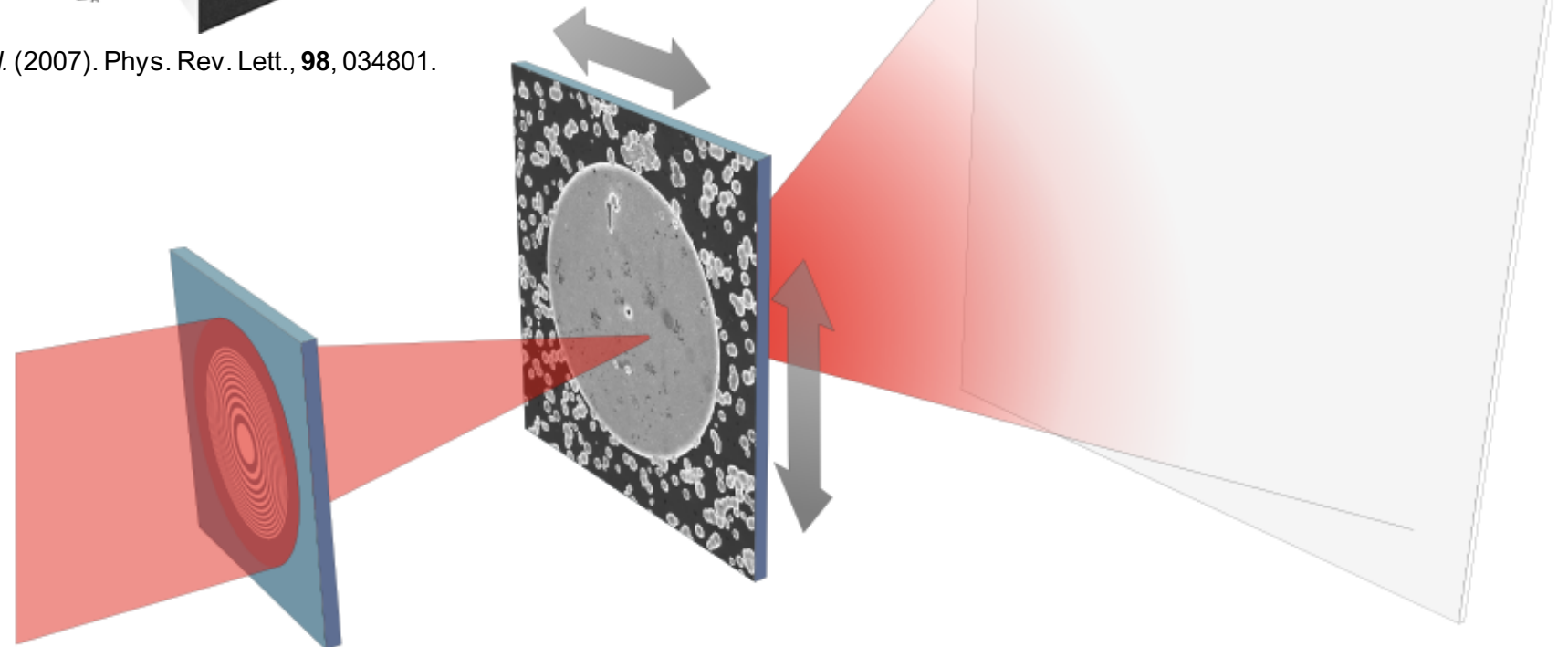
Slide courtesy of P. Thibault, PSI

Scanning X-ray diffraction microscopy

X-ray ptychography with a focused probe



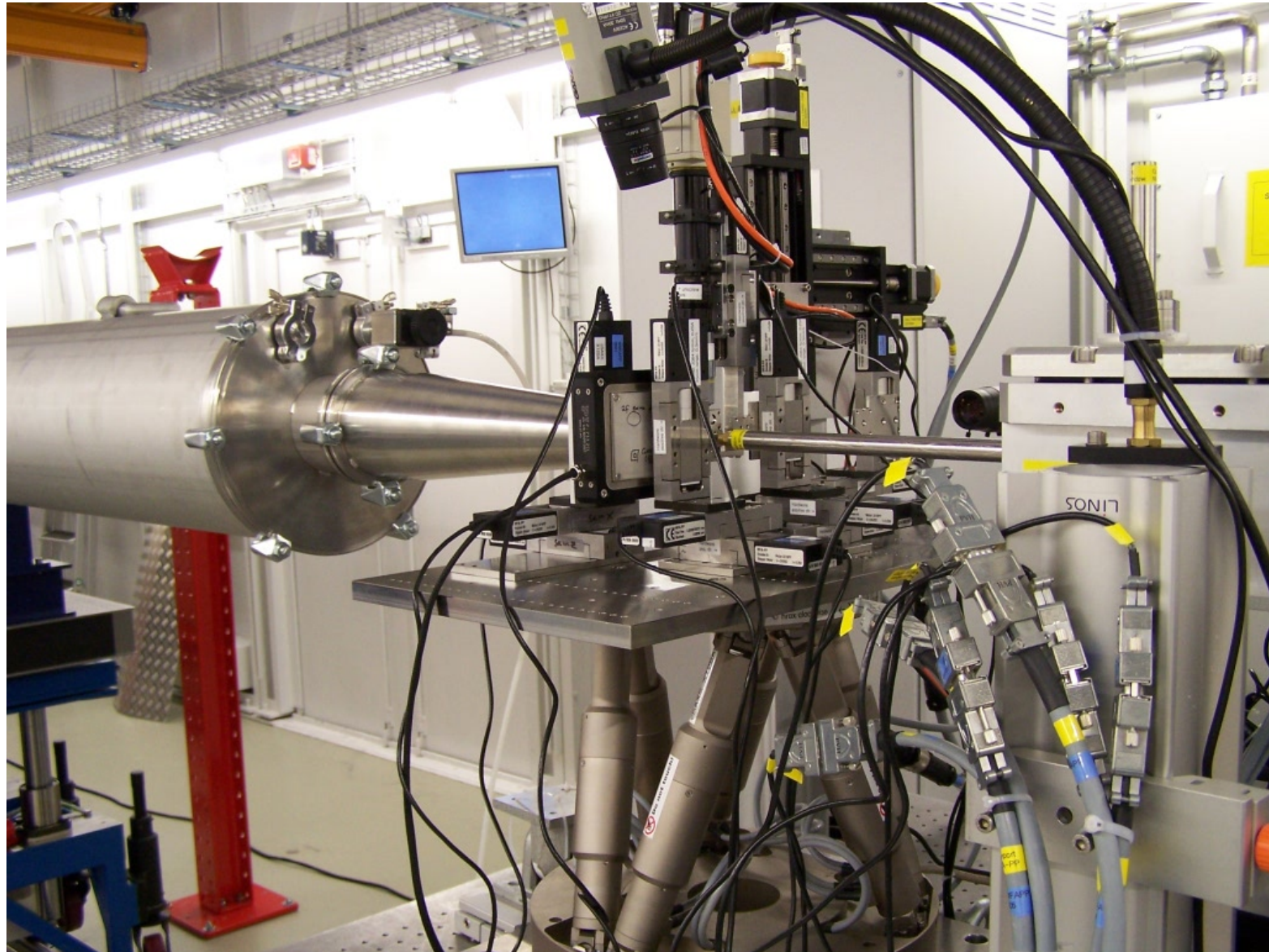
Rodenburg et al. (2007). Phys. Rev. Lett., **98**, 034801.



P. Thibault et al., Science, 321, 379-382 (2008).

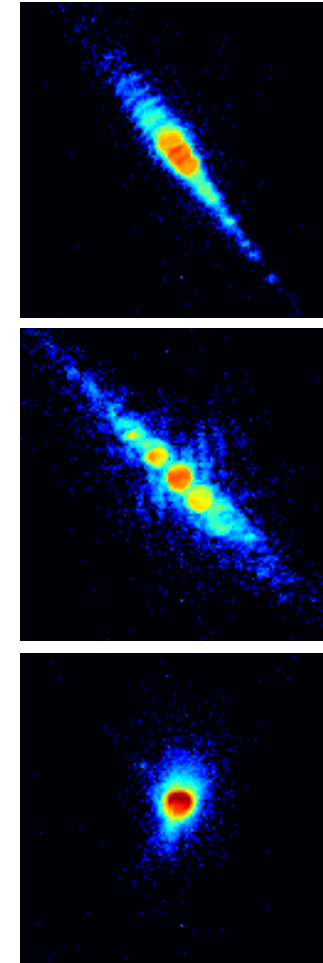
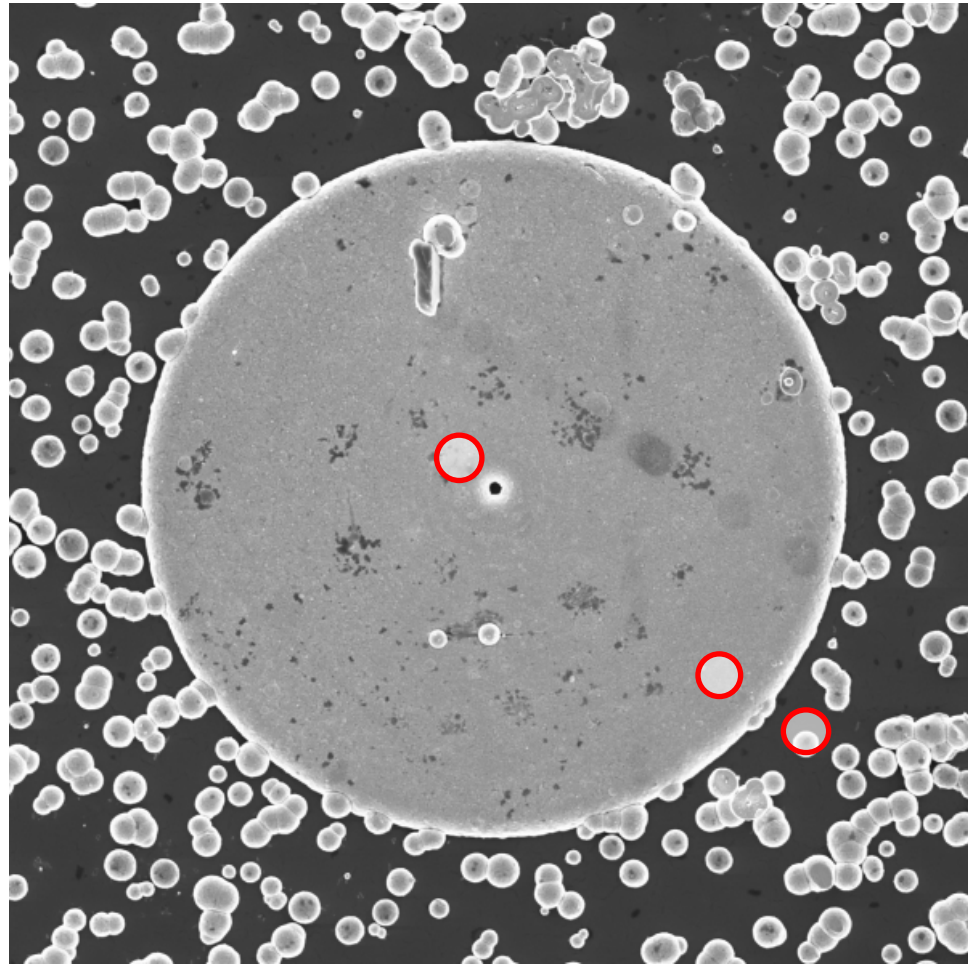
Scanning X-ray diffraction microscopy

X-ray ptychography with a focused probe



Scanning X-ray diffraction microscopy

Test specimen : buried Fresnel zone plate



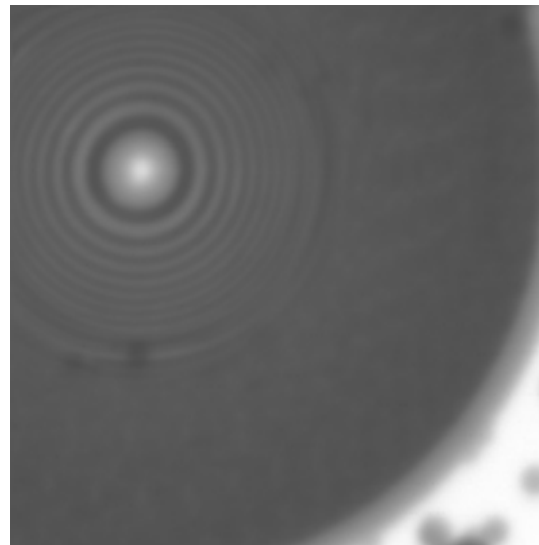
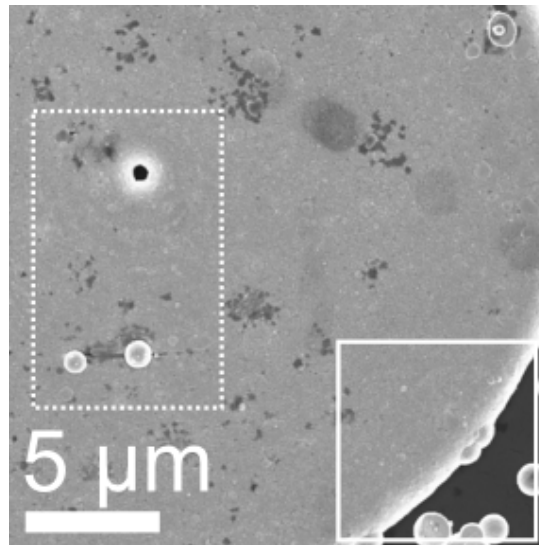
... and 40,389 more ...

Again, keep in mind: spotsize here 300 nm!

Slide courtesy of P. Thibault, PSI

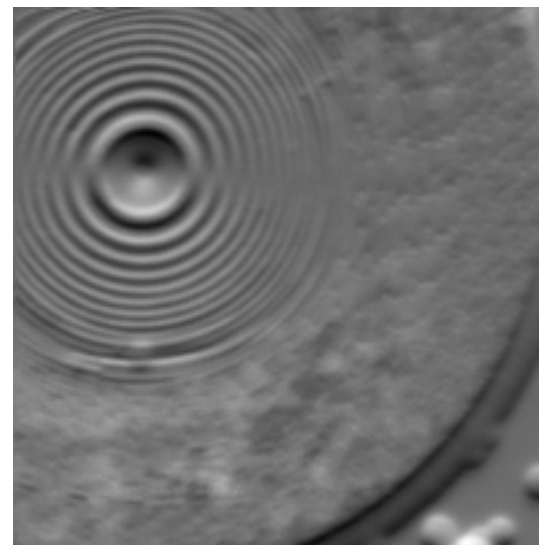
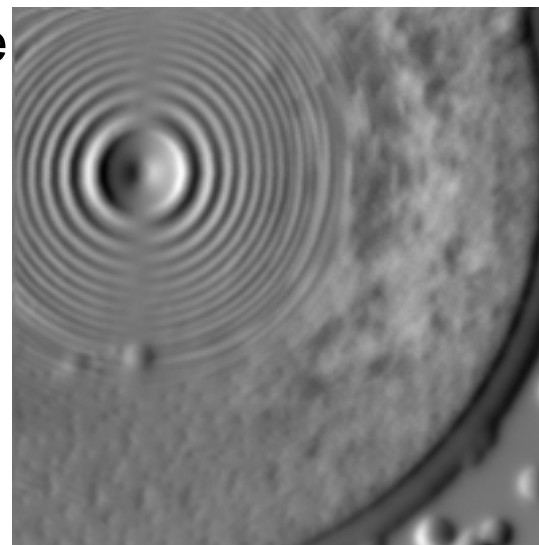
Scanning X-ray diffraction microscopy

First analysis of the dataset “à la STXM”...300 nm res. at best...



Absorption

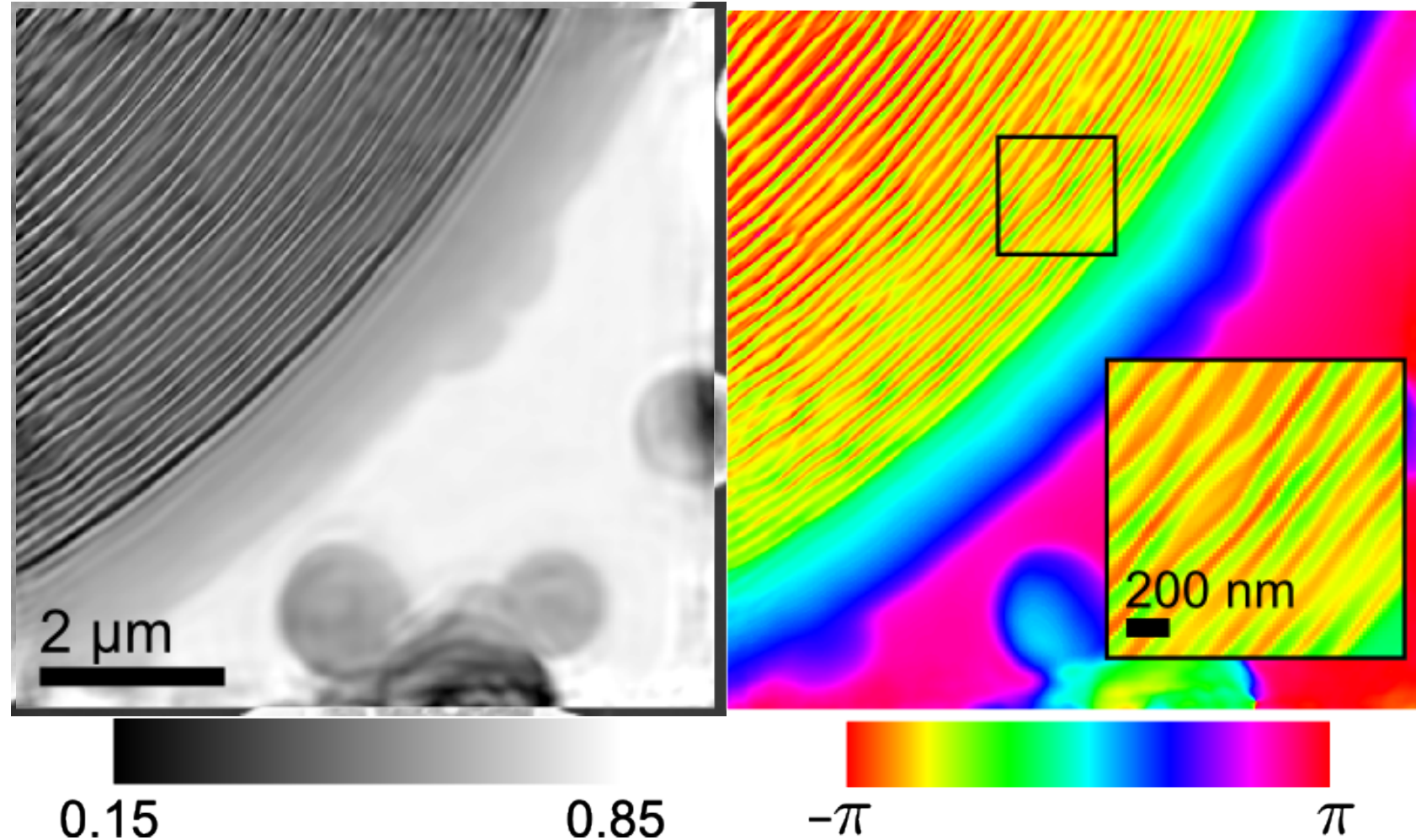
Differential phase contrast



Slide courtesy of P. Thibault, PSI

Scanning X-ray diffraction microscopy

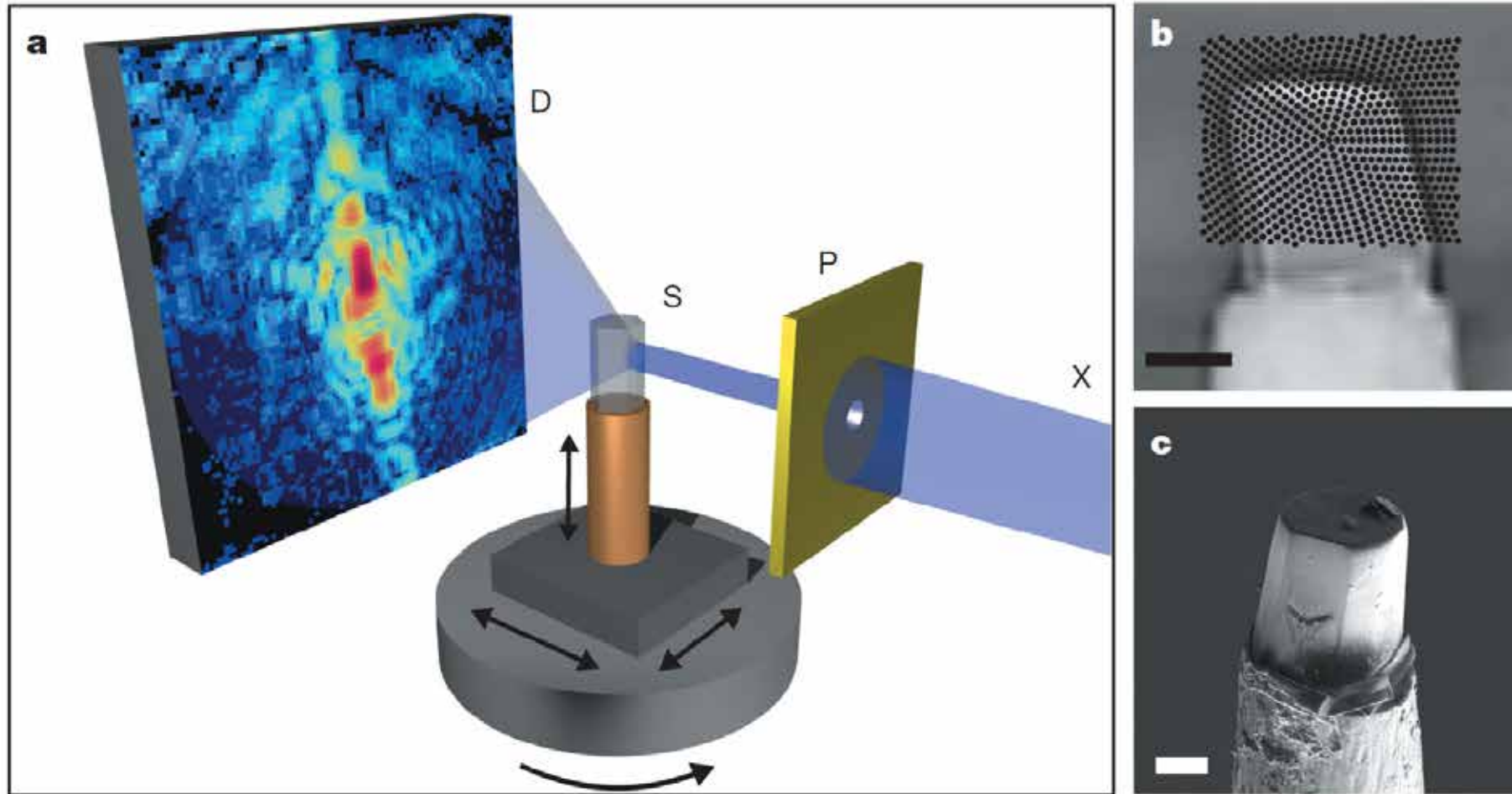
Reconstruction of a selected region



Resolution estimated around 20 nanometers !!

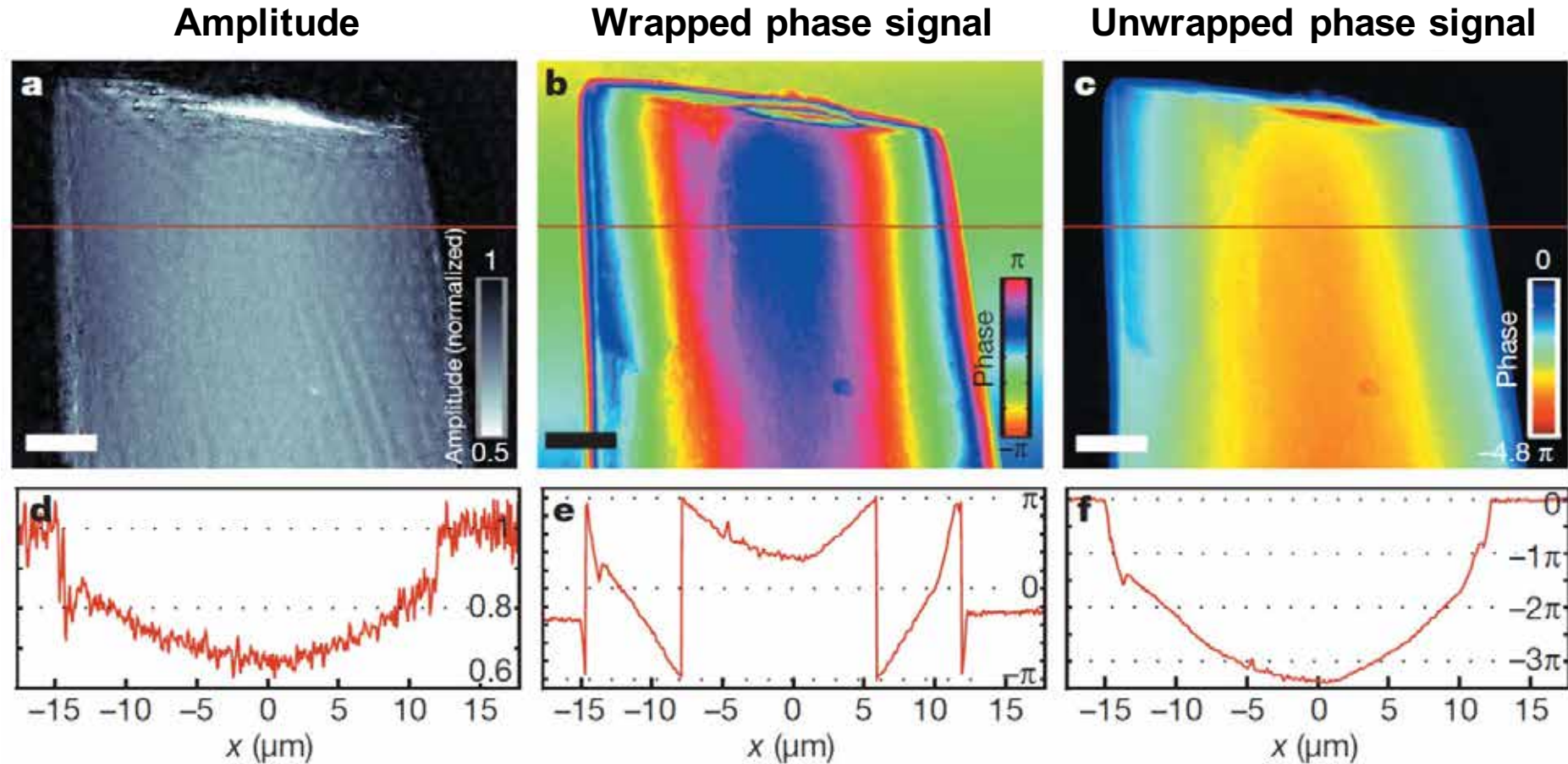
Slide courtesy of P. Thibault, PSI

Extending ptychographic SXDM to 3D



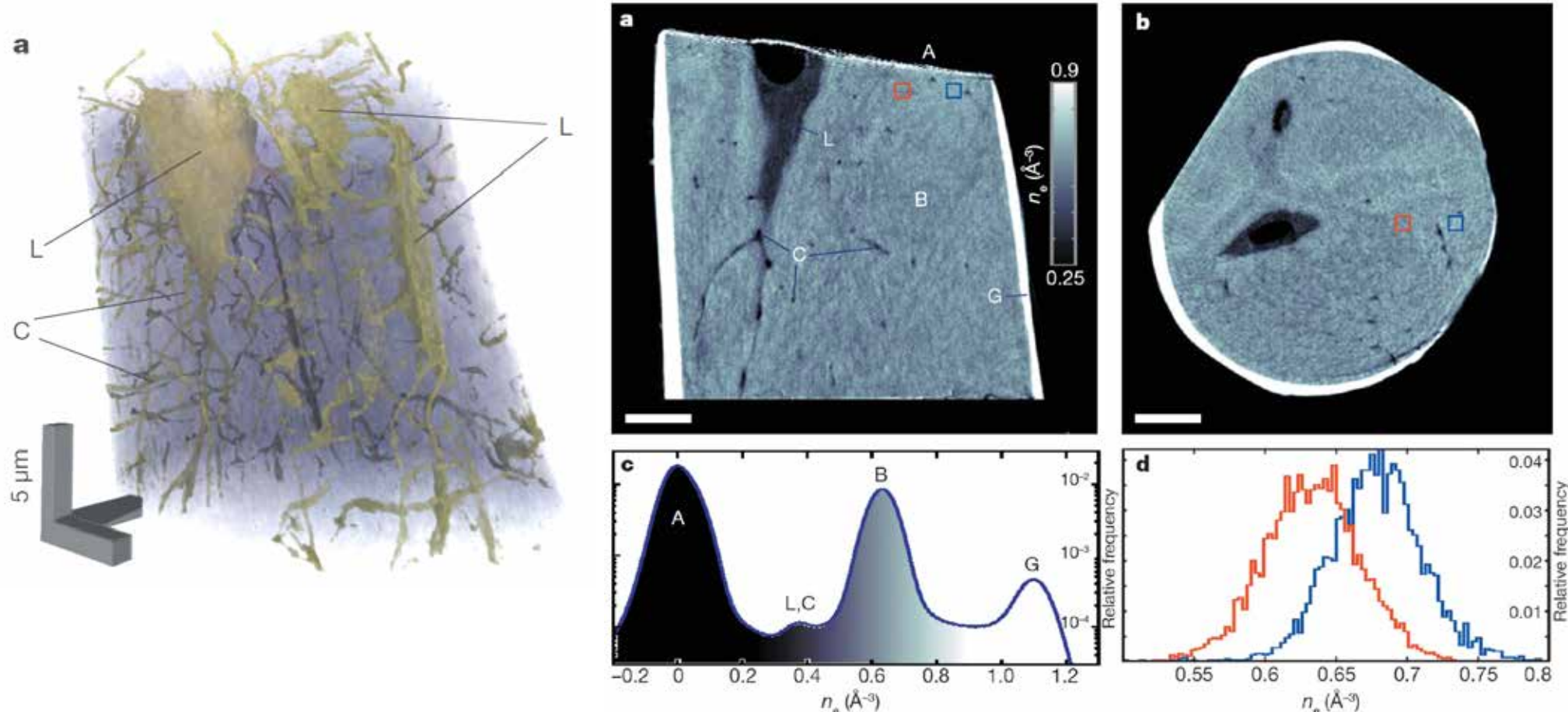
From Dierolf *et al.*, Nature 467, 2010

Extending ptychographic SXDM to 3D



From Dierolf *et al.*, Nature 467, 2010

3D quantitative information at nanoscale



The phase values have been converted to quantitative electron density. The labelled structures are air (A), bone matrix (B), canaliculi (C), gallium coating (G), which is a result of focused ion beam preparation, and osteocyte lacuna (L). b, Cut perpendicular to the rotation axis. The two large dark areas are osteocyte lacunae, and small dark dots are sections through individual canaliculi. The slight variations in the shades of grey in a and b indicate inhomogeneity in the bone density at the submicrometre scale. c, Histogram of electron density values in the reconstructed volume (500 equally sized bins for n_e values between -0.2 and 1.3Å^{-3}). The labels correspond to the ones in panel a and indicate the grey values that can be associated with the aforementioned features. d, Comparison of the bone peak (label B) of the histogram for two cubic sub-volumes of 1mm^3 , indicated by the red and blue boxes in a and b. At the micrometre scale, the detection threshold of density fluctuations is slightly less than 0.001Å^{-3} or about 0.2% of the mean bone density. Scale bars in a and b, 5 microns.

From Dierolf *et al.*, Nature 467, 2010

Ptychography on cement samples

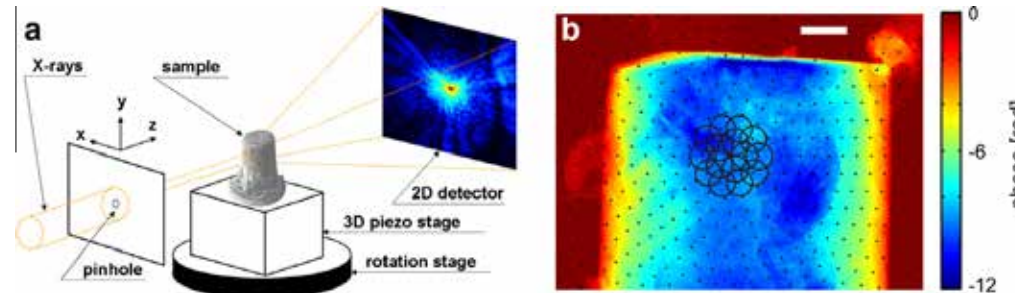


Fig. 1. (a) Sketch of the experimental setup for ptychographic X-ray computed tomography. At each incidence angle coherent diffraction patterns are recorded by a pixelated detector for a number of overlapping scanning positions, which allows the projected complex-valued transmission function to be reconstructed. (b) Example of a single reconstructed phase projection of the epoxy resin impregnated hardened cement paste sample. The black dots indicate the scanning positions at which diffraction patterns were recorded, and the black circles represent the approximate shape of the beam – shown for the first two shells of the circular scan only. The scale bar corresponds to 5 μm .

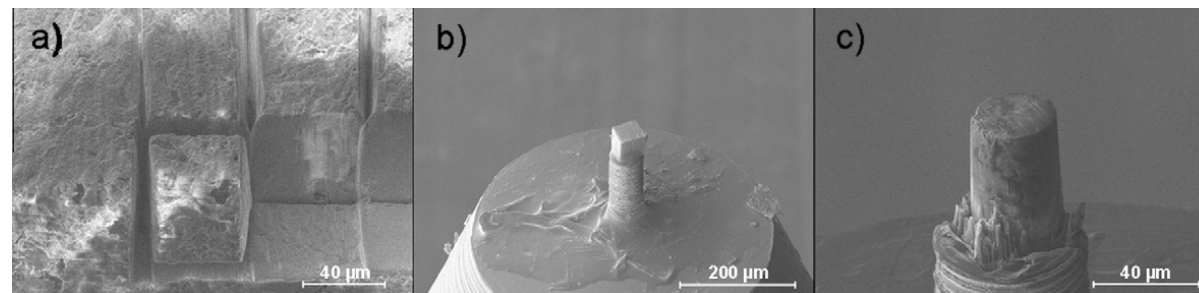
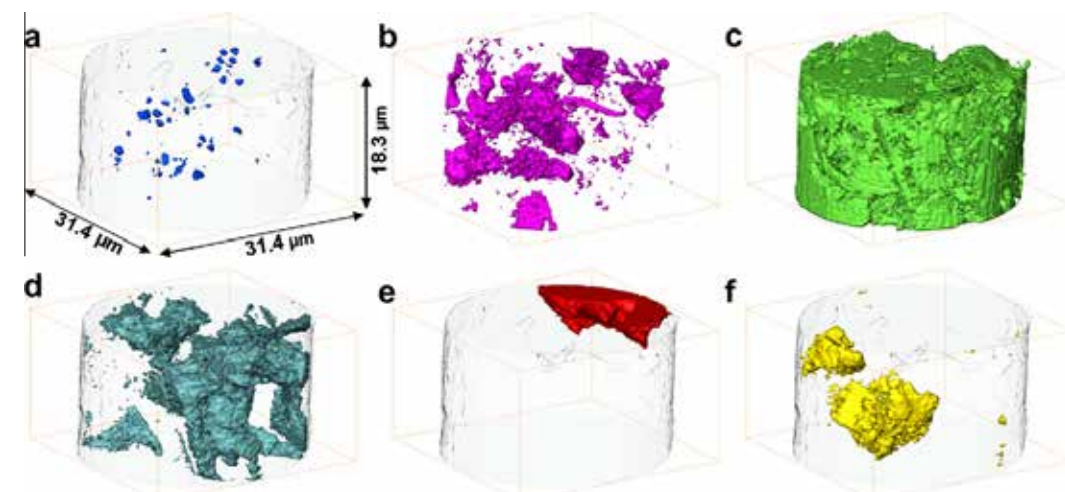
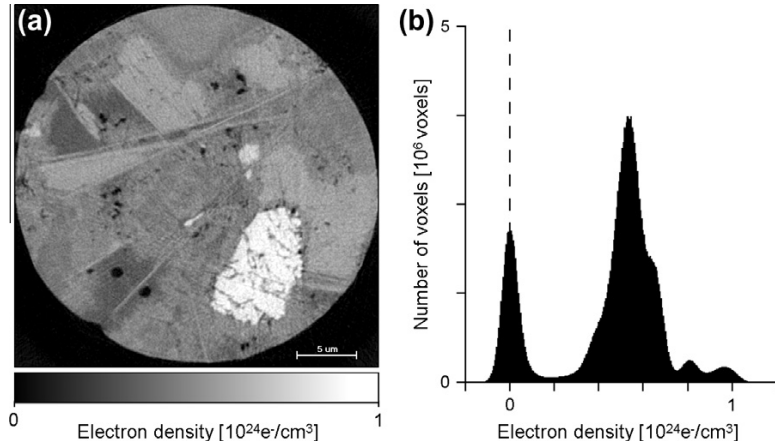


Fig. 2. (a) A view of the 90° sharp edge of epoxy-impregnated hardened cement paste from which a cube-like object was machined using focussed ion beam (FIB) milling. One of the objects is visible in about the centre of the image with the recesses remaining on the right after other similar objects were extracted. (b) The cube-like object positioned on the top of a stainless steel sample holder and (c) the final specimen produced by micromachining of the object in Fig. 2b into cylindrical shape using FIB milling.



OPEN

X-ray ptychographic computed tomography at 16 nm isotropic 3D resolution

SUBJECT AREAS:
TECHNIQUES AND
INSTRUMENTATION
IMAGING TECHNIQUES

M. Holler¹, A. Diaz¹, M. Guizar-Sicairos¹, P. Karvinen¹, Elina Färm², Emma Härkönen², Mikko Ritala², A. Menzel¹, J. Raabe¹ & O. Bunk¹

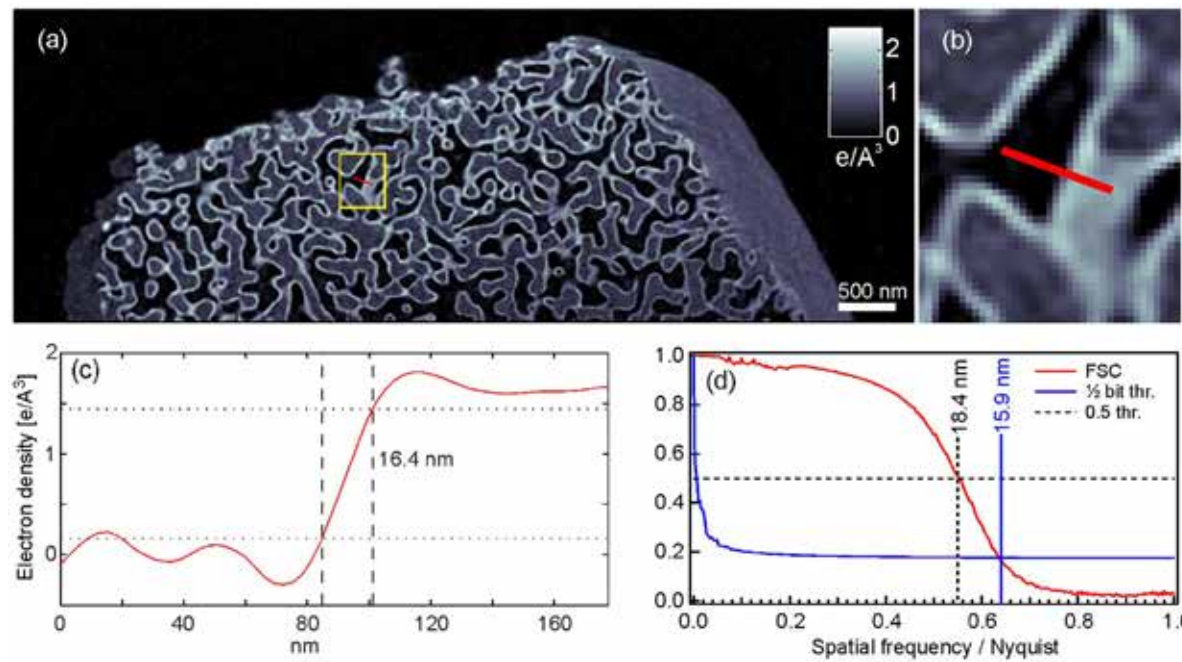


Figure 4 | Results of the tomographic reconstruction. (a) Section of the tomogram parallel to the rotation axis. Three distinct gray levels are visible for air (black), glass (gray), and a thin layer of Ta_2O_5 (white) conformal to the pores. (b) Zoom in of a region indicated by the yellow rectangle in (a). (c) Line profile indicated by a red line in (a) and (b) showing 16.4 nm edge response using the 10%–90% criteria. (d) Resolution estimation by Fourier shell correlation (FSC) computed using all 720 projections.

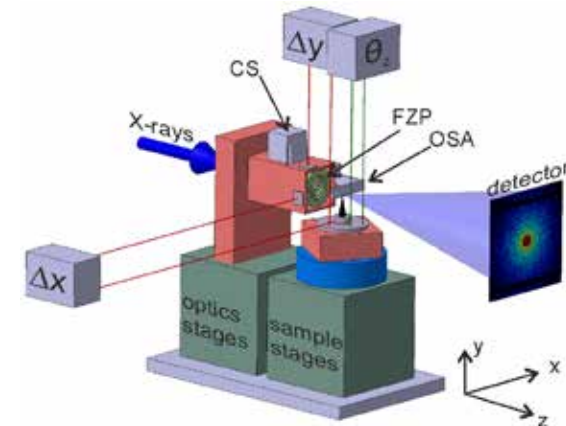
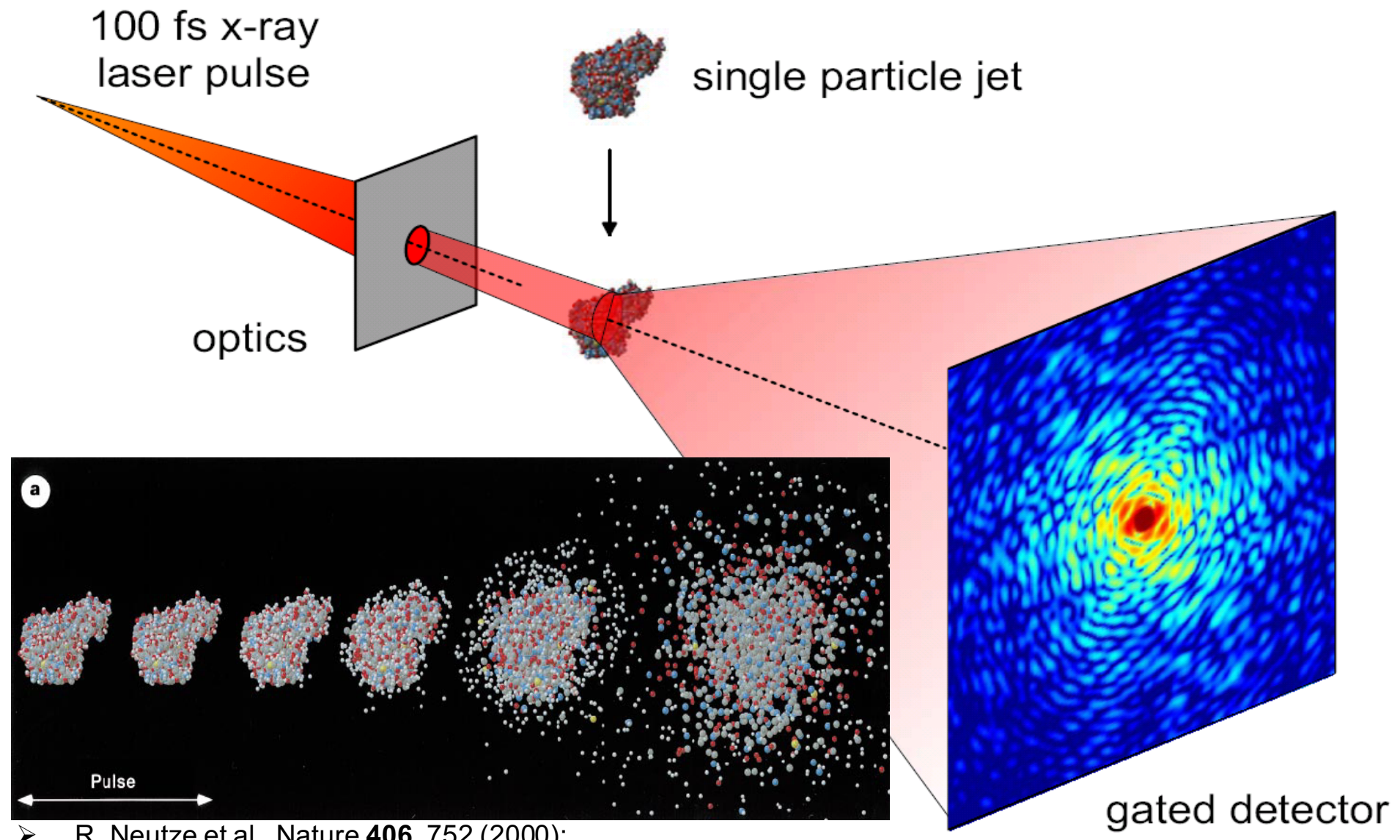


Figure 1 | Tomography setup, composed of X-ray optics and sample stage units. The optics stage contains a central stop (CS), a Fresnel zone plate (FZP) and an order-sorting aperture (OSA) for conditioning the X-ray beam. The sample stage performs the 2D scans and allows a rotation θ_y around the y-axis for tomography. The relative position of sample and optics Δx and Δy , as well as the wobble angle of the sample stage θ_z is measured via optical interferometry.

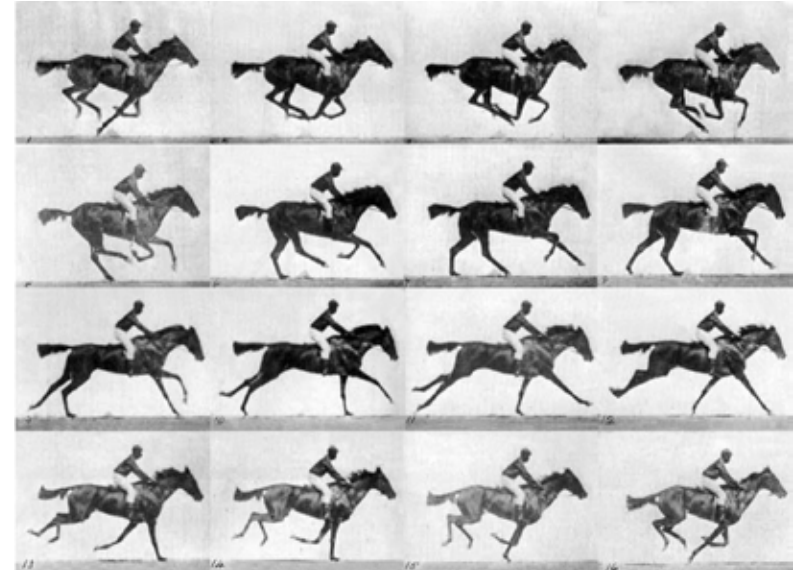
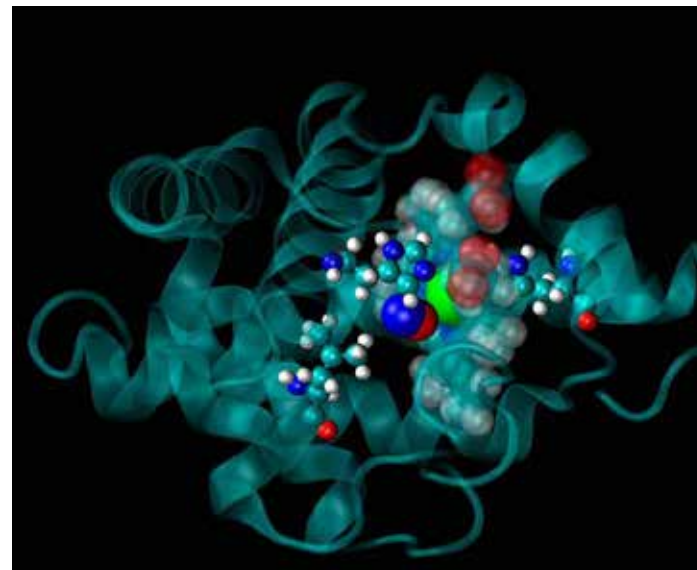
3D sample preparation. The tomography sample is based on nanoporous glass with a mean pore size of 139 nm, which is intended for use in the calibration of high pressure mercury porosimeters. As a reference material it has the advantage of being already well characterized by several methods²². A Ta_2O_5 film was fabricated on the surface of this glass material by atomic layer deposition from $\text{Ta}(\text{OC}_2\text{H}_5)_5$ and H_2O at 250°C using a SUNALE reactor (Picosun Oy, Finland)²⁸. The final film thickness was 37 nm in the outermost region of the glass beads. Using a focused ion beam, a cylinder of 6 microns diameter of this material was milled and mounted on a sample holder. This sample allows tomographic data to be taken at any projection angle without missing wedge, providing isotropic 3D resolution. It is ideal for evaluating the performance of high-resolution X-ray tomography instrumentation as it is radiation tolerant, and it provides features of 37 nm and 139 nm that are well distributed in their three-dimensional position and orientation at two distinct high-contrast levels.

Holler M. et al., Sci. Rep. 4, 3857 (2014)

Future: Atomic Resolution from Single Macromolecules ?



- R. Neutze et al., Nature **406**, 752 (2000);
- J. Hajdu et al., JSB **144**, 219 (2003);
- H. Chapman et al., Nat. Physics **2**, 839 (2007)



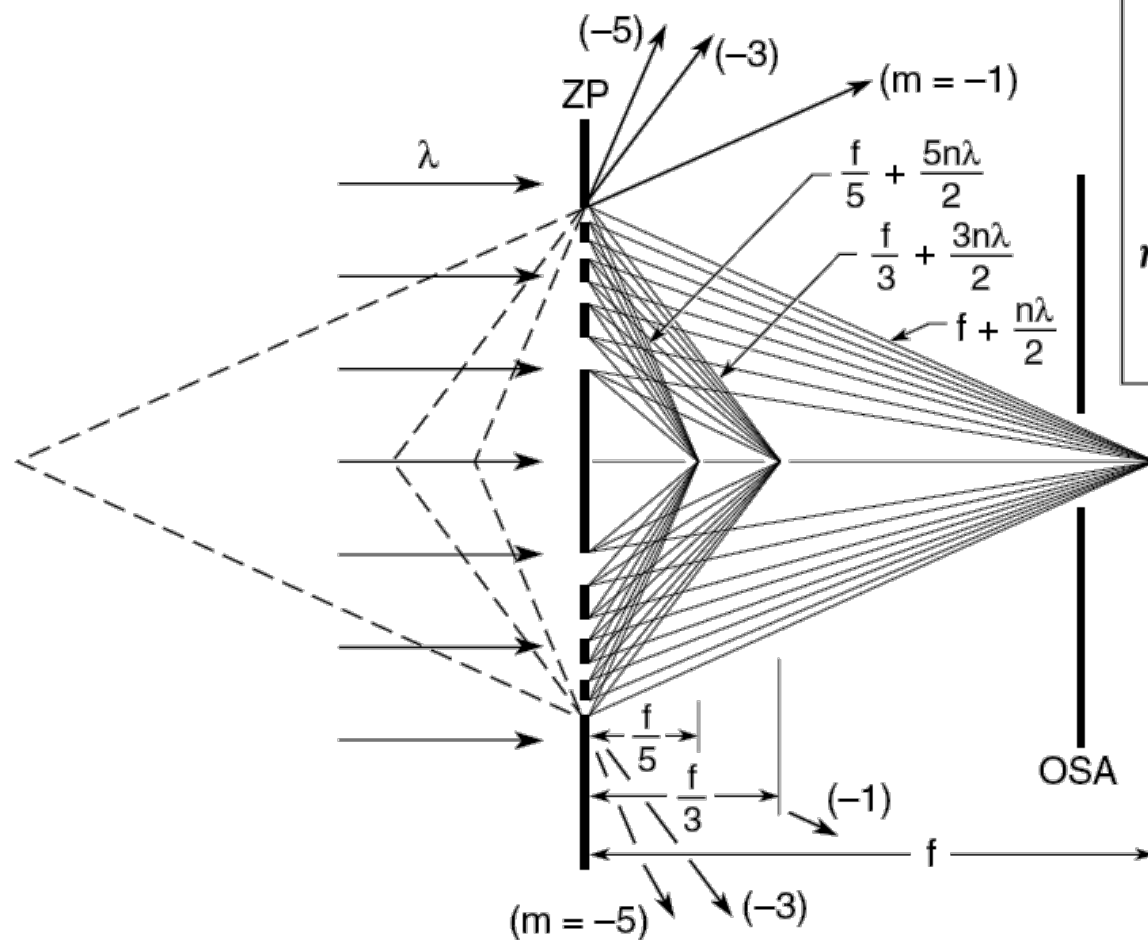
Swiss FEL

Swiss Free Electron Laser

Ultra-high brilliance within a few femtoseconds

Watch the movie....

Appendix A: Fresnel zone plates are diffracting object



$$r_n^2 \simeq mn\lambda f_m$$

$$\eta_m = \begin{cases} \frac{1}{4} & m = 0 \\ 1/m^2\pi^2 & m \text{ odd} \\ 0 & m \text{ even} \end{cases}$$

$$f_m = \frac{1}{m} \frac{r_N^2}{N\lambda}$$

$$f_m = \frac{1}{m} f_1$$

Appendix A: Fraunhofer Single Slit

